

Series 03 Control and Simulation 02

A System Look at Electromechanical Actuation for Primary Flight Control

E.A. Lomonova



Delft University Press



706395

A System Look at Electromechanical Actuation for Primary Flight Control

Bibliotheek TU Delft



C 3021886

2392
340
3

Series 03: Control and Simulation 02



A System Look at Electromechanical Actuation for Primary Flight Control

E.A. Lomonova



Delft University Press / 1997

Published and distributed by:

Delft University Press
Mekelweg 4
2628 CD Delft
The Netherlands
Telephone +31 (0)15 278 32 54
Fax +31 (0)15 278 16 61
e-mail: DUP@DUP.TUdelft.NL

by order of:

Faculty of Aerospace Engineering
Delft University of Technology
Kluyverweg 1
P.O. Box 5058
2600 GB Delft
The Netherlands
Telephone +31 (0)15 278 14 55
Fax +31 (0)15 278 18 22
e-mail: Secretariaat@LR.TUdelft.NL
website: <http://www.lr.tudelft.nl>

Cover: Aerospace Design Studio, 66,5 x 45.5 cm, by:
Fer Hakkaart, Dullenbakkersteeg 3, 2312 HP Leiden, The Netherlands
Tel. +31 (0)71 512 67 25

90-407-1581-5

Copyright © 1997 by Faculty of Aerospace Engineering

All rights reserved.

No part of the material protected by this copyright notice may be reproduced or utilized in any form or by any means, electronic or mechanical, including photocopying, recording or by any information storage and retrieval system, without written permission from the publisher: Delft University Press.

Printed in The Netherlands

Contents

Introduction.....	1
Chapter 1 Aircraft power system analysis and comparison.....	5
1.1 Overview of generating systems.....	5
1.1.1 Constant speed drive.....	8
1.1.2 Cycloconverter various speed constant frequency (VSCF) power system.....	8
1.1.3 DC-link various speed constant frequency (VSCF) power system.....	8
1.1.4 High voltage direct current (270 V) power system.....	11
1.2 Advanced power system.....	11
1.2.1 Basis of 20 kHz AC power system.....	11
1.2.2 Rationality for system selection.....	17
1.2.3 System description.....	17
1.2.4 System operation.....	17
Chapter 2 Brushless Motors.....	19
2.1 Main circuit configuration.....	28
2.2 The inverter.....	33
2.3 Sine wave PWM circuit.....	34
2.4 Power supplies for brushless motors.....	36

2.4.1. Pulse-width modulated (PWM) transistor inverter operating at high switching frequency.	36
2.4.2 Pulse-width modulated thyristor converter with constant direct voltage supply (voltage source inverter.	38
2.4.3 Thyristor converter with impressed direct current supply (current source inverter).	39
2.5 Trigger control circuit.	41
2.6 Construction and function of the resolver.	43
2.7 Energy product of brushless motor.	47
2.7.1 Magnetic materials.	47
Chapter 3 Brushless motor control.	54
3.1 Torque production.	55
3.1.1 Field and torque production with rectangular current.	55
3.1.2 Field and torque with sinusoidal current.	58
3.1.3 Design of sinusoidal-fed PM motor.	60
3.1.4 Square-wave current control system.	61
3.1.5 On-off square-wave current controller.	61
3.2 Mathematical models of brushless motor drive system.	64
3.2.1 Mathematical model of brushless motor in d,q-axes presentation.	64
3.2.2 Position control system of brushless motor using d,q-axes presentation.	67
3.2.3 Mathematical model of brushless motor in phase coordinates.	68

3.3 Synthesis of controllers.	71
3.3.1 Decoupling current control of a brushless motor. . .	72
Chapter 4 Preliminary system approach to design of electromechanical actuators for aircraft control surfaces.	76
References.	92
Appendix 1.	95
Appendix 2.	96
Appendix 3.	100
Appendix 4.	103

List of Symbols

\bar{c}	mean aerodynamic chord
C_{ha}	hinge moment coefficient (a function of surface and tab position)
E_a	induced voltage in phase a
E_b	induced voltage in phase b
E_c	induced voltage in phase c
f_0	fixed clock frequency
F_{mf}	“fictitious” magnetomotive force
H_M	hinge moment coefficient
H_P	horse power
I_d	direct (d-axis) component of the armature current
I_D	intermediate direct current of power source
I_q	quadrature (q-axis) component of the armature current
J_L	load inertia
J_M	motor inertia
K_b	winding factor
l	axial length of the machine
L_d	motor d-axis inductance
L_q	motor q-axis inductance
M_d	mutual inductance in d,q -axes presentation
p	number of pole pairs
R	motor resistance

S	surface reference area Laplace operator
T_{ML}	actuator (motor) load torque (flight control surface moment)
T_0	minimum time interval between switching operations
t_b	acceleration time
T_{ek}	peak motor torque (electromagnetic torque)
T_M, T_e	motor torque (electromagnetic torque)
T_{ML}	motor load torque
U_D	intermediate direct voltage of power source
U_d	d - axis component of voltage
U_q	q- axis component of voltage
V	true air speed (TAS)
W_b	number of turns per pole per phase

Greek symbols

Δ	difference operator
ξ	motor damping coefficient
α	advance angle for maximum torque per ampere position
ρ	air density (the function of temperature and altitude)
ν	interger number
ω_L	load (surface) speed in revolutions per minute
μ_0	coefficient of permeability

θ_a	motor (rotor) position
θ_M	permanent magnet space
ψ_d	d - axes flux linkage
ψ_F	field flux linkage
ψ_q	q - axes flux linkage
ω_b	base speed
ω_M	angular velocity of the brushless motor
2Δ	hysteresis band

Matrixes

$[\psi]$	flux linkage matrix
$[U]$	voltage matrix
$[R]$	resistance matrix
$[L]$	inductance matrix
$[I]$	current matrix

Abbreviations

AC	Alternating Current
AC/AC	Alternating Current to Alternating Current Converter

AC/DC	Alternating Current to Direct Current Converter
A/D	Analog to Digital Converter
AEA	All Electric Aircraft
ALNICO	Aluminium Nickel Cobalt magnet
BJTs	Bipolar Junction Transistor
BM	Brushless Motor
CR _A , CR _B , CR _C	Conduction Rates
CSD	Constant Speed Drive
D/A	Digital to Analog Converter
DC	Direct Current
EMAs	Electromechanical Actuators
EMI	Electromagnetic Interference
FBW	Fly-by-Wire
FCS	Flight Controlled Surface
FETs	Field effect transistors
GTOs	Gate Turn-Off thyristors
HVDC	High Voltage Direct Current
IGBT	Insulated Gate Bipolar Transistors
LC	Inductor-Capacitor circuit
MCA	Isotropic (ALNICO) Magnet Material
MCB	Anisotropic (ALNIKO) Magnet Material
MOSFET	Metal Oxide Semiconductor Field Effect Transistor
MPA	Isotropic (Ceramic) Magnet Material
MPB	Anisotropic (Ceramic) Magnet Material
PBW	Power-by-Wire

PM	Permanent Magnet
PWM	Pulse Width Modulation
RMS	Root Mean Square
SCR	Selicon Controlled Rectifier
SR	Series Resonant invertor
VSCF	Various Speed Constant Frequency

List of Tables

1.1	Main types of aircraft power systems.	6
1.2, 1.3	Weight of power systems and their equipment for All Electric Aircraft --TU-204.	7, 9
2.1	Advantages of brushless drive systems.	20
2.2	Comparison of brushless motors control hardware.	42
2.3	Types of Alnico magnets and their magnetic characteristics.	48
2.4	Types and magnetic characteristics of ferrite magnets.	49
2.5	Types of rare-earth cobalt magnets and their magnetic characteristics.	50
2.6	Varieties and magnetic characteristics of <i>NeFeB</i> magnets.	51
3.1	Phase voltages for wye-connected stator.	70
4.1	Electromechanical actuation system model parameters.	80
4.2	Motor model parameters.	81
4.3	Motor design constraints.	86
4.4	Design constraint nomenclature.	88
4.5	Design equation nomenclature.	89
4.6	General constraints for design of an electromechanical actuator.	90

Acknowledgements

I sincerely thank Prof. ir.J.Schoonhoven for being my official supervisor and the scholarship I received. I sincerely thank Chairman of Stability and Control Department, Prof.dr.ir. J.A.Mulder, for his most supportive attitude, attention, and assistance.

I owe much thanks to my Russian teachers: Prof.dr. S.R.Miziurin, Academician, Pr.dr.D.A.Bout, and Prof.dr. L.K.Kovalev for their permanent support.

I sincerely thank my father, son, husband and his parents for never letting me down although my "home absence" has been awful during the last year.

I thank all my colleagues at the Stability and Control Department, and Faculty of Aerospace Engineering who created the brilliant friendship atmosphere, unique conditions to work, who tolerated and supported me.

I thank Holland for making me welcome.

Introduction

Current aircraft use three main forms of onboard secondary power, that is, electrical power, pneumatic and hydraulic power. In general, hydraulic power is generated, distributed, and utilized for the majority of high power output functions such as primary and secondary flight control surfaces, landing-gear extension and retraction, brakes, nosewheel steering, etc., while electrical power is used for everything else. This division of functions over these forms of power developed over the years, largely as a result of the ever increasing demands of high performance aircraft for higher levels of control. There are two problems with this arrangement. The first is that each power source must be oversized to meet the system reliability requirements, which results in a heavier power system. The second is that the power cannot in general be shared among the systems. For example, if the hydraulic power source fails, the hydraulic loads cannot be powered by pneumatic or electric power sources.

Using a single type of power for all aircraft secondary functions would allow load sharing. With load sharing the duty cycle of the secondary power system could be optimized over the entire flight duty cycle. This would result in a smaller overall capacity power system and significant weight reduction.

Because avionics, lighting and the galley require electric power, it is the only type of power that can supply all of the aircraft's loads. If electric power is chosen as the only source, these hydraulic actuators must be replaced by electromechanical ones and environmental control and icing protection must be powered electrically instead of pneumatically.

In its basic form, a primary flight control system (FCS) consists of movable control surfaces connected by cables and rods to cockpit controls that are directly operated by the pilot. If there are no powered actuators, the surfaces are aerodynamically balanced to reduce the pilot's physical effort in controlling the aircraft. In some aircraft the mechanical sections of these systems also include powered actuators. Since hydraulic actuators were felt to have many advantages over electromechanical actuators for high torque, high power applications, hydraulic power became the choice for all high-power demand applications. However, in the 25 years since hydraulics achieved its current level of acceptance, many changes have occurred in the electrical power field that indicated that the time had come for a critical re-evaluation of electrical power's place in the power arena [Ref. 36]. It has long been recognized that, if all secondary power used on board an aircraft could be generated, distributed, and used by one type of power system rather than two, there would be significant potential savings involved. The technology to build electromechanically actuated primary flight control systems is now available. The past few years have seen the emergence of fly-by-wire (FBW) and

power-by-wire (PBW). The conception of fly-by-wire refers to the input signal path being electrical rather than mechanical and fly-by-power refers to the actuator using electrical rather than hydraulic power. The incentives for this are definitely clear:

- Aircraft reliability is significantly increased by the elimination of distributed high pressure hydraulic lines from the fuselage and wing box.
- System complexity is reduced in a major way by the elimination of a complex hydraulic system.
- Weight of the aircraft is reduced.
- Development and life cycle costs are reduced.
- Requirements to the logistic and maintenance support are reduced.
- Aircraft production costs are reduced.

The development of advanced power systems and primary flight control Electromechanical Actuators (EMAs) are the main steps in the realisation of the concept of the All Electric Aircraft.

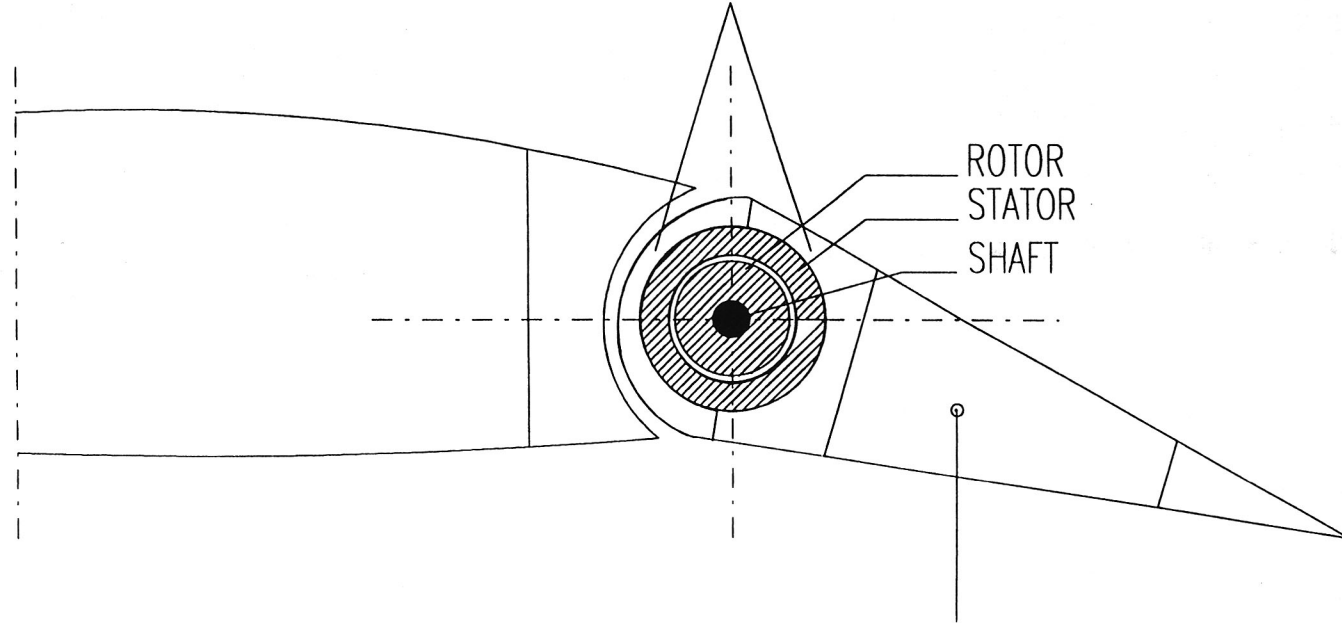
To determine the effect of an advanced power system on aircraft, it is necessary to select a baseline aircraft. Then an advanced power system concept has to be identified that would satisfy all of the requirements of the aircraft. Next an electrically powered flight control systems has to be integrated with the secondary power system. The system weight reductions have to be calculated, and the baseline aircraft will be resized to get full advantage of the weight reductions.

The next steps of this work are to define a baseline aircraft power system and engines. This baseline design has then to be modified by replacing the baseline secondary power system with an advanced electric power generation- and distribution system. The advanced electric system has to be designed to support all the functions previously supplied by the baseline secondary power system.

With all secondary power being furnished by an electric power system, other aircraft systems have to be modified to accept electric power. The flight control system requires the most substantial modifications. The hydraulic flight control actuators, their associated servovalves, and the mechanical cables and pulleys (in case of mechanical control input signals) will be completely eliminated from the baseline design. These components have to be replaced with electromechanical actuators, their associated power receivers, and a fly-by-wire control system. The actuators have to be replaced on a one-for-one basis to keep the same level of redundancy as the original flight control system.

An important criterion in specifying an electric actuation system is the duty cycle to which it must be designed. The mission profile (altitude and velocity vs. time) of an aircraft along with actuator force and rate requirements are the starting points for this research work. From these data, a fundamental duty cycle, load, heat dissipation, and power required are estimated as a function of mission time. This generally leads to a discussion on electric actuation system and power generation system circuits design.

ELECTRO-MECHANICAL ROTARY ACTUATORS
WITH DC BRUSHLESS MOTORS



ACTUATED TRAILING EDGE SURFACE:
ELEVATORS, RUDDERS, AILERONS

Fig. 1.1 THE ILLUSTRATION OF ACTUATION GEOMETRY

The configuration of the Electromechanical Actuator (Figure I.1) will be dependent on the FCS requirements, but generally consists as a minimum of electro-actuators and mechanical drives. According to the numerous advantages of the brushless drive systems (high torque, light weight, low torque ripple, etc.), they are becoming an attractive candidate for EMAs.

In the following sections several different power systems will be considered in order to investigate the main advanced electrical systems for More Electric Aircraft. It will be presented a theoretical investigation of EMAs based on the brushless motor and inverter description: electromechanical architecture, magnet materials, operating principles, electromagnetic processes, etc. In order to design current, position, torque, and speed controllers for brushless motors, the general theory of electromechanical and electromagnetic processes in electrical machines and power converters will be used. Finally, this system look at EMAs investigation will be presented as a preliminary design strategy.

Chapter 1

Aircraft power system analysis and comparison

1.1 Overview of generating systems

The role of electric energy in aircraft is one of ever increasing magnitude and importance. Continuity and stability of electric power now affect every facet of modern aircraft from passenger convenience and comfort to flight safety and mission completion [Ref. 7].

The evolution of aircraft electrical power systems has been driven by the ever increasing demand to make aircraft designs safer and more reliable while increasing the number of functions performed electrically by new and improved subsystems at reduced weight.

The constant speed drives served their purpose and have been the back-bone of aircraft electric power generating systems (Fig. 1.1). Technology, however limits the life of this device to levels inconsistent with the reliability and maintainability demanded of new generation of aircraft.

Today, airframe developers are proposing new electrical power system architecture based on the use

1. High voltage direct current , 270 V (HVDC)
 2. Cycloconverter various speed constant frequency (VSCF), 115/200 Volt, 400 Hz alternating current, (Fig.1.2)
 3. DC-Link Variable Speed Constant Frequency (VSCF), 115/200 Volt, 400 Hz alternating current, (Fig.1.3)
 4. High voltage cycloconverter VSCF alternating current (HVAC), 231/400 V
 5. High frequency alternating current, 20 kHz (HFAC)
- seeking to optimise generating and secondary systems reliability and weight.

Although electrical system components and utilisation equipment comprise only a small part of the overall aircraft weight, the weight issue has become the foremost argument in development of a HVDC (270 volt DC), HVAC, VSCF, HFAC electrical systems.

The preliminary estimation of power system weight for different structures is presented in Table 1.1. The simulation results of power system weight for All Electric Aircraft TU-204 (Table 1.2, 1.3) with HVDC and HVAC show that they will be more attractive also for EMAs implementation, and allow to decrease significantly the system mass. The new design approach to power systems introduces the reliability of solid-state electronics to the largely hydromechanical conventional systems, and EMAs. The cycloconverter VSCF (AC, $f = 400$ Hz) , DC-Link VSCF (AC, $f = 400$ Hz), HVDC systems are compatible with operational avionics systems but are complex also. Let us briefly present the main power system architectures.

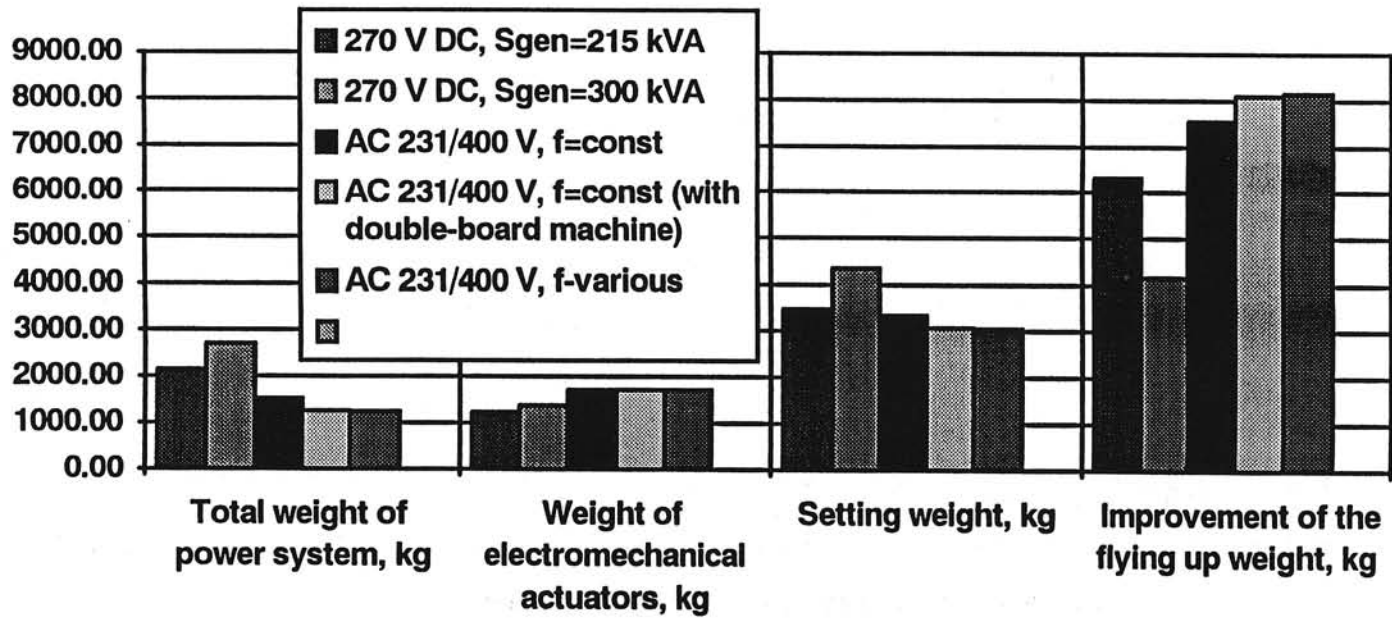
The main types of aircraft power systems

Table 1.1

power system	type of aircraft	power system parameters	
		reached parameters	expected parameters
1. AC power system (with IDG) $f=\text{const}$	Civil and transport subsonic and supersonic ($M \leq 3$) aircraft, military supersonic ($M \leq 6$) aircraft of special destination	* $M = 0,6 \pm 0,8 \text{ kg/kVA}$ $U = 115/200 \text{ V}$ $f = 400 \text{ Hz}$ $S_{\text{gen}} \leq 120 \text{ kVA}$	* $M = 0,4 \pm 0,6 \text{ kg/kVA}$ $U = 200 \pm 400 \text{ V}$ $f = 400 \pm 1000 \text{ Hz}$ $S_{\text{gen}} = 200-300 \text{ kVA}$
2. AC power system with VSCF (converter or DC-link types) $f=\text{const}$	Subsonic and supersonic civil and transport ($M \leq 3$) aircraft, military supersonic ($M \leq 6$) aircraft of special destination	* $M = 0,7 \pm 1,2 \text{ kg/kVA}$ $U = 115/200 \text{ V}$ $f = 400 \text{ Hz}$ $S_{\text{gen}} \leq 100 \text{ kVA}$	* $M = 0,5 \pm 0,7 \text{ kg/kVA}$ $U = 200-400 \text{ V}$ $f = 400-1000 \text{ Hz}$ $S_{\text{gen}} \leq 500 \text{ kVA}$
3. AC power system f -various	Aircraft with turbofan engines $n_{\text{max}}/n_{\text{min}} = 1,2 \pm 1,3$	* $M = 0,5 \pm 0,7 \text{ kg/kVA}$ $U = 115/200 \text{ V}$ $f = 350 \pm 600 \text{ Hz}$	* $M = 0,5 \pm 0,7 \text{ kg/kVA}$ $U = 200 \pm 400 \text{ V}$ $f = 350 \pm 600 \text{ Hz}$
4. Combined (hybrid) AC and DC power system	Civil and transport subsonic aircraft, military supersonic ($M \leq 10$) aircraft of special destination	* $M = 0,6 \pm 1 \text{ kg/kVA}$ $U = 115/200 \text{ V}$ $f = 350 \pm 600 \text{ Hz}$ $U = 28 \text{ V}$ $\sum S = 300 \pm 400 \text{ kVA}$	* $M = 0,4 \pm 0,6 \text{ kg/kVA}$ $U = 200 \pm 400 \text{ V}$ $f = 400 \pm 1000 \text{ Hz}$ $U = 270 \text{ V}$ $\sum S = 500 \pm 600 \text{ kVA}$
5. High voltage DC power system (HVDC)	civil and military aircraft (realisation of all electric aircraft conception)	—	* $M = 0,45 \pm 0,65 \text{ kg/kVA}$ $U = 270 \text{ V}$ (except distribution system) $S_{\text{gen}} \approx 500 \text{ kVA}$
6. High-frequency (20 kHz) AC power system: -on the base of a resonance inverter; -on the base of an inductor generator with a rowing active zone	aircraft of special destination	— —	 $U = 200 \pm 600 \text{ V}$ $f = 20 \text{ kHz}$ $S_{\text{gen}} = 500 \text{ kVA}$ $U = 200 \pm 600 \text{ V}$ $f \approx 20 \text{ kHz}$ $S_{\text{gen}} = 500 \text{ kVA}$

Table 1.2

Weight of power systems and their equipment for All Electric Aircraft TU-204



1.1.1 Constant speed drive

Conventional systems used in aircraft to generate (AC, $f=400$ Hz) electrical power have used the design approach presented in Figure 1.1. The engine output is coupled through a gearbox to a mechanical/hydraulic constant speed drive (CSD). Variations in engine speed (typically a 2:1 range) are reduced at the constant speed drive output, thus the generator input speed is maintained at a constant value. A synchronous generator is used to maintain constant frequency output. Generator output voltage amplitude is controlled by a generator control unit, which also controls the aircraft bus tie contactor.

More advanced CSD designs incorporate the generator and constant speed drive into one package. These integrated drive generator (IDGs) systems have the advantage of a lower weight as compared to discrete CSD systems.

1.1.2. Cycloconverter various speed constant frequency (VSCF) power system

One approach to VSCF systems is shown in Figure 1.2. A cycloconverter system eliminates the constant speed mechanical/hydraulic drive and couples the engine gearbox directly to the cycloconverter generator. With variations in engine speed, the frequency of the generator output frequency of 400 Hz by means of an electronic converter. The converter uses solid-state switches to select the proper input generator phase at each instant in time to synthesise a constant 400 Hz output. To date, the electronic switches used in cycloconverters have been silicon controlled rectifiers (SCR), which limit the steady state operating oil temperature of the cycloconverter system to approximately 80°C [Ref.18].

1.1.3. DC-link various speed constant frequency (VSCF) power system

Another approach to VSCF systems is the DC-link concept shown in Figure 1.3. With the availability of high voltage, high power transistors, DC-link Variable Speed Constant Frequency (VSCF) electrical systems have become practical for aircraft generating systems. The basic difference between the DC-link approach and the cycloconverter is the type of electronic switch used in the converter and the type of input to the converter. In the case of the cycloconverter, the input is a multi phase, varying frequency waveform. The DC-link system, as the name implies, uses a DC voltage as the converter input. The electronic switch in the cycloconverter is a SCR, while transistors are used in DC-link systems as the switching elements.

Since the DC-link system uses DC voltage as an input, the electronic switching array and the switching control scheme can generally be simplified compared to a cycloconverter. The number of switches in the converter can be reduced since most cycloconverters (in VSCF cycloconverter system for the F-18 aircraft, use a six phase input which requires a minimum of thirty-six switching elements [Ref. 35]). The DC-link converter requires a minimum of six active switching devices and six commutating diodes. A higher temperature cooling oil can also be used in DC-link systems (120°C), since transistors are used instead of SCR.

Either cycloconverter or DC-link approach has specific advantages over the constant speed drive now in general use. By replacing the mechanical/ hydraulic CSD with a solid-state power converter, the reliability of the generating system is improved. Also,

Table 1.3

Weight of power systems and their equipment for All Electric Aircraft TU-204 (with turbofan engines)

Power system	Power system with cooling, kg	Switching equipment, kg	Power distribution network, kg	Auxiliary power unit, kg	Protection automatic equipment, kg	Total weight of power system, kg	Electro-mechanical actuators, kg	General setting weight, kg	Improvement and changing of the flying up weight, kg
270 V dc, S _{gen} =215 kVA S _{gen} =300 kVA	233	103,8	190	37,1	117,2	2146,5	1237,8	3489,1	6313,7
	325	135,8	249	97,1	123,2	2704	1381,5	4343,5	4166
AC 231/400 V f=const (with AC-AC converter)	175,5	70,5	213,5	15	72	1526,1	1714,4	3338,6	7552,8
AC 231/400 V f=const (with double-board machine)	118,8	70,5	213,5	15	72	1256,1	1714,4	3077,9	8101,4
AC 231/400 V f=various	109,5	80,5	213,5	15	72	1242,1	1714,4	3054,4	8150,4

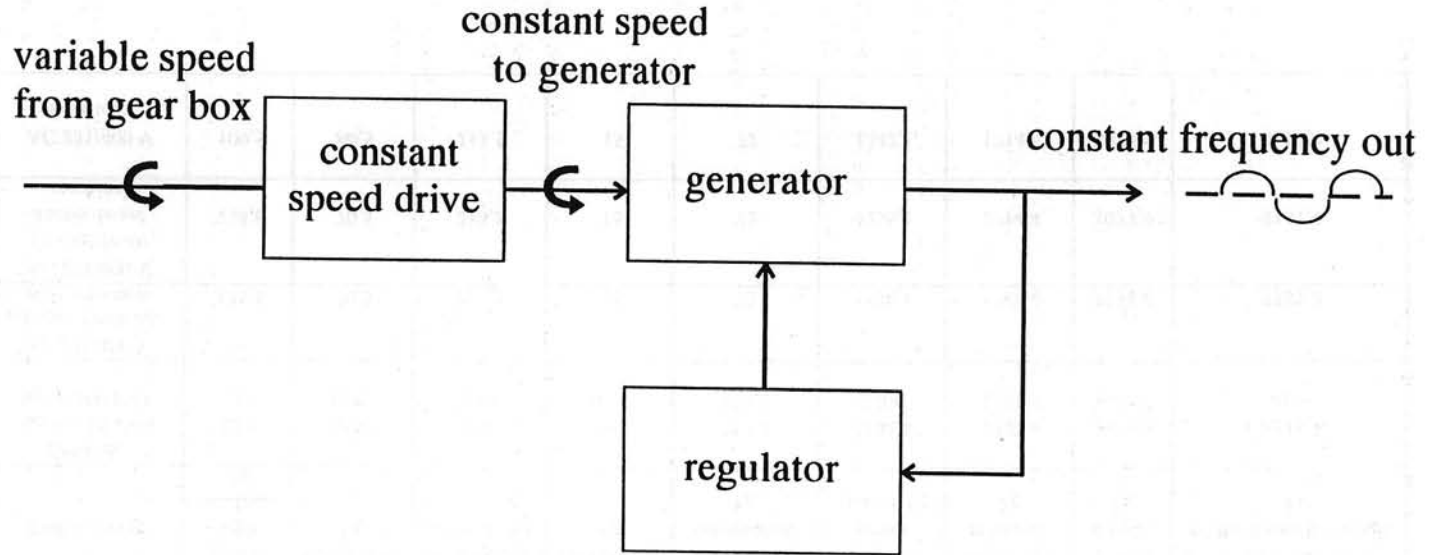


Fig. 1.1 CONSTANT SPEED DRIVE SYSTEM

since the DC-link VSCF system output frequency is crystal controlled, the output frequency variations inherent with CSD drivers are eliminated.

1.1.4. High voltage direct current (270 V) power system

The choice of an electric power system for aircraft applications must be based on total airframe impact. Rapid advance in semiconductor technology makes possible the direct utilisation of the high speed engine mounted generator output directly as high voltage (270 V) DC power (analog to the DC-link VSCF power system), especially for the implementation of EMAs [Ref.37]. This approach greatly reduces the generator system complexity and should result in the lowest cost and weight. Selection of a HVDC power system offers the following advantages

1. High efficiency-- only generator-rectifier losses are effective in the conversion from engine shaft power to electric bus distribution power. No constant speed driver (CSD), AC filter components or other converter losses.
2. High reliability--only the generator shaft and bearings are subject to mechanical wear and the elimination of the CSD or other complex power conditioner greatly enhances reliability.
3. Light weight--high speed light weight machine designs can be used. For larger loads and the main power distribution feeders, the wire weight savings will be about 25-30% in comparison with AC, 115 V, 400 Hz, 3-phase [Ref. 44].
4. Power Continuity--proliferation of volatile memory in avionics systems requires uninterruptable power. DC system concepts offer the greatest versatility in power continuity.
5. Safety--presents a lesser shock hazard to personnel than AC, 115 V, 400 Hz, etc.

1.2 Advanced power system

When evaluating a power system for an all-electric aircraft, the effect on other systems and the overall effect on the aircraft must also be considered. This includes such factors as *the types of controllers required for control surface actuators, the size and weight of the circuit breakers, and the system failure modes.*

The substantial gain is provided by a high-frequency AC distribution system based on a bi-directional resonant power converter. Let us consider this type of power system as candidate for advanced all electrical aircraft.

1.2.1 Basis of 20 kHz AC power system

The primary technology used in the high-frequency AC power distribution system is resonant power conversion. Preliminary converters of this type have been built and tested for space applications[Ref. 18].

Although there are many topological variations of the resonant converter, let us highlight their common features.

First, the switches in a resonant converter create a square-wave AC waveform from the DC source. Inductors and capacitors then remove the unwanted harmonic components from this square wave. As the difference in frequency between the fundamental component and the lowest third harmonic of the square wave is so small, we can use

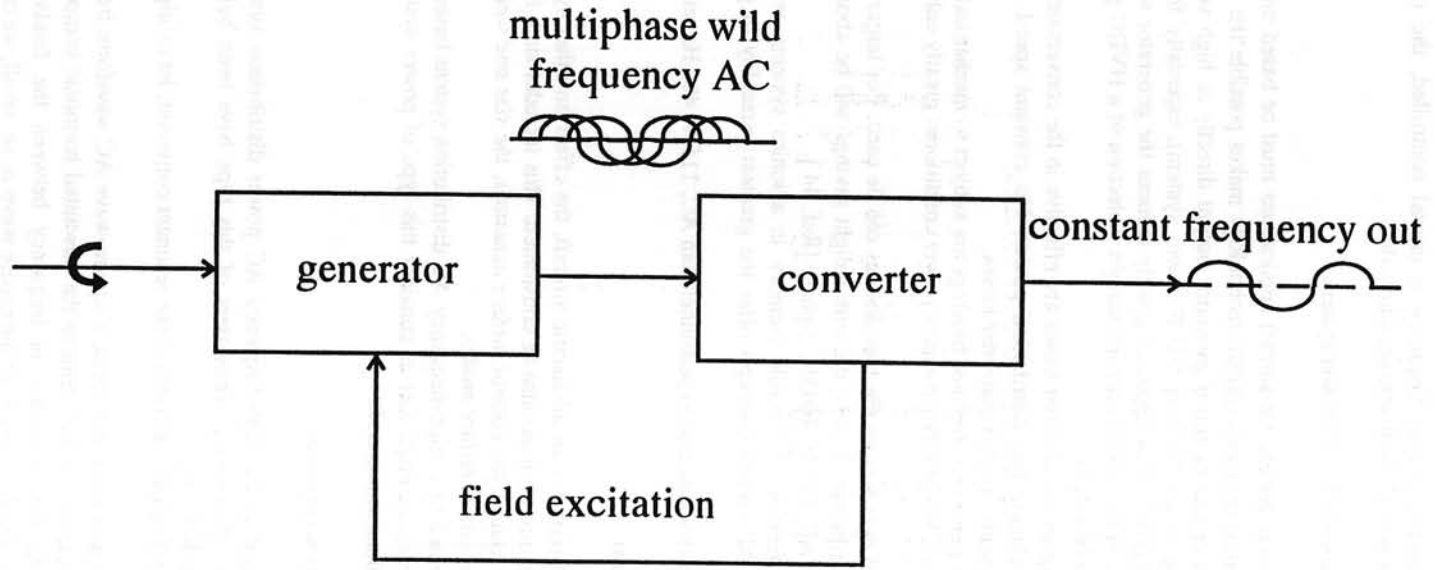


Fig. 1.2 CYCLOCONVERTER VSCF SYSTEM (VARIOUS SPEED CONSTANT FREQUENCY)

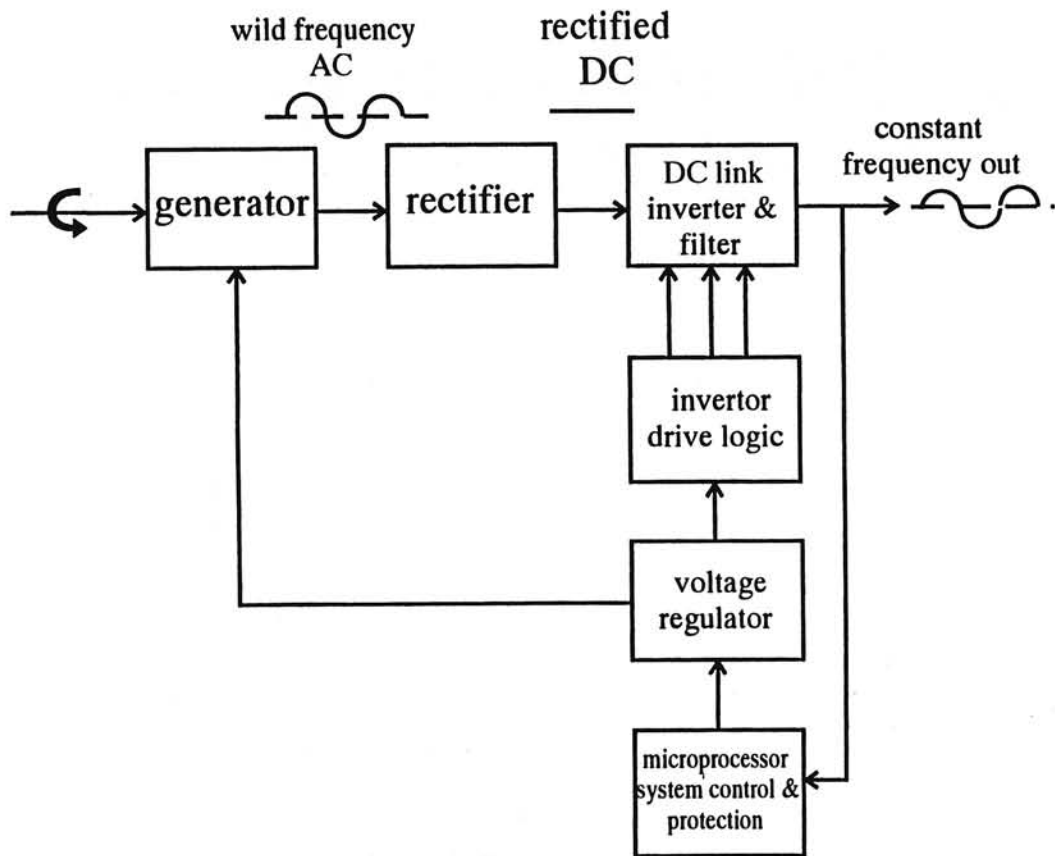


Fig. 1.3 DC LINK VSCF GENERATING SYSTEM

a resonant LC circuit tuned to approximately the switching frequency, rather than a simple low-pass filter, to remove harmonics from the fundamental. Hence is the name resonant converter.

Second, because the network composed of the resonant filter and the external AC system has a reactive impedance at all but its resonant frequency, the switches in a resonant converter must be able to transfer energy in both directions. Thus we can also use a resonant converter designed for average power flow from the DC system to the AC system to transfer energy in the other direction should the application require it.

Third, the resonant converter's semiconductor devices can have significantly lower switching losses than those of the semiconductor devices in a high-frequency DC/DC or DC/AC converter.

Finally, there are two approaches to design the resonant converter - one complementing the other. In the first, the switches create a square wave of voltage that is applied to a series resonant circuit. This is called a series resonant converter. In the second, the switches create a square wave of current that is applied to a parallel resonant circuit, resulting in the parallel resonant converter. In each of its topological states, a resonant converter is generally a second-order system [Ref. 22].

Additionally, in many topologies of resonant converters the switch currents oscillate and would reverse direction if the switch could carry bidirectional current. These circuits are especially well suited to the use of SCRs, as they can be turned off by the resonant action of the circuit trying to force the current to become negative.

To simplify the discussion, we assume that the converter is designed to deliver AC power to a resistive load. If the load is reactive, we can use its reactive elements as a part of the resonant filter.

The series resonant (SR) inverter is a DC-to-AC conversion device. The main advantage of the SR converter over other types is the natural commutation of the switching devices when the resonant tank is driven below its natural resonant frequency. This greatly simplifies the use of thyristors as switching devices. Also, it improves the operating efficiency, because turn-off losses (which can be quite significant at high frequency) are virtually zero. A typical bipolar switching transistor can turn on faster than it can turn off, so the requirements of the SR converter match the capabilities of a bipolar transistor more closely than do those of other converters. At high operating frequencies, the leakage inductance of the converter transformer becomes significant to the operation of most switching converters. Usually the energy stored in the leakage inductance at the switch turn-off time must be dissipated in the switch protection network. In the SR converter the leakage inductance appears in series with the desired tank inductance and is therefore not a factor in the switching losses. Because of the importance of switching losses at high frequency, SR converters can be built for higher frequency operation than other types. The SR converter also offers lower electromagnetic interference (EMI) and lower capacitive coupling between the input and output sides.

In the basic concept of the resonant power converter (Fig. 1.5) switches 1 and 2 are alternately switched in such a way as to present the series inductor-capacitor (LC) circuit with square-wave voltage. The LC circuitry, performing the function of a low-pass filter, allows only the fundamental (sinusoidal) current to flow in the series circuit. The load is placed across the capacitor and thus provides a low-impedance sinusoidal voltage source. Since the current in the inductor is sinusoidal, the switch can be opened as the current passes through zero. Zero-cross switching yields an advantage that cannot be

overemphasized: the absence of energy loss during power switch turn off is a major advantage of resonant power conversion [Ref. 18]. Not only will silicon-controlled

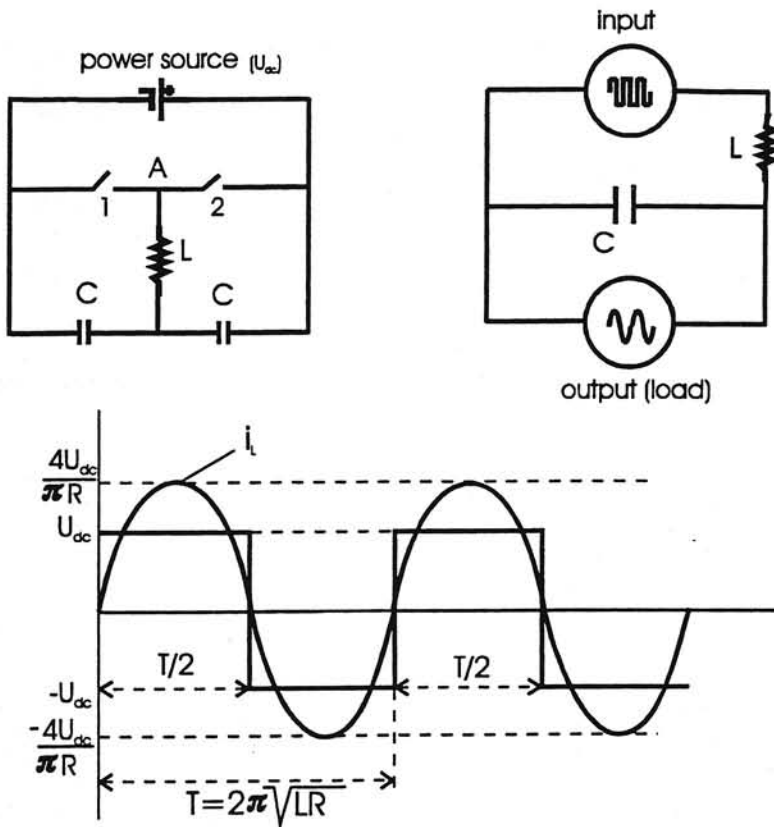


Fig. 1.5 Basic topology of the resonant converter for 20 kHz AC power system

rectifier (SCR) switches self-commutate, but also there is no frequency-proportional converter power loss at turn off. As a result power devices may be safely and efficiently operated at power and frequency levels unobtainable by other conversion techniques.

Lower frequency waveforms can be synthesized from this high-frequency carrier as required to satisfy load requirements. A basic circuitry connection to allow this is shown in Figure 1.6. In this circuit, switch pairs 1-1' and 2-2' operated in such a manner as to perform synchronous rectification of the 20-kHz source and thus synthesize a lower frequency output. In this respect the circuit operates as a conventional cycloconverter. Proper sequencing of the switch pairs will also allow reverse power flow by chopping a lower frequency (including DC) into 20 - kHz source.

The inherent symmetry of the high-frequency inversion system is presented by the bi-directional implementation in Figure 1.7. In this configuration port A can act as a source,

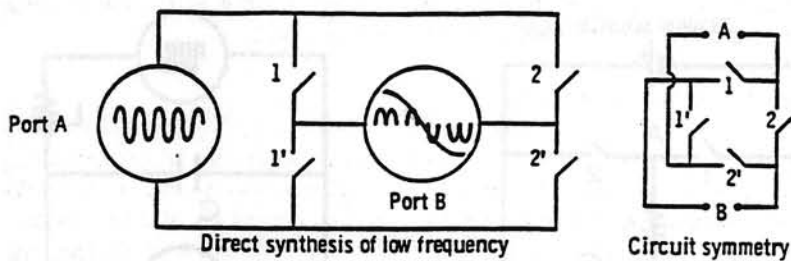


Fig. 1.6 Basic circuitry for waveform synthesis in 20 kHz power system

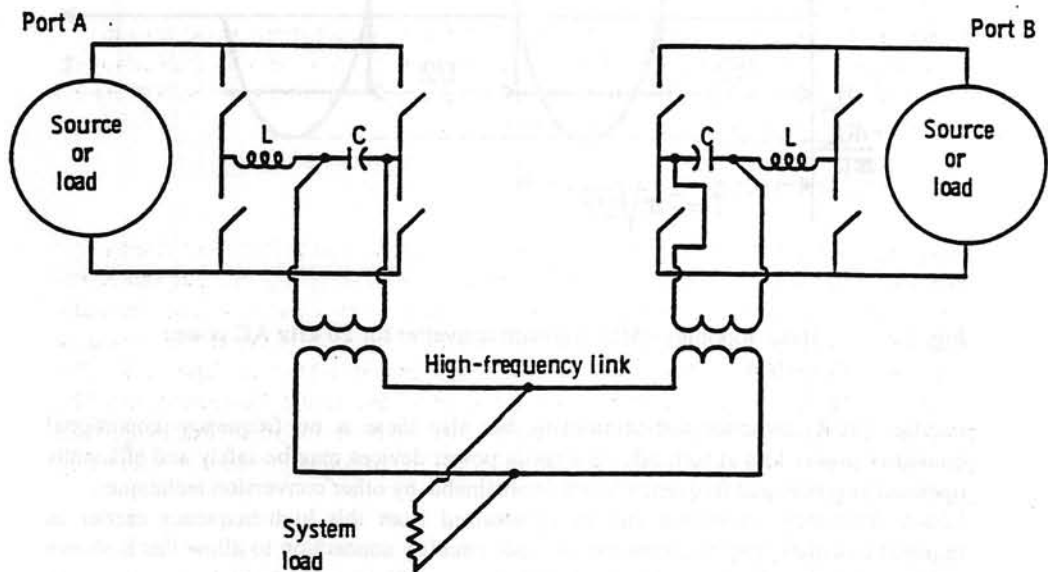


Fig. 1.7 Bi-directional high-frequency power interface in 20 kHz AC system

and port B as a load, or vice versa. Also both ports can act as sources with other loads connected across the high-frequency link. The circuitry illustrated in Fig.1.6 is for a DC or single-phase AC sources, but it can be expanded for multiphase sources. This configuration illustrates the interface between multiple power sources, power generation and storage, and power sources and system loads [Ref. 20].

1.2.2 Rationality for system selection

The proposed electric distribution system is a single-phase, sinusoidal alternating-current, 440 V, 20 kHz power system. This particular configuration is selected for the following reasons and numerous advantages of the high-frequency power distribution system:

- a high operating frequency minimizes the weight of magnetic devices such as transformers
- the fundamental operating frequency, and in particular the power frequency, are above the audio range, and this will provide a quiet power system
- the energy available per cycle is inversely proportional to the operating frequency, and this minimizes the damage occurring during electrical faults
- the low energy content (a 400-Hz power system would have 50 times more available energy per cycle than an equivalent 20-kHz system) improves personnel safety over conventional power systems
- a high-frequency power system allows to synthesize lower frequency waveforms with minimum of distortion
- lower distortion waveforms result in more efficient operation of electrical devices
- waveform synthesis allows the load and power sources to be tailored with relatively simple circuitry, which in turn easily implements such concepts as variable speed control of brushless motors for actuation systems

1.2.3 System description

Using resonant power conversion as the core technology, an aircraft power system (for CESSNA CITATION II) would be configured in a following way: the outputs of the starter-generators (two three-phase, 24 000 rpm, 1200 Hz induction machines mounted on the accessory gearbox of each engine) are fed to three-phase bi-directional, resonant converters. Each phase of these converters has configuration shown in Figure 1.7. The outputs of the three phases are connected in series and tied to the distribution bus. The loads are fed from the main distribution bus through isolators and controllers to protect the bus from load faults. The amount of power conditioning varies considerably depending on the load.

1.2.4 System operation

Under typical conditions the induction generators provide 1200-Hz, three phase power to the resonant converters. The frequency of the converter is controlled by its resonant circuit and is therefore independent of the input frequency. The result is a constant-frequency 20 kHz, constant level of voltage, single-phase output to the distribution bus. In most instances 20 kHz AC power cannot be used directly by the loads. Load receivers

(AC-DC, AC-AC converters) are used to synthesize the output required by the load. Even though the bus is a single phase, motors can be driven from power receiver by using an AC-AC converter or AC-DC converter and inverter. Basically, in first case the power flow from the main distribution bus can be managed in half-cycle increments by the AC-AC converter. The pulses would generate a sinusoidal energy pattern by using the proper switching sequence. To maintain a constant voltage-to-frequency ratio into the motor, the pulse pattern can be varied by inserting blank spaces into the pattern. It can be done by leaving all AC-AC switches off for one half-cycle. For variable brushless motor loads the voltage and frequency can be varied to satisfy the load requirements all the way from DC for holding actuator motors in a fixed position to approximately 1000 Hz for providing fast slew rates. Higher frequencies can be obtained by selecting other pulse patterns. The overall management of the power system should be accomplished through a digital data and control system. The second approach for driving scheme of a brushless motor is presented in a Chapter "Brushless motors".

Chapter 2

BRUSHLESS MOTORS

The servomotor is an important component of the electromechanical actuator. Servomotor and motion-control technologies are based on mechatronics engineering (which is the combination or fusion of electronics and mechanical engineering and is interdisciplinary). The application of brushless motors became attractive due to several factors: reduction of the price of powerful transistors, creation and establishment of the technique of current control of PWM (pulse width modulator) inverters, development of varieties of highly precise and accurate detectors, and the manufacture of these components in a compact form. In this way, brushless motors combined the strong structure of AC motors and delicacy of dc motors. Additionally, they are completely free from the output power reduction due to commutator and from complex maintenance. Thanks to recent remarkable progress in power electronics and microelectronics, more advanced servomotor and motion control is now available. In particular, digital signal processors (DSP), although developed for application in the field of communications, will be used as controllers and sensor signal processors owing to their fast computational capability and suitable architecture.

Brushless servomotors can be classified (Figure 2.1) as alternating current (AC) machines: induction synchronous motor, induction reluctance motor, brushless motor (synchronous motor), and vector-control motors.

The optimal capacity ranges for each motor type such as the mechanism of torque generation, operational efficiency, cooling, control devices, control technique, ease of manufacture, profitability are different. Brushless (synchronous) motors (Fig. 2.2) are becoming more attractive (see Table 2.1) for powerful applications (5 - 100 kW). The general technical parameters of the brushless (synchronous) motors are presented in Appendix 1.

The components necessary for the control of the brushless motor are: a main frame, sensors for angle, angular velocity, current, voltage, magnetic flux, and temperature, and a semiconductor power converter (power amplifier), including various analog or digital ICs for triggering control (Fig. 2.3). In addition to these, a small motor-driven gear (resolver) having a position and speed sensor is also mounted on the motor shaft. A digital controller (DSP) should be included too. The whole system and hardware are shown in Figures 2.3, 2.4, 2.5. In the signal generation part, motor voltage, current, flux, and frequency should be controlled so as to obtain accurate and fast torque response. Motion control (position, speed, and force control) should be also obtained in the control part (Figure 2.5).

Usually brushless motors are supplied in one of three ways by the manufacturer:

- A complete motor and electronics package

Table 2.1

ADVANTAGES OF BRUSHLESS DRIVE SYSTEMS

Characteristics	Description
<u>More Power per Dimension</u> <ul style="list-style-type: none"> • Small size $T_M / V [Nm/dm^3]$ • Light weight $T_M / M [Nm/kg]$ • High dynamics $T_M / J [s^{-2}]$ 	<ul style="list-style-type: none"> • due to an extremely high torque/volume ratio, provides better packaging and uses less valuable space • due to a high torque/ weight ratio, provides easier installation and may improve machine performance and load capacity • due to the high torque/inertia ratio, higher acceleration provides faster response and reduced cycle time
<u>High torque</u>	<ul style="list-style-type: none"> • over a wide speed range due to absence of mechanical commutator, high acceleration is available throughout the speed range
<u>High load capacity</u>	<ul style="list-style-type: none"> • heat generation is confined to the stator, thus ensuring direct heat dissipation to the outside and larger thermal time constant, higher peak torques are available for longer times, external cooling to increase machine performance is very effective
<u>Direct temperature monitoring</u>	<ul style="list-style-type: none"> • of the stator windings and use of a controller heatsink provide full protection of motor and controller against thermal overload (ntc-thermistor)
<u>Low torque ripple</u>	<ul style="list-style-type: none"> • improves operating smoothness especially at a low speed
<u>No maintenance</u>	<ul style="list-style-type: none"> • no regular maintenance required. There are no brushes to wear out or commutators to maintain. Bearings and optional shaft seal can be replaced, if it is necessary
<u>Easy installation</u>	<ul style="list-style-type: none"> • due to modular principle of the controller packaging and power supply with minimum interconnections
<u>System expansion and service</u>	<ul style="list-style-type: none"> • of control electronics easily achievable due to multi-level modularity.

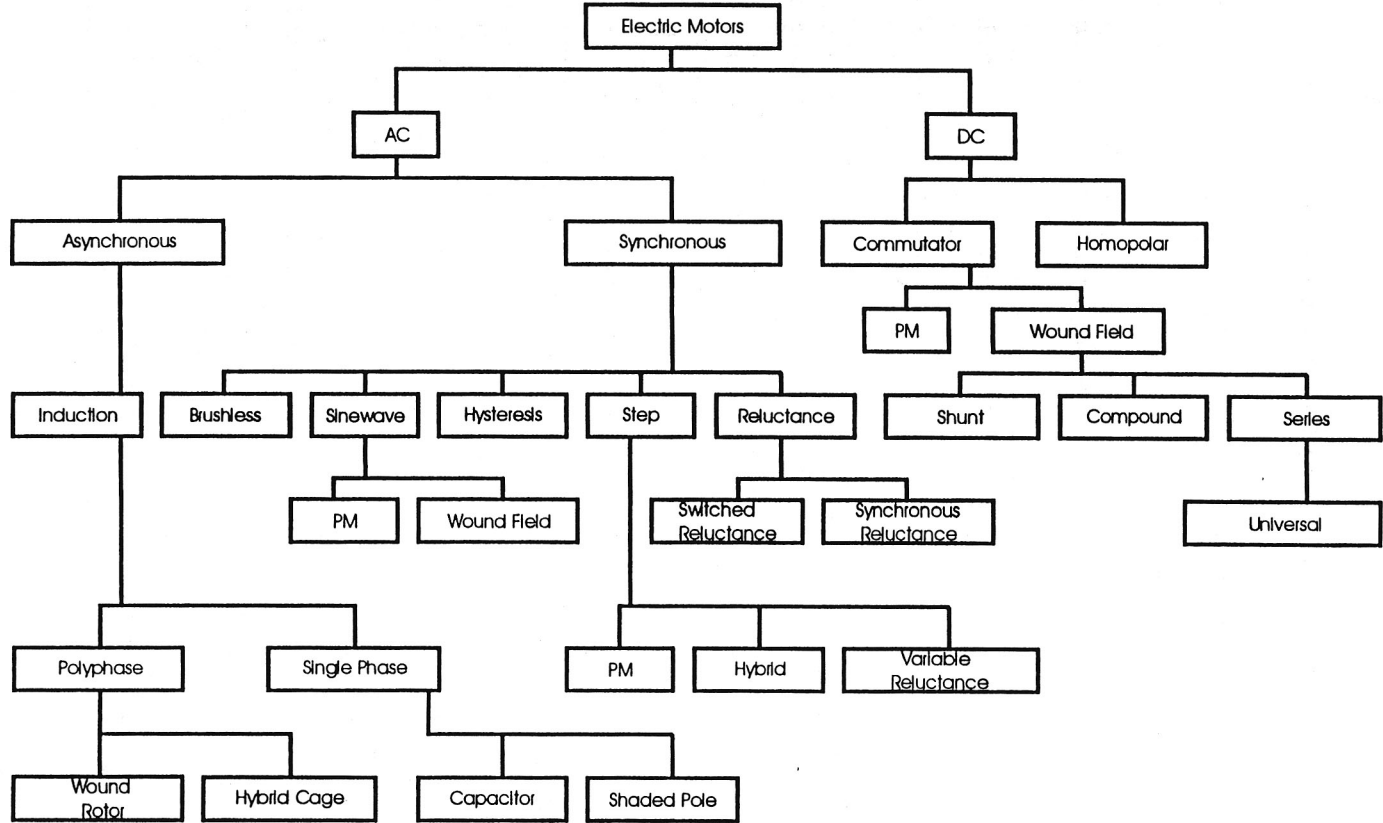


Fig. 2.1 A classification of electric motors

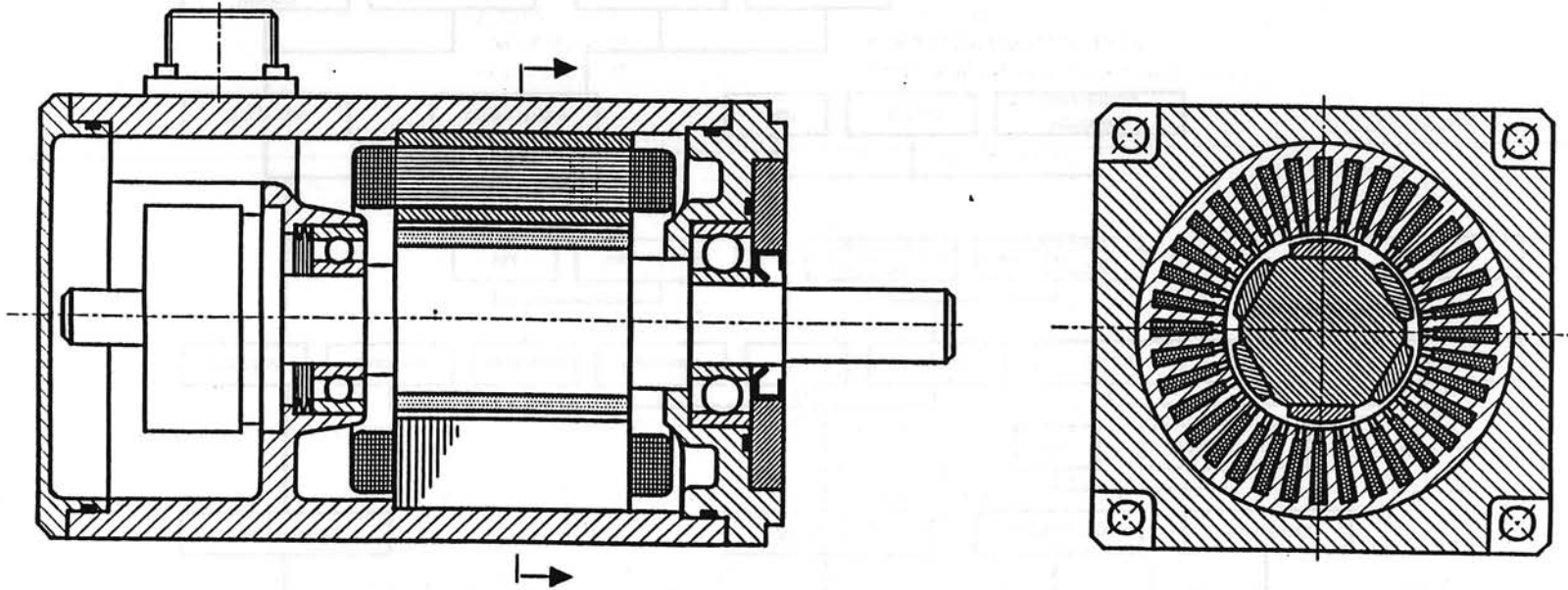


Fig. 2.2 Schematic design of the brushless motor with rotor position transducer

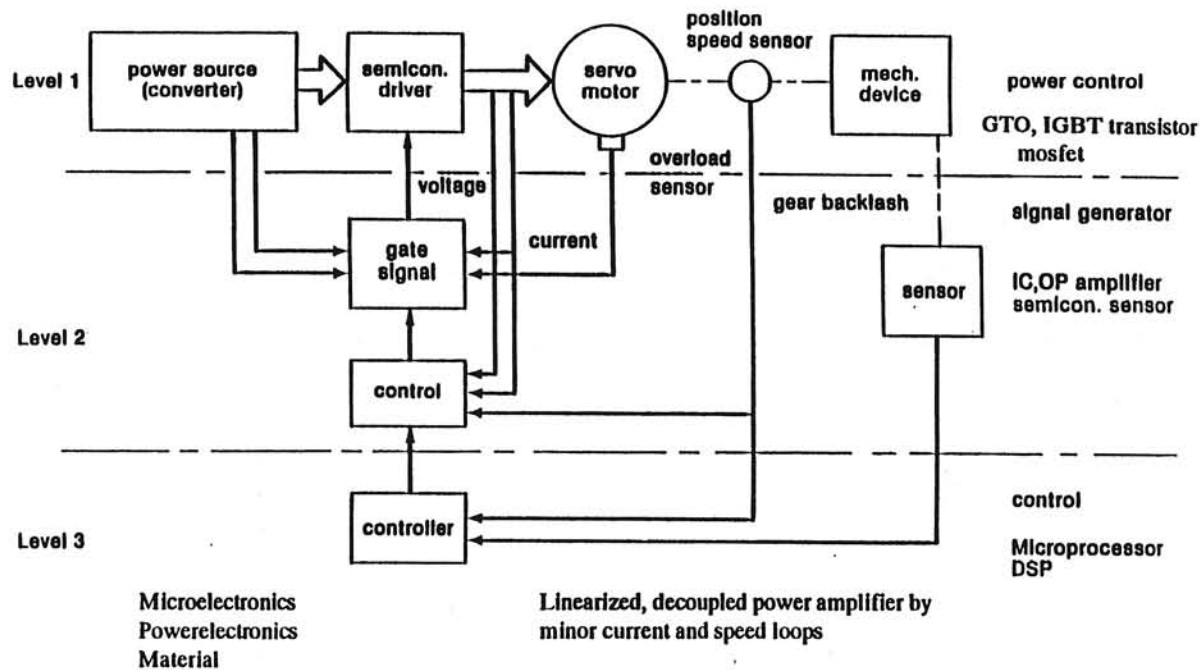


Fig. 2.3 Hardware for the servomotor (brushless motor) control system

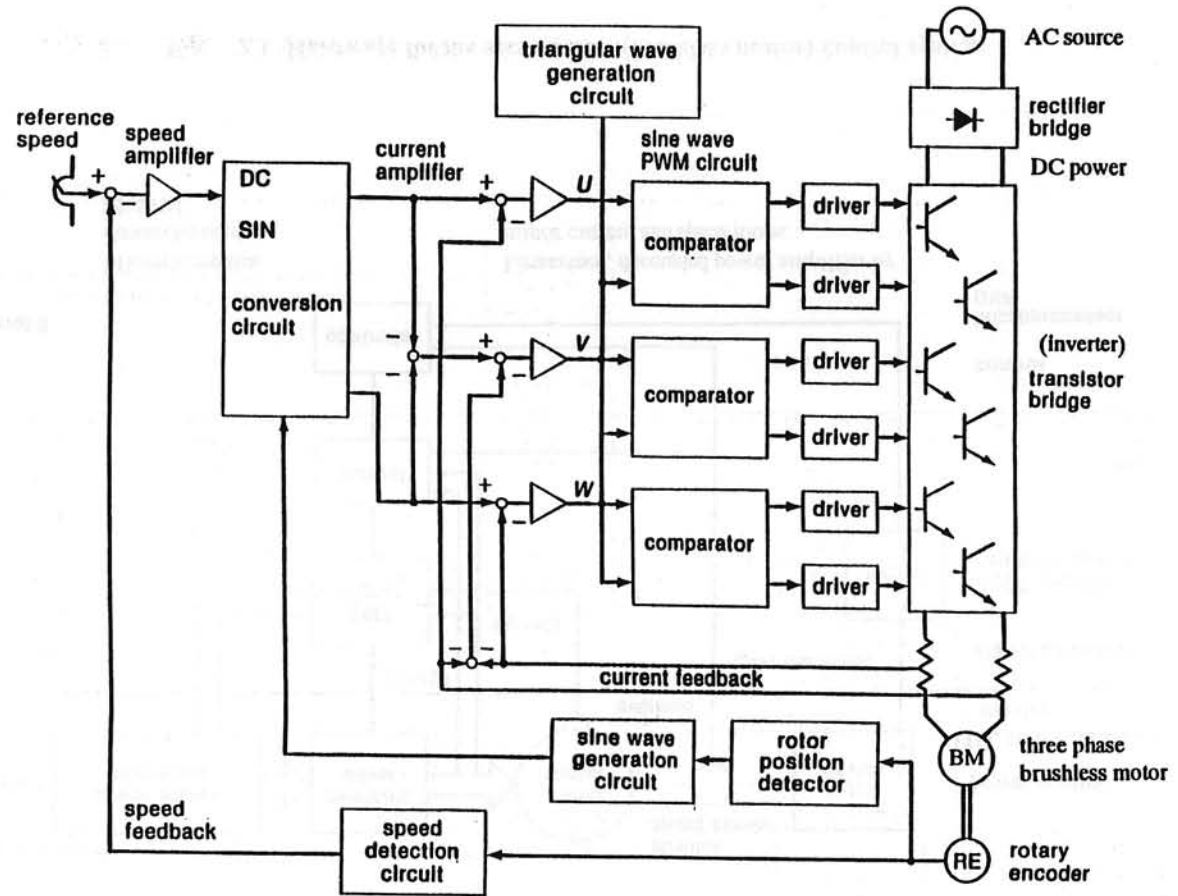


Fig. 2.4 Block diagram of the system of brushless motor

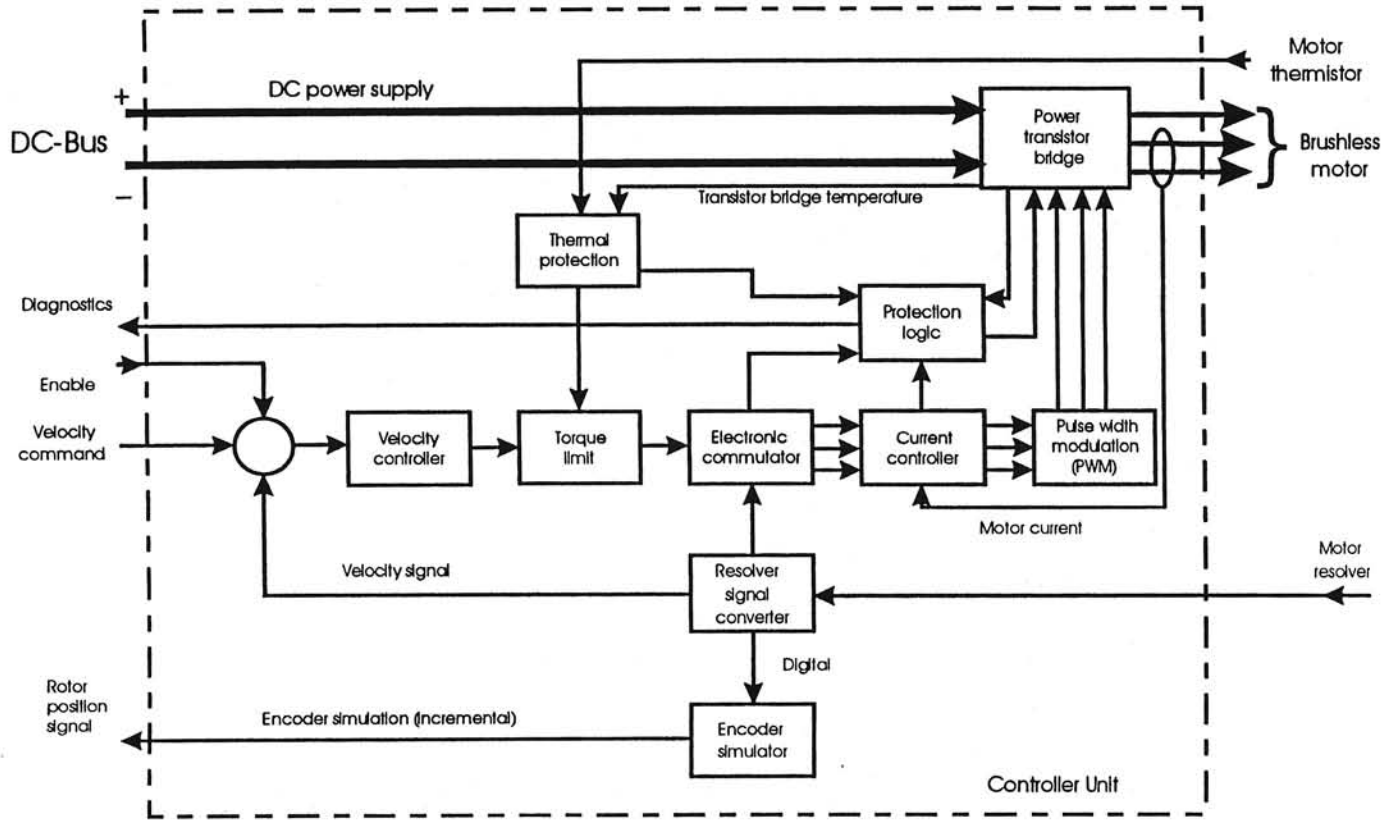


Fig. 2.5 Operating principle of a controller unit for brushless motor

- Brushless motor with sensing systems. This option is very frequently made available for further designing drive system
- Motor without electronic drive or sensing system. This option is mostly supplied to manufactures of electronic control systems

The driving system needs to be designed and applied as a single body to make the best use of the features of the semiconductor power inverter, the detectors, and the main frame of the motor. these components should be designed to support performance of electromechanical actuator. In other words, the control system has to be designed as a single unit of which the objective is the control of a high-performance motor for the aircraft electromechanical actuation system application. In evaluating a servomotor driving system, the control performance and speed ratio are stressed, along with the speed of the motor, the applicable torque range, and acceleration performance. The deciding factors in control performance and the speed ratio are the power rate and the accuracy of detectors both in the motor's main frame and in the power inverter.

Detectors need to be able to detect rotational position for position control and to detect speed for response rate and/or speed control. The speed signal is calculated from the position (encoder) signal in most applications of digital control. A resolver or an encoder is used for the purpose. However, if the necessary resolution cannot be obtained by a position sensor, then a brushless tachogenerator must be used.

The main circuit of a brushless motor is equipped with semiconductor devices (transistors or thyristors) capable of self switching off and high-speed switching. Two types of transistor are extensively used in power switching circuits, namely the bipolar junction transistor (BJTs) and the power metal oxide semiconductor field effect transistor (MOSFETs) [Ref. 46]. The BJTs consists of a pnp or npn single-crystal silicon structure. It operates by the injection and collection of minority carriers, both electrons and holes, and is therefore termed a bipolar transistor. Bipolar transistors are connected by means of Darlington connection and packed together with diodes. The MOSFETs depends on the voltage control of a depletion width and is a majority carrier device. It is therefore a unipolar transistor. Unlike the BJTs, MOSFETs do not exhibit minority carrier storage delays, and their switching times are ultra fast. The high off-state and low on-state voltage characteristics of the bipolar junction transistor are combined with the high input impedance properties of the MOSFETs to form the insulated gate bipolar transistor (IGBTs). The IGBT is suitable for numerous applications in power electronics, especially in Pulse Width Modulated servo and three-phase drives requiring high dynamic range control and low noise. IGBTs are equally suitable in resonant converter circuits [Ref. 1]. Gate turn-off thyristors (GTOs) are more suitable for use with high voltage and large current than are bipolar transistors. In addition, GTOs permit high current density. In spite of these advantages, with GTOs one must have longer gate trigger circuits and snubbers to perform protection co-ordination. GTOs therefore applied in the region of 300-400 kVA or above, where transistors cannot be employed [Ref. 14 , 46]. The main characteristics of modern semiconductor devices are presented in Appendix 2.

Let us briefly present the main circuit and trigger control circuit of the brushless motor.

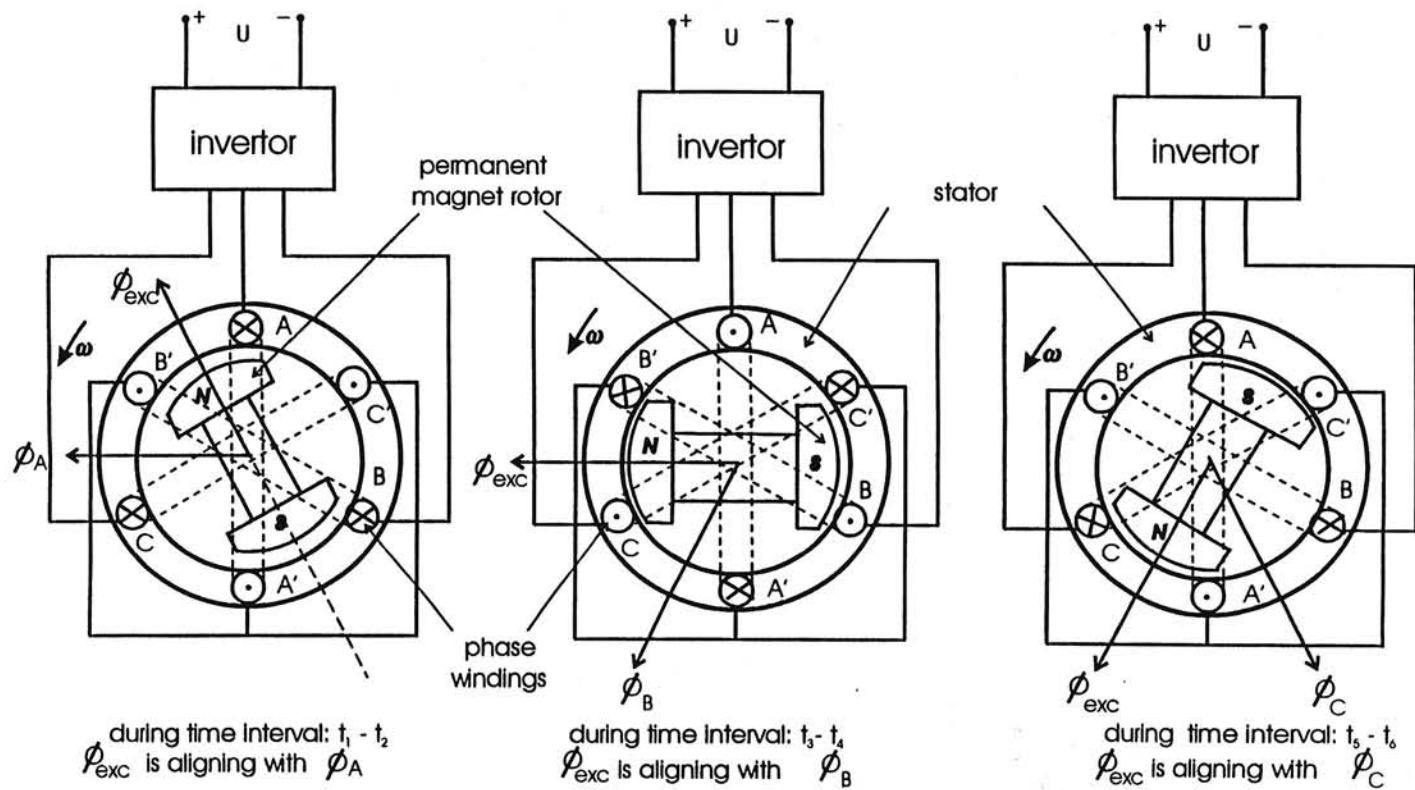


Fig 2.6a Basic scheme of the brushless DC motor with permanent magnets

2.1 Main circuit configuration

As shown in Figure 2.6a, 2.6b, the main circuit of BM (3 phases, wye connection) comprises converter transforming the alternating current into the direct current, inverter (source of AC power for motor stator windings) having six power switches (transistors or thyristors) with six associated reactive feedback diodes, and motor [Ref. 11,45,]. Figure 2.6a is a cross-sectional view of three-phase brushless motor, with A^+ , A^- , B^+ , B^- , C^+ , C^- indicating the beginning or the end of the coil of each phase. When a motor is energised by three-phase alternating current, during time interval $t_1 - t_2$ (or 60 electrical degrees), the magnetic flux is induced by the current in winding A as shown in Fig.2.6a. If there is an exciting magnetic flux at right angles, torque is generated to rotate the rotor counter-clockwise owing to the magneto-motive force, etc. It follows from the above that a continuously rotating field can be obtained by making three-phase currents flow in the stator coil. If the sine wave phase and the rotor position can be made to be always at right angle, it becomes possible to obtain a highly efficient motor with smooth torque using electronic switching devices (transistors or thyristors). The rotational direction may be reversed by rearranging of switching ON-OFF sequence of the electronic switches in inverter. Three-phase inverter bridge is operated in 180° or 120° conduction mode.

180° conduction mode Figure 2.7 shows voltage-fed inverter bridge quasi-square output waveforms for a 180° switch conduction pattern. Each switch conducts for 180° , such that no two switches across the voltage rail conduct simultaneously. Six patterns exist for one out put cycle and the rate of sequencing these patterns specifies the bridge output frequency. The conducting switches during the six distinct intervals are shown and can be summarised as follows

Interval (electrical deg)	Conducting switches
$0--\pi/3$	$T_1 T_2 T_3$
$\pi/3--2\pi/3$	$T_2 T_3 T_4$
$2\pi/3--\pi$	$T_3 T_4 T_5$
$\pi--4\pi/3$	$T_4 T_5 T_6$
$4\pi/3--5\pi/3$	$T_5 T_6 T_1$
$5\pi/3--2\pi$	$T_6 T_1 T_2$
$2\pi--7\pi/3$	$T_1 T_2 T_3$

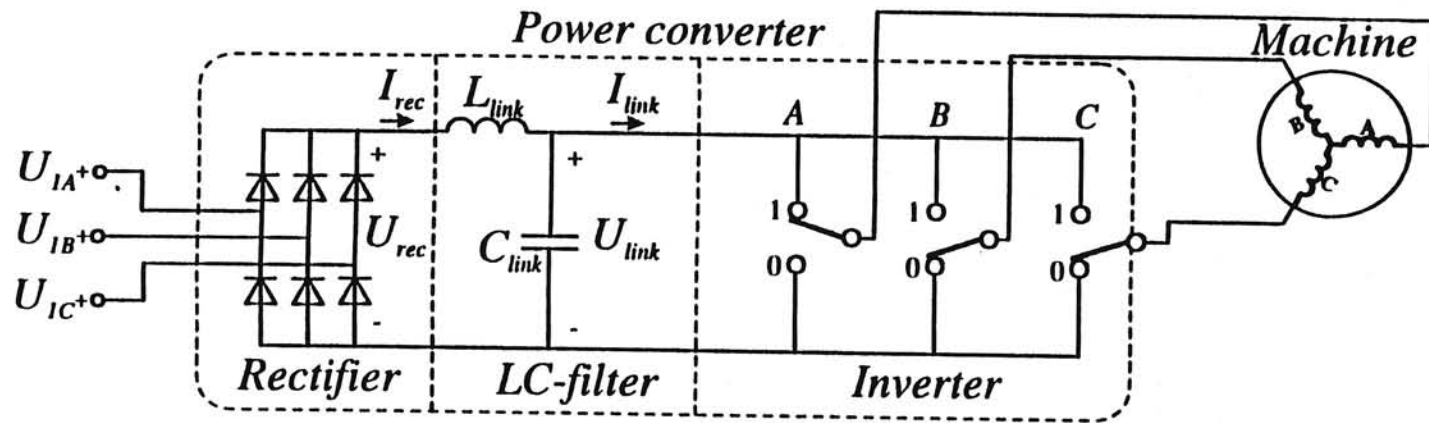


Fig. 2.6b MAIN ELECTRICAL CIRCUIT OF BRUSHLESS MOTOR

(power supply: AC, 3-phase, $f=400$ Hz)

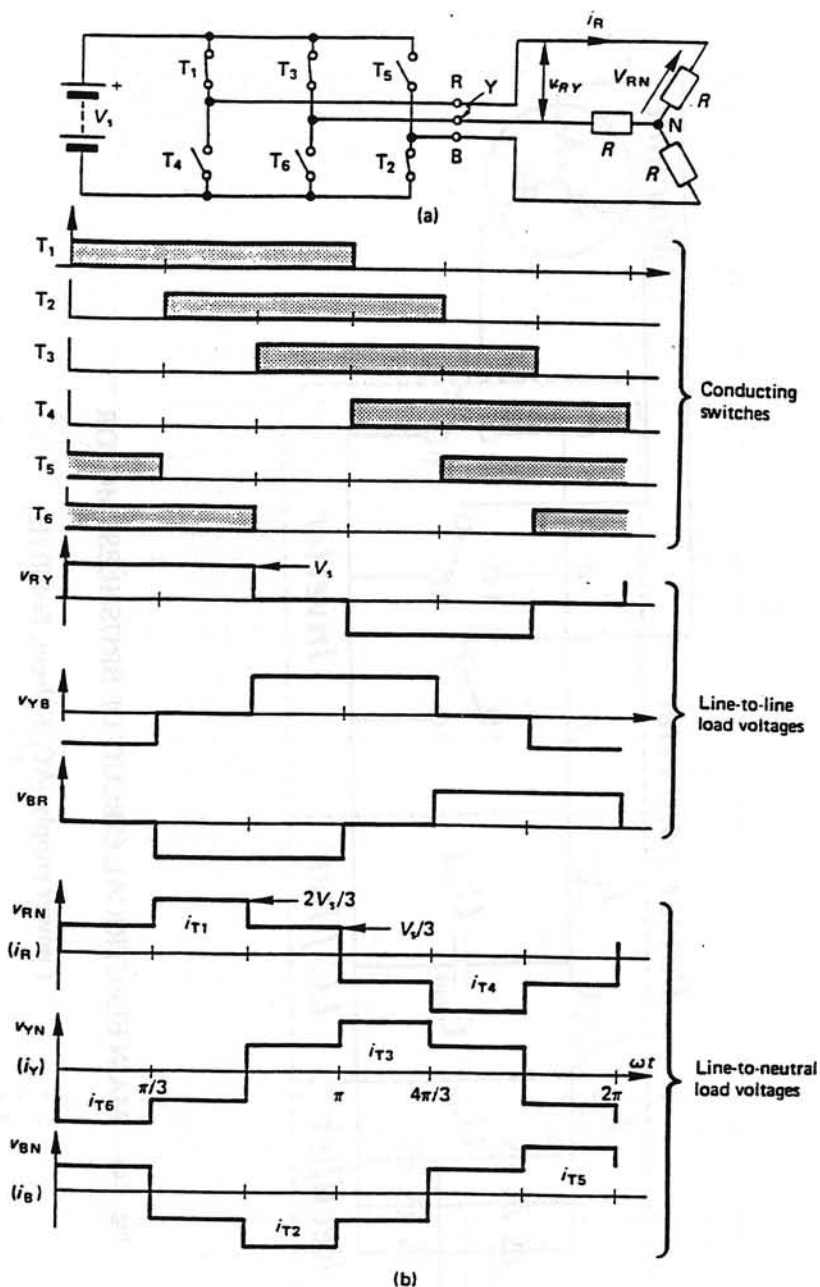


Fig. 2.7 A three-phase bridge inverter employing 180° switch conduction with a star (Y) connected load
 (a) the bridge circuit with conducting T_1, T_2, T_3 switches;
 (b) circuit voltage and current waveforms

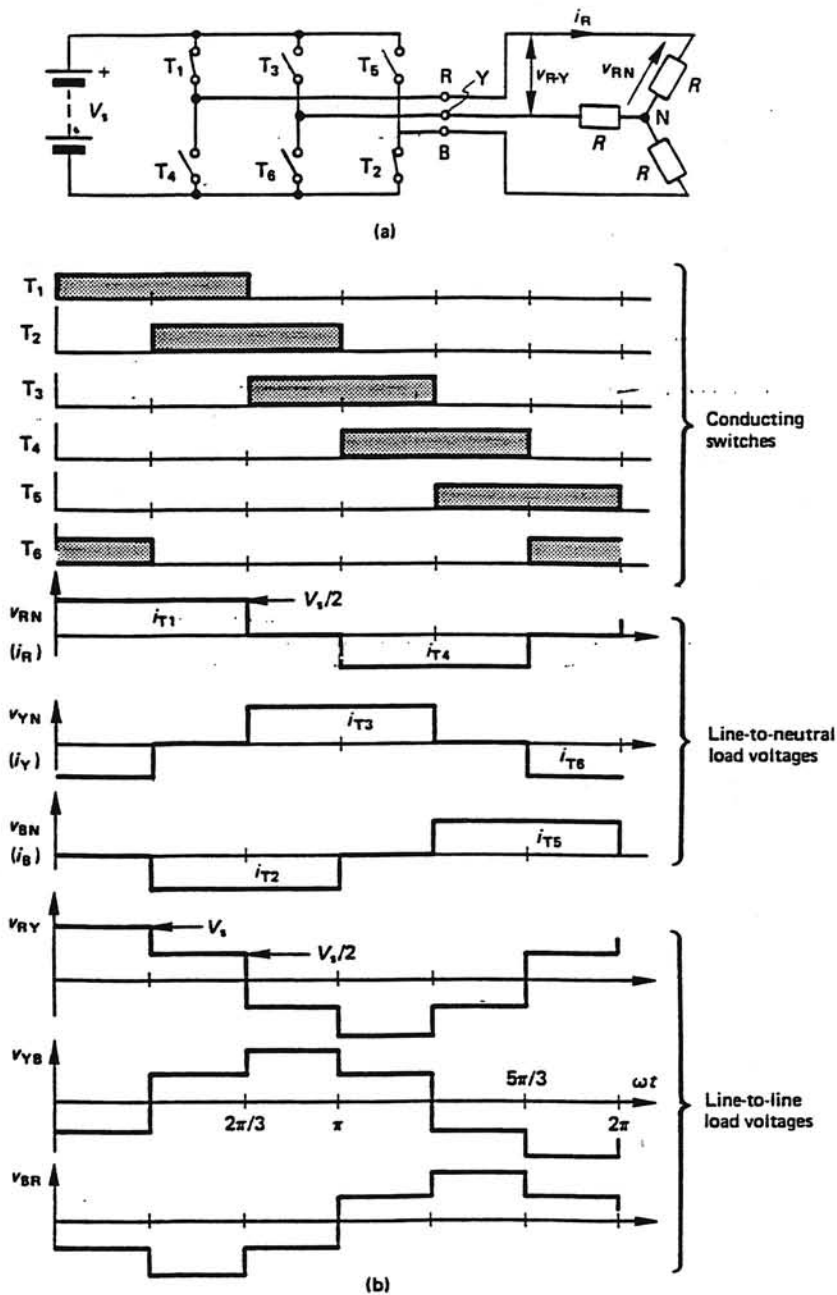


Fig. 2.8 A three-phase bridge inverter employing 120° switch conduction with a star (Y) connected load
 (a) the bridge circuit with conducting T_1, T_2 switches;
 (b) circuit voltage and current waveforms

The three output voltage waveforms can be derived by analysing a resistive star load and considering each of the six connection patterns. The line-to-neutral voltage is defined by

$$\begin{aligned}
 U_{RN} &= 2/\pi U_s [\sin \omega t + 1/5 \sin 5\omega t + 1/7 \sin 7\omega t + 1/11 \sin 11\omega t + \dots] \\
 U_{BN} &= 2/\pi U_s [\sin (\omega t + 2\pi/3) + 1/5 \sin 5(\omega t + 2\pi/3) + \\
 &\quad 1/7 \sin 7(\omega t + 2\pi/3) + 1/11 \sin 11(\omega t + 2\pi/3) + \dots] \quad (2.1) \\
 U_{YN} &= 2/\pi U_s [\sin (\omega t - 2\pi/3) + 1/5 \sin 5(\omega t - 2\pi/3) + \\
 &\quad 1/7 \sin 7(\omega t - 2\pi/3) + 1/11 \sin 11(\omega t - 2\pi/3) + \dots]
 \end{aligned}$$

The line-to-line voltage ($\alpha = \pi/3$) is defined

$$\begin{aligned}
 U_{RY} &= 2\sqrt{3}/\pi U_s [\sin \omega t - 1/5 \sin 5\omega t - 1/7 \sin 7\omega t - 1/11 \sin 11\omega t - \dots] \\
 U_{YB} &= 2\sqrt{3}/\pi U_s [\sin (\omega t + 2\pi/3) - 1/5 \sin 5(\omega t + 2\pi/3) - \\
 &\quad 1/7 \sin 7(\omega t + 2\pi/3) - 1/11 \sin 11(\omega t + 2\pi/3) - \dots] \quad (2.2) \\
 U_{BR} &= 2\sqrt{3}/\pi U_s [\sin (\omega t - 2\pi/3) - 1/5 \sin 5(\omega t - 2\pi/3) - \\
 &\quad 1/7 \sin 7(\omega t - 2\pi/3) - 1/11 \sin 11(\omega t - 2\pi/3) - \dots]
 \end{aligned}$$

Figure 2.7b shows that U_{RY} is shifted $\pi/6$ with respect to U_{RN} , hence to obtain the three line voltages while maintaining a U_{RN} reference, ωt should be substituted with $\omega t + \pi/6$, $\omega t - \pi/2$, and $\omega t - 5\pi/6$, respectively.

Since the interface voltages consist of two square waves displaced by $2\pi/3$, no triplen harmonics (3,6,9,...) exist. The output comprise harmonics given by the series $n = 6r \pm 1$ where $r \geq 0$ and is an integer. The n -th harmonic has a magnitude of $1/n$ relative to the fundamental.

By examination of the interphase output voltages in Figure 2.7 it can be established that the mean half-cycle voltage is $2U_s/3$ and an rms value of $\sqrt{(2/3)} U_s$, namely $0.8166 U_s$. From equation (2.2) the rms value of the fundamental is $\sqrt{6} U_s/\pi$, namely $0.78 U_s$, that is $3/\pi$ the total rms voltage value.

120° conduction mode

The basic three-phase inverter bridge in Figure 2.8 can be controlled with each switch conducting for 120°. As a result, at any instant only two switches conduct and the resultant quasi-square output voltage waveforms are shown in Figure 2.8. A 60° dead time exists between two series switches conducting, thereby providing a safety margin against simultaneous conduction of the two series devices across the DC supply rail. This safety margin is obtained at the expense of a lower semiconductor device utilisation than

with 180° device conduction. The device conduction pattern can be summarised as follows.

Interval (electrical deg)	Conducting switches
0-- $\pi/3$	T ₁ T ₂
$\pi/3$ -- $2\pi/3$	T ₂ T ₃
$2\pi/3$ -- π	T ₃ T ₄
π -- $4\pi/3$	T ₄ T ₅
$4\pi/3$ -- $5\pi/3$	T ₅ T ₆
$5\pi/3$ -- 2π	T ₆ T ₁
2π -- $7\pi/3$	T ₁ T ₂

Figure 2.7b for 180° conduction and 2.8b for 120° conduction show that the line to neutral voltage of one conduction pattern is proportional to the line to line voltage of the other.

$$U_{RN} (120^\circ) = 1/2 U_{RY} (180^\circ) = \sqrt{3}/\pi U_S [\sin \omega t - 1/5 \sin 5\omega t - 1/7 \sin 7\omega t - 1/11 \sin 11\omega t - \dots] \quad (2.3)$$

$$U_{RY} (120^\circ) = 3/2 U_{RN} (180^\circ) = 3/\pi U_S [\sin \omega t + 1/5 \sin 5\omega t + 1/7 \sin 7\omega t + 1/11 \sin 11\omega t + \dots] \quad (2.4)$$

Also $U_{RY} = \sqrt{3}U_{RN}$ and the phase relationship between these line and phase voltages, of $\pi/6$, has not been retained. That is, with respect to Figure 2.8b, substitute ωt with $\omega t + \pi/6$ in equation (2.3) and $\omega t + \pi/3$ in equation (2.4).

2.2 The inverter

The voltage source inverter can be considered ideally as three 2-way switches that can switch between two levels; the + (state 1) and - (state 0) DC-link terminals. The switches drive the three terminals of a 3-phase brushless motor. The three 2-way switches with each 2 possible states result in a total of $2^3 = 8$ distinct switch states (Figure 2.9) [Ref. 4 , 46]

$$S_{SW} \in [000, 100, 110, 010, 011, 001, 101, 111] \quad (2.5)$$

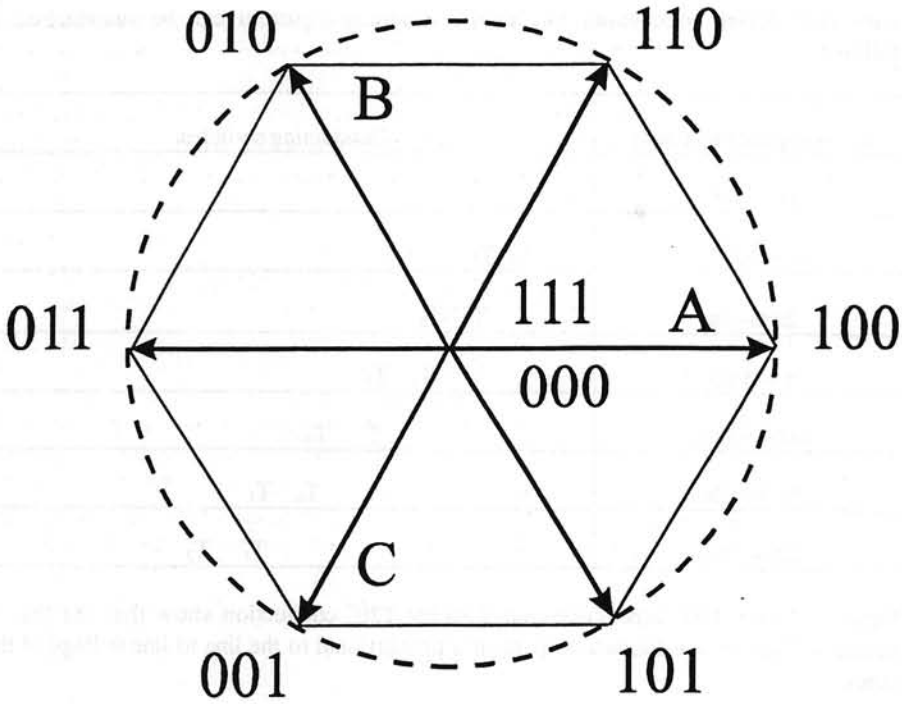


Fig. 2.9 Inverter switching mode as a 2-D representation of switch states

The set of states in (2.5) is divided into two subsets, an active subset and a short-circuit subset or zero-voltage subset

$$S_{SW}|_{\text{active}} \in [100, 110, 010, 011, 001, 101] \quad (2.6)$$

$$S_{SW}|_{\text{zero}} \in [000, 111] \quad (2.7)$$

2.3 Sine wave PWM circuit

The aim of brushless motor is to make sine wave currents flow in the motor, so it is ideal for BM to have the output of the current amplifier of the sine waves applied directly to the motor after amplifying the power. However, amplification of the sine waves is not practical, because that means using a power transistor in the proportional region. This makes it difficult to solve the problem of high temperature due to power loss.

Consequently, the power loss is reduced by switching the power transistor. This method is called PWM (pulse width modulation). In this method, the current of a motor is converted into a controlled pulse or width proportional to the amplitude of the sine wave so that it may become a sine wave on the average. Figure 2.10, shows the principles of

the method. A triangular carrier wave oscillating with constant frequency and amplitude, and the sine wave output from the current amplifier are compared by a comparator. As shown in the Figure 2.10, pulses of unequal widths are output by extracting the portions where the values of the sine wave exceed those of the carrier wave. The duty ratio of the pulse width is increased or decreased, centring around 50%, by the sine wave and modulated to make a sine wave on the average, because the inverter output is 0 V when the duty ratio is 50%.

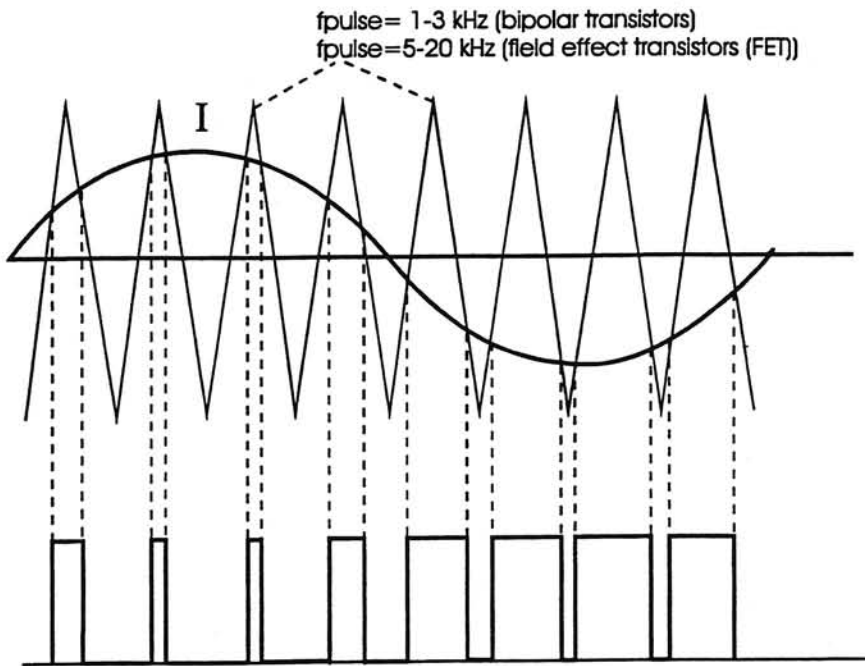


Fig. 2.10 Principle of sine wave PWM

It is important to decide the method of selecting the oscillating frequency of the chopping wave. As the carrier frequency equals the switching loss proportionally as it is made higher, and it reduces the speed of response of the servomotor as it is made lower. Furthermore, ripples appear more frequently, and the torque change and the core losses are increased [Ref.12, 14, 16, 18].

Generally speaking, a carrier frequency of 1-3 kHz, is selected when the inverter consists of bipolar transistors; 5-20 kHz is selected when the inverter is consists of FETs. The current ripples developed at these levels of frequency make the iron core of the motor vibrate and this generates unpleasant noises when the frequency is within audio range. To resolve this problem, the carrier frequency is made 16 kHz, or more by using FETs.

2.4 Power supplies for brushless motors

An important aspect of the presentation brushless motors is that their application in continuous duty variable speed electromechanical actuators calls for static inverters of adequate power, generating three-phase voltages of variable amplitude and frequency. This is necessary in order to maintain at all speeds a low rotor frequency, which is a precondition for acceptable overall efficiency of the drive. As presented earlier, inverters of this type are available today employing thyristors including gate turn-off thyristors (GTO) or switched power transistors (IGBT). The basic lay-out of a variable speed AC drive (brushless) motors is shown in Fig. 2.6b; it consists of an brushless motor, static converter, which generates a variable voltage, variable frequency AC system and the associated control equipment. The increased complexity of the converter is caused by the fact that thyristor inverters with forced commutation involve additional components and a more complicated mode of operation. Similar arguments apply to the control structure which is also much more complex than for a DC motor. The reason for this is that the AC (brushless) motor with its simple mechanical construction represents a very complex non-linear multivariable control plant. In contrast to the DC motor which has a more complicated mechanical design but a simple control structure, the brushless motor must be fed with alternating currents of variable amplitude, frequency and phase.

It is for these reasons that no standard solution for the control of brushless motors has emerged as in the case of the DC brush motor.

There is a large variety of solutions for the inverter- and control-problems, designed personally for special applications and operating conditions.

Let us briefly present a few basic converter schemes for brushless motors.

2.4.1. Pulse-width modulated (PWM) transistor inverter operating at high switching frequency

A switched transistor inverter for the power supply of three phase brushless motor in the lower power range ($< 40 \text{ kW}$) for servo drives with on-off current control is shown in Figure 2.11 [Ref. 23]. With the choice of suitable transistors having a switching time in the order of $1 \mu\text{sec}$ the mean switching frequency may be above 15 kHz , i.e. beyond the audible range in order to avoid objectionable interference by a audio noise [Ref.14]. This has an additional advantage that the inverter then exhibits a large band width for control. If the intermediate direct voltage U_D is of sufficient magnitude (270 V for aircraft with EMAs), fast current control loops may be designed which keep the stator currents in close agreement with the alternating reference values. This effectively results in current sources for the stator windings of the motor, thus eliminating the influence of the stator voltage equation of brushless motor on the dynamics of the drive [Ref. 27, 28]; as a consequence, considerable simplification of the control plant is achieved because the stator voltage interactions are now dealt with by the current controllers. The controllers could either employ a pulse width modulator or they could be of the simple on-off type as shown in Figure 2.11, having a small hysteresis band 2Δ which creates a lower limit for the time interval between two subsequent switching operations; at the same time the tolerance band is helpful in avoiding interference between the three current control loops since, because of the isolated neutral of the stator winding, one of the three controllers is

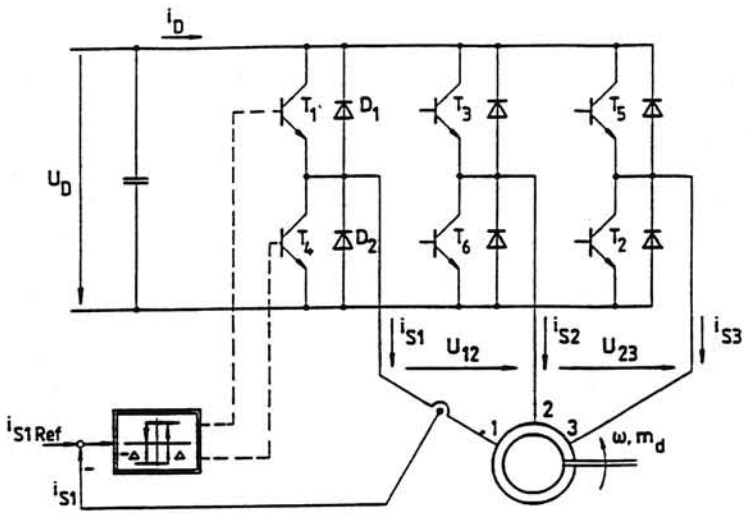


Fig. 2.11 Switched transistor inverter for brushless motor with on-off current control

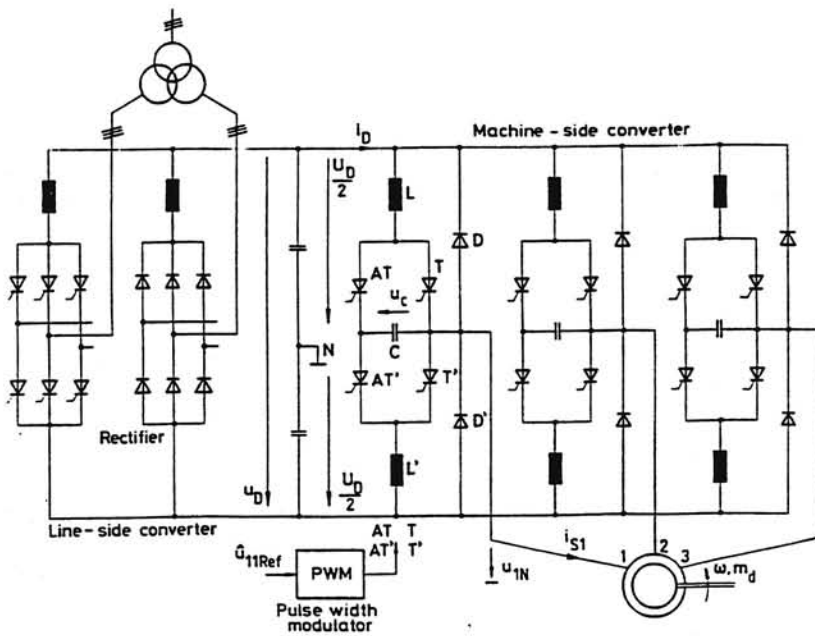


Fig. 2.12 Thyristor converter with constant intermediate direct voltage

redundant but is retained for reasons of symmetry. The line-to-line voltages have three-level waveform, assuming the values $-U_D$, 0 , $+U_D$. In order to produce a preferred switching frequency, a triangular clock signal may be added at the summing points of the controllers. Another possibility consists in synchronising the on-off controller, i.e. allowing a switching operation to occur only at equidistant sampling instants $t = \nu T_0$ defined by a fixed clock frequency $f_0 = 1 / T_0$. If synchronised on-off controllers are employed, the hysteresis band Δ can be omitted because it will be a minimum interval T_0 between subsequent switching operations. When a very low ripple content of the currents is specified, the use of a pulse-width modulator in combination with a linear current controller is preferable to on-off current control. The audible noise is of course more pronounced with PWM control but the current waveform is much more acceptable. The assumption of virtual current sources for the stator windings is, of course, only valid as long as the ceiling voltage of the inverter is not approached. In the case of using a free-running on-off controller, the frequency of the current reference is gradually increased. Due to the inductive load impedance the peak value of the fundamental component of voltage rises with frequency according to

$$\hat{U}_1 = \sqrt{R^2 + (\omega L)^2} \hat{I}_1$$

This results in a rising control error between the sinusoidal reference and the piecewise exponential feedback signal and must be taken into account when designing the drive control system [Ref. 25, 43].

As an alternative to the bipolar transistors shown in Fig. 2.11, field effect transistors for relatively high power rating (500 V, 20 A) are becoming available. They may be regarded as a solid state equivalent of the vacuum tube, combining extremely low steady state control current ($< \text{nA}$) with high switching speed ($< 1 \mu\text{sec}$), thus allowing higher switching frequencies ($> 25 \text{ kHz}$) far beyond the audible range. The control circuit may be greatly simplified for example by using optical devices as isolating signal transmitters to the transistors operating at high potential. A disadvantage of field effect transistors is the large voltage drop in on-state, causing higher conduction losses, and the relatively large gate capacitance.

2.4.2 Pulse-width modulated thyristor converter with constant direct voltage supply (voltage source inverter)

The use of transistors is presently restricted to relatively lower power applications (EMAs) even though experimental drivers at higher power have been developed. With thyristors the power of semiconductor converters extends into the MW-region. The circuit that resembles the transistor inverter in Fig. 2.12 (AC power system source -- 115/208 V, 3 phase, 400 Hz) supply most closely is the thyristor converter with constant direct voltage supply as shown in Fig. 2.11. Because of the low AC impedance of the DC link it is also called a voltage-source inverter. Instead of the line-side converter, DC power system source (270 V) could be used for feeding the inverter. Since normal thyristors cannot be blocked by gate signals, additional components comprising auxiliary thyristors are required for the forced commutation of the machine-side inverter. Hence, natural commutation of the machine-side converter is not possible

[Ref. 26, 27]. The machine-side converter depicted in Fig. 2.12 is an example of a large variety of different circuits; it is considerably simplified, showing only the main components. Instead of a pair of transistors as in Fig. 2.11, each contains a force-commutated thyristor switch, comprising two main thyristors T, T' , with antiparallel diodes D, D' , two auxiliary thyristors AT, AT' , a commutation capacitor C and two air cored inductors L, L' . Briefly, a commutating process takes place as follows: the main thyristor T initially carries the load current i_{s1} and the commutating capacitor C is positively charged, $U_C > 0$; then firing of the auxiliary thyristor AT causes T to be blocked almost instantaneously so that the load current flows temporarily through AT and C thus recharging the capacitor. At the same time a resonant circuit is created consisting of L, AT, C and the diode D ; when about a half period of the oscillation is concluded and the current through AT tends to reverse its sign, AT is also blocked, which leaves the capacitor with opposite voltage, ready for the next commutating transient when T' has to be extinguished. The load current is now flowing through D' . If the current pulse through the resonant circuit is of sufficient magnitude as compared to the load current, the commutation is almost independent of the load so that the voltage U_{IN} can be approximated by a square wave $\pm U_D / 2$ with short but continuous commutating transients. A detailed analysis of converter circuits, taking all these effects into account, should be best performed by digital simulation. Hence the accurate analysis of the commutating transients is of major concern to the circuit designer. Special types of thyristors with short recovery time ($< 20 \mu\text{sec}$) are usually specified for pulse-width modulated inverters, which limits the power rating. Also, the occurrence of unacceptable load currents must be prevented by fast control action.

The firing instants for the main- and auxiliary thyristors are determined by voltage and/or current controllers. In view of the limited switching frequency, which is usually below 1 kHz for thyristor inverters of higher power rating, the load currents can no longer be considered to be sinusoidal as was possible with the transistor inverter operating at a higher switching frequency. Hence PWM-thyristor inverters of the type shown in Fig.2.12 are naturally suited to act as low impedance voltage sources, presenting to the load pulse-width modulated rectangular voltages, the fundamental components of which are prescribed by voltage command signals. Because of the large superimposed harmonics, caused by the chosen switching strategy, closed loop control of fundamental voltages having variable frequency is not practical. Therefore open loop voltage control through a pulse-width modulator is the standard solution while the current loops are normally closed on the next higher level of drive control.

2.4.3 Thyristor converter with impressed direct current supply (current source inverter)

The converter circuit shown in Fig. 2.13, comprises once again a line-side and a machine side converter connected through a dc link; the two converters operating at different frequencies are decoupled by a smoothing reactor L_D which, in combination with a current control loop, serves to maintain a constant direct current I_D as prescribed by the current reference. Thus the machine side converter is supplied from what amounts to a current source [Ref.9, 27, 43].

The simplifications made possible with this circuit are twofold:

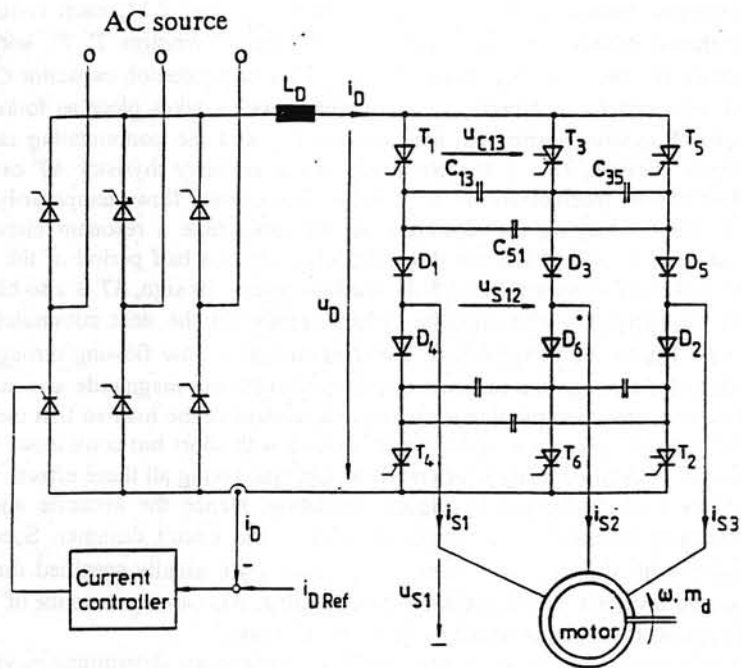


Fig. 2.13 Thyristor converter circuit with DC link

- The unidirectional link current I_D allows the use of a two-quadrant line converter where the mean of the link voltage, U_D , may be inverted by delayed firing for reverse power flow.
- The link reactor permits the supply voltage U_D to be temporarily raised or lowered during a commutation of the machine-side converter. Thus the auxiliary thyristors may be eliminated while commutating capacitors and decoupling diodes are still required.

Altogether there is a total of 12 thyristors. It is noted that, instead of the line side converter, the DC link could also be supplied from another force commutated converter such as a chopper with current control. The mode of operation of the machine-side converter in Fig. 2.13 differs considerably from that of the voltage source converter in Fig. 2.12. While the load current supplied from a PWM voltage source inverter was at least crudely sinusoidal, it has now a three step square waveform, assuming the values $-I_D$, 0 , $+I_D$. The commutating transients are more involved now because the motor impedance is a part of the commutation circuit which means that the commutating time depends on the loading of the motor and increases at light load [Ref. 25]

The commutating transient may be briefly described as follows:

with no commutation in progress, two thyristors, for example T_1 and T_2 carry the direct current I_D and the capacitor C_{13} is positively charged as a result of the preceding commutation. If thyristor T_3 is now fired, T_1 is extinguished in a rapid transient and T_3 assumes the direct current; this is the starting condition of the commutating transient proper. While the current I_{S1} is now reduced towards zero, I_{S2} is rising towards I_D ; during this interval phase 1 of the motor is fed through C_{13} as well as through the series-connected capacitors C_{35} , C_{51} . Eventually diode D_1 is blocked and the commutation is completed with T_2 and T_3 conducting. Clearly the motor transient impedance between terminal 1 and 2 is part of the commutation circuit, as mentioned before. The diodes are required for decoupling in order to prevent the capacitors from losing their charge necessary for commutation. The commutating interval can be reduced by choosing a motor with low leakage reactance.

2.5 Trigger control circuit

Transistor PWM inverters (as mentioned before) are voltage controlled. They have the following features.

- The transistors are highly efficient, having little forward loss and a small number of switching devices.
- As they are capable of performing high-speed switching, they can be used as PWM control inverters. In particular, those utilising MOSFETs are able to perform switching of more than several kilohertz without increasing the loss. The application of PWM control simplifies the main circuit, improves input power factor, efficiency and responsibility, and makes current control easier.

Transistor PWM inverters perform sinusoidal current drive control with the following features [Ref. 12]

- It enables to obtain smooth torque independently of the angle of rotation.
- It makes it easy to execute phase compensation.

Table 2.2

COMPARISON OF BRUSHLESS MOTORS CONTROL HARDWARE

METHOD	FEATURE
<i>Digital</i>	<ul style="list-style-type: none"> • A/D is necessary between the circuit and the analogue sensor • Manipulates current waveforms easily: waveform manipulation, phase compensation, phase compensation, etc. • General-purpose I/F has not been established yet (parallel, serial, etc.) • Performs sequence processing easily and it can made multifunctional (fault, overload curve, diagnostic) • Speed of computation and processing is slow Speed sampling time < 1 ms is necessary • Little temperature drift • Can be regulated easily. Having repeatability and small amount of dispersion
<i>Analogue</i>	<ul style="list-style-type: none"> • Response speed is high Operation time of devices is of order of microseconds • Temperature drift is large, of order of millivolts • Difficult to be regulated • I/F with the analogue sensor is easy • Cannot easily manipulate current waveforms • The input I/F is general-purpose • Performs current control easily (current amplification, pulse width modulation, etc.)
<i>Hybrid</i>	<ul style="list-style-type: none"> • Gives both analogue and digital advantages <i>Analogue:</i> input speed command calculations, current control, PWM circuit, base-drive circuit <i>Digital:</i> speed signal processing, current wave generator, protections, sequence control, input-output sequence control • Input: general analogue interface • Computational time: less than 1 ms, fast speed and current controls • Multifunction: sequence control and protections

- It performs phase compensation even if the delayed current flow is generated.

In spite of these advantages, the sensor and the controller necessary for that control are expensive.

Ignition control circuits are classified into three types according to the method of connection: analog, the digital, or hybrid. The features of the control hardware of the three methods are compared in Table 2.2.

Vector control (current is orthogonal to flux) requires a pole sensor. Resolver or optical encoder are the devices which can be used for these purposes.

2.6 Construction and function of the resolver

A resolver is a detector of the position and the angle of rotation. It is used as a sensor for the motor controller. The encoder converts the amount of displacement into the digital form, while the resolver converts it into an analogue form. In general, a resolver equipped with a rotary transformer is called a brushless resolver. Resolver consists of rotor and stator as well, and the energy is transformed by magnetic fields. The stator winding, which is the excitation winding, is of two-phase structure, with an electrical phase difference of 90° . The rotor winding is the output winding. The resolver can be mounted in the brushless motor housing (a hollow shaft of the resolver with stator and rotor is fixed on the motor shaft). As it is presented in the cross section view (Fig.2.14a), the resolver can be split into stator and rotor as well as into its functional groups. The equivalent circuit diagram of the resolver (Fig.2.14b) shows the position of the windings in the resolver.

The transformer section is transforming a high frequency (typical values 3-11 kHz) signal to the resolver rotor. The axis of the coils on the rotor and stator is the same as the symmetry axis. Therefore the position of the coils does not change when the motor is turning. The transformer works by similar way as an ordinary non-rotating transformer.

The resolver section is detecting the motor position and rotating direction. It can be compared with a transformer again. In this case, the axes of the coils do not align with the symmetry-axes. Additionally, there are two secondary windings with axis turned on 90 degrees. According to the rotor position (angle α) the flux linkage changes between these two secondary windings. During the operating cycle of the motor two high frequency signals (U_{cos} , U_{sin}) with mechanical rotating frequency f are modulated within (Fig.2.15).

Transformation of the resolver signal The signal of the resolver has to be transformed into an analogue signal that can be converted into a digital position signal. Therefore it is converted in a sinusoidal and a cosinusoidal signals. Two different methods of transforming the resolver signal are presented here.

- sample and hold at the maximum of the input signal - to sample and hold both output signals during the operating time, when the input signal is at its maximum. The output voltage signal (U_{cos}) is shown in Fig. 2.16. This method is used with the VECON-chip.
- demodulation by a synchronous demodulator - to rectify the high-frequency input signal ($f=3-11$ kHz, $U_{input} = 4$ V). At first, the input signal is converted into the digital output reference signal $U_{ref} +1$ and -1 (Fig. 2.17), and multiplied with the

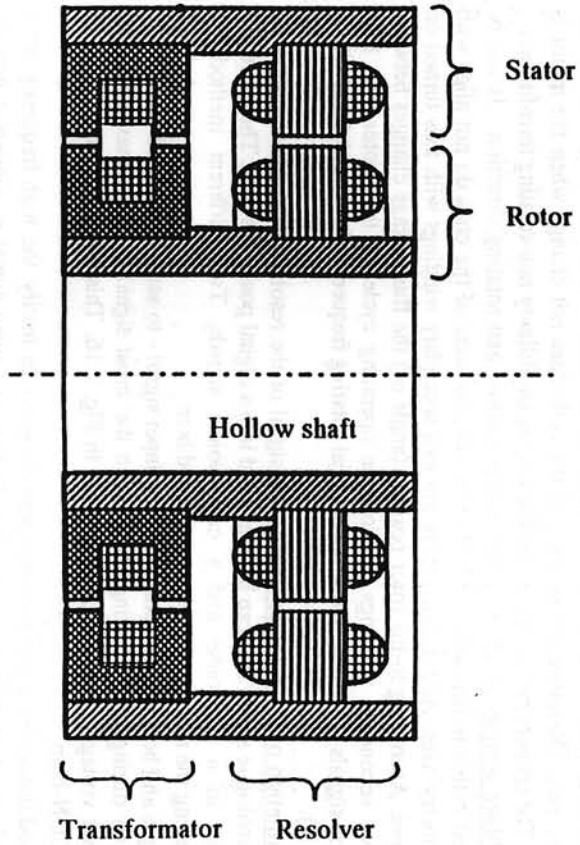


Fig. 2.14a Construction of the resolver

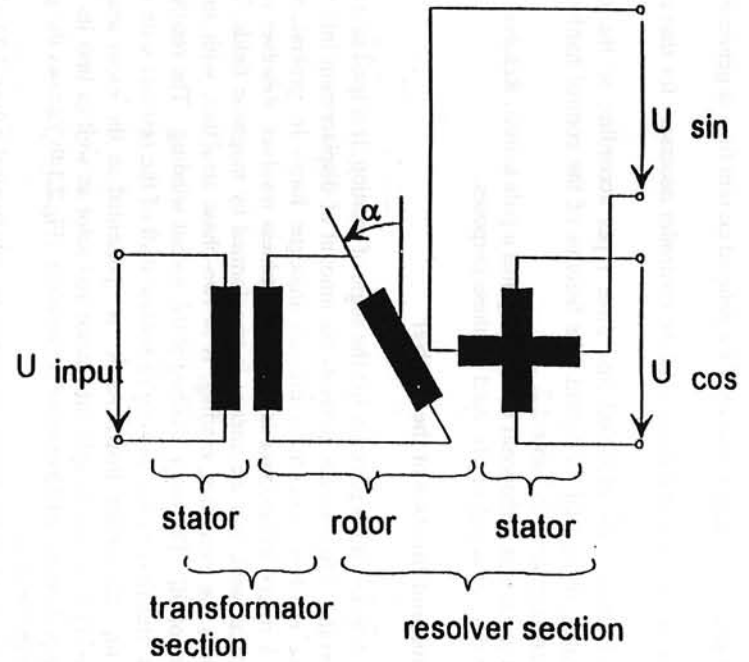


Fig. 2.14b Equivalent circuit of the resolver

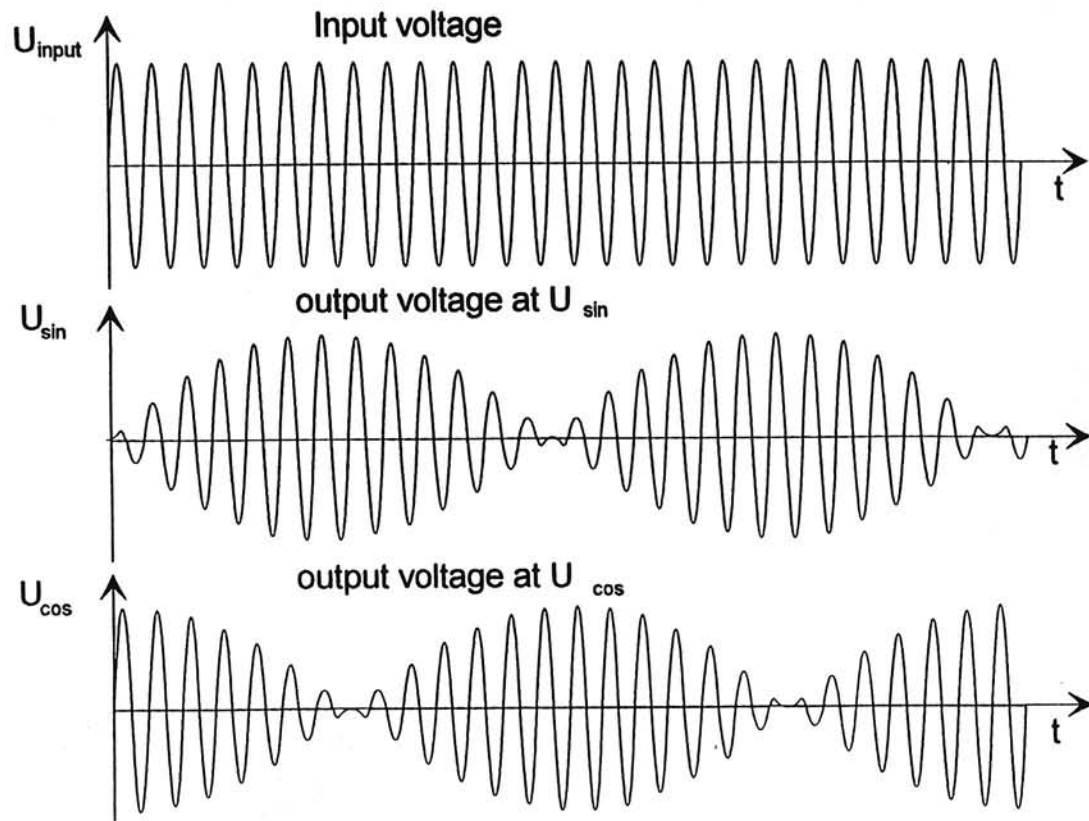


Fig. 2.15. Input and output signals of the resolver

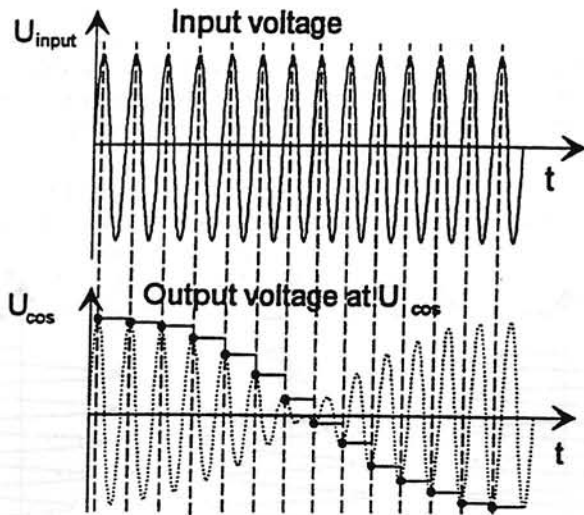


Fig. 2.16 Output signal of the resolver with sample and hold

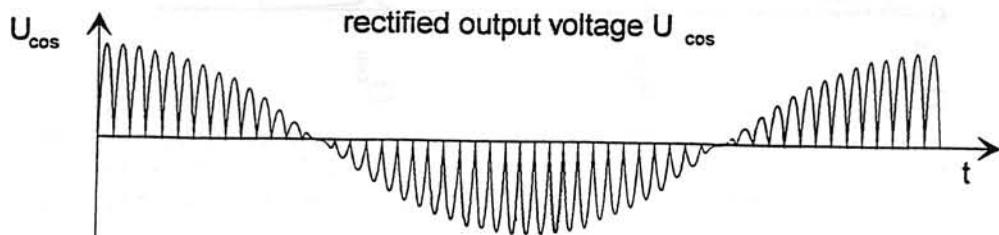
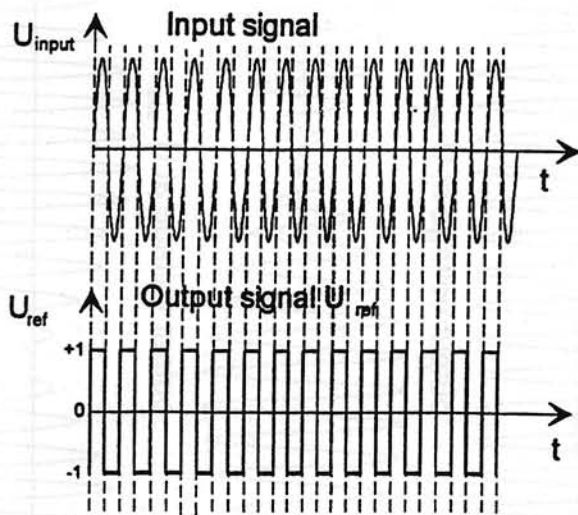


Fig. 2.17 Resolver output signal after the synchronous demodulation

two output signals. An example for the rectified output signal U_{\cos} is shown in Fig. 2.17. In this case the noise signals have less effect. The frequency of the input signal is dependent on the frequencies used in the controller with a trend to higher values. The transformation ratio of the resolver varies with the frequency. Usually, the resolver is specified for one single frequency.

In both transforming methods there is a phase shift between input and output signals, therefore the output signal is getting lower. In digital controllers this resolver signal will be converted into a digital signal. If the range of the A/D converter is not totally used, the quantization error is increases. For reducing the error, the adjustable delay element could be added in the demodulator.

2.7 Energy product of brushless motor

The maximum energy product is a key parameter in evaluating brushless motors with permanent magnets for any type of application. The maximum energy product $(BH)_{max}$ is obviously the maximum product of flux density B_r , coercive force H_c , and several typical values are listed below in Tables 2.4, 2.5, 2.6, 2.7, for different groups of magnets.

2.7.1 Magnetic materials

Brushless motors of small mechanical time constant and excellent fast speed response for electromechanical drive system. applications should be equipped with permanent magnets of high performance.

The magnetic characteristics of permanent magnets are usually shown accurately by a demagnetisation curve. However, they can be roughly determined by residual magnetic flux density B_r , holding power H_c , and maximum energy product $(BH)_{max}$. The energy stored in the gap of a magnetic circuit including permanent magnets is proportional to the product of the magnetic flux density and holding power. Therefore, the better magnetic a material is, the more magnetic energy it possesses. The different magnetic characteristics of various kinds of magnets are presented in Tables 2.3,2.4,2.5,2.6.

The magnetic flux density when the magnetising force is completely taken away from a saturated magnetic flux density, or magnetic flux density when $H=0$, is called the residual magnetic flux density. The magnetic field intensity when the magnetic flux density $B=0$, after the magnetising force is taken away from the saturated magnetic flux density and when the magnet is magnetised in the opposite direction, is called the coercive force H_c . The product of the magnetic flux density on the demagnetisation curve and the magnetising field intensity is called the energy product $(BH)_{max}$, which is expressed in units of joule cubic metre ($J m^3$) or Gauss (G) [Ref. 28].

Let us consider and compare the main properties of the basic magnetic materials for brushless motors.

Alnico magnets

Alnico magnet is ferroalloy consisting of aluminium, nickel, and cobalt as its main components, plus copper, titanium, and other elements. Called "Alnico" from the symbols of its main components, the magnet is widely used for general purposes. Alnico

Table 2.3

Types of Alnico magnets and their magnetic characteristics

Type	Residual magnetic flux density, B_r		Coercive force, H_c		Maximum energy product, $(BH)_{max}$		Notes	
	(T)	(kG)	(kA/m)	(Oe)	(kJ/m ³)	(MG·Oe)	Recoil permeability, ^a	Density, D
							μ_{rec}	(g/cm ³)
MCA 140	0.55 ~ 0.70	5.5 ~ 7.0	41.4 ~ 49.4	520 ~ 620	9.5 ~ 11.9	1.2 ~ 1.5	3 ~ 5	7.0
MCA 160	0.60 ~ 0.73	6.0 ~ 7.3	49.4 ~ 57.3	620 ~ 720	11.9 ~ 13.5	1.5 ~ 1.7	3.5 ~ 5	7.3
MCA 230	0.56 ~ 0.66	5.6 ~ 6.6	79.6 ~ 87.6	1000 ~ 1100	15.9 ~ 19.9	2.0 ~ 2.5	3 ~ 4	7.3
MCB 360	0.95 ~ 1.05	9.5 ~ 10.5	55.7 ~ 60.5	700 ~ 760	25.5 ~ 31.8	3.2 ~ 4.0	4 ~ 5	7.3
MCB 420	1.15 ~ 1.25	11.5 ~ 12.5	49.4 ~ 54.1	620 ~ 680	28.6 ~ 38.2	3.6 ~ 4.8	4 ~ 5	7.3
MCB 500	1.23 ~ 1.33	12.3 ~ 13.3	46.2 ~ 52.5	580 ~ 660	35.8 ~ 43.8	4.5 ~ 5.5	2.5 ~ 3.5	7.3
MCB 580	1.25 ~ 1.35	12.5 ~ 13.5	50.2 ~ 58.1	630 ~ 730	42.2 ~ 50.1	5.3 ~ 6.3	2.5 ~ 3.5	7.3
MCB 750	1.30 ~ 1.40	13.0 ~ 14.0	54.1 ~ 59.7	680 ~ 750	53.3 ~ 65.3	6.7 ~ 8.2	1.5 ~ 2.5	7.3
MCB 400H	0.80 ~ 0.90	8.0 ~ 9.0	95.5 ~ 111.5	1200 ~ 1400	27.9 ~ 35.8	3.5 ~ 4.5	2 ~ 3	7.3
MCB 500H	0.85 ~ 0.95	8.5 ~ 9.5	107.5 ~ 119.4	1350 ~ 1500	35.8 ~ 43.8	4.5 ~ 5.5	2 ~ 3	7.3

^a Recoil permeability is the ratio of the variation of the magnetic flux density to the magnetizing force when the magnetizing force is subtracted from the value of the maximum energy product or the neighbouring value on the demagnetization curve.

Types and magnetic characteristics of ferrite magnets

Table 2.4

Type	Residual magnetic flux density, B_r		Coercive force, H_c		Maximum energy product, $(BH)_{max}$		Notes	
	(T)	(kG)	(kA/m)	(Oe)	(kJ/m ³)	(MG·Oe)	Recoil permeability, μ_{rec}	Density, D
							(G·Oe)	(g/cm ³)
MPA 100	0.20 ~ 0.23	2.0 ~ 2.3	127.4 ~ 151.3	1600 ~ 1900	6.4 ~ 8.7	0.8 ~ 1.1	1.2	4.8
MPB 280	0.33 ~ 0.36	3.3 ~ 3.6	159.2 ~ 207.0	2000 ~ 2600	19.9 ~ 23.9	2.5 ~ 3.0	1.1	4.8
MPB 320	0.36 ~ 0.40	3.6 ~ 4.0	135.4 ~ 159.2	1700 ~ 2000	22.3 ~ 27.9	2.8 ~ 3.5	1.1	4.9
MPB 330	0.36 ~ 0.40	3.6 ~ 4.0	183.1 ~ 207.0	2300 ~ 2600	23.9 ~ 28.6	3.0 ~ 3.6	1.1	4.9
MPB 380	0.40 ~ 0.43	4.0 ~ 4.3	143.3 ~ 175.2	1800 ~ 2200	27.9 ~ 31.8	3.5 ~ 4.0	1.1	5.0
MPB 270H	0.32 ~ 0.36	3.2 ~ 3.6	207.0 ~ 238.9	2600 ~ 3000	18.3 ~ 23.9	2.3 ~ 3.0	1.1	4.8
MPB 330H	0.36 ~ 0.40	3.6 ~ 4.0	238.9 ~ 270.7	3000 ~ 3400	23.9 ~ 28.6	3.0 ~ 3.6	1.1	4.9

Table 2.5

Types of rare-earth cobalt magnets and their magnetic characteristics

		Characteristics						Notes	
Series	Name of product ^a	Residual magnetic flux density, B_r		Coercive force, H_c		Maximum energy product, $(BH)_{max}$		Recoil permeability, μ_{rec}	Density, D
		(T)	(kG)	(kA/m)	(kOe)	(kJ/m ³)	(MG·Oe)	(G·Oe)	(g/cm ³)
1-5 series	REC-18	0.83 ~ 0.87	8.3 ~ 8.7	598 ~ 677	7.5 ~ 8.5	136 ~ 151	17 ~ 19	1.05 ~ 1.10	8.2
	REC-20	0.88 ~ 0.92	8.8 ~ 9.2	677 ~ 717	8.5 ~ 9.0	151 ~ 167	19 ~ 21	1.05 ~ 1.10	8.2
	LM-10	0.60 ~ 0.66	6.0 ~ 6.6	462 ~ 510	5.8 ~ 6.4	72 ~ 88	9 ~ 11	1.00 ~ 1.05	8.1
	LM-16	0.78 ~ 0.84	7.8 ~ 8.4	605 ~ 653	7.6 ~ 8.2	120 ~ 140	15 ~ 17.5	1.00 ~ 1.05	8.2
	LM-19	0.84 ~ 0.90	8.4 ~ 9.0	653 ~ 700	8.2 ~ 8.8	140 ~ 160	17.5 ~ 20	1.00 ~ 1.05	8.3
	LM-22	0.90 ~ 0.96	9.0 ~ 9.6	700 ~ 750	8.8 ~ 9.4	160 ~ 184	20 ~ 23	1.00 ~ 1.05	8.3
	REC-18B	0.82 ~ 0.90	8.2 ~ 9.0	510 ~ 637	6.4 ~ 8.0	128 ~ 160	16 ~ 20	1.05 ~ 1.10	8.3
	REC-22	0.92 ~ 0.98	9.2 ~ 9.8	621 ~ 674	7.8 ~ 9.4	160 ~ 191	20 ~ 24	1.05 ~ 1.10	8.4
	REC-22B	0.92 ~ 1.00	9.2 ~ 10.0	558 ~ 685	7.0 ~ 8.6	160 ~ 191	20 ~ 24	1.05 ~ 1.10	8.3
	REC-24	0.98 ~ 1.02	9.8 ~ 10.2	478 ~ 542	6.0 ~ 6.8	175 ~ 191	22 ~ 24	1.00 ~ 1.05	8.4
2-17 series	REC-26	1.02 ~ 1.08	10.2 ~ 10.8	669 ~ 796	8.4 ~ 10.0	199 ~ 215	25 ~ 27	1.05 ~ 1.10	8.4
	REC-30	1.08 ~ 1.12	10.8 ~ 11.2	478 ~ 542	6.0 ~ 6.8	231 ~ 247	29 ~ 31	1.00 ~ 1.05	8.4
	LM-21B	0.93 ~ 1.01	9.3 ~ 10.1	358 ~ 477	4.5 ~ 6.0	151 ~ 184	19 ~ 23	1.00 ~ 1.05	8.2
	LM-24B	1.04 ~ 1.12	10.4 ~ 11.2	517 ~ 636	6.5 ~ 8.0	175 ~ 207	22 ~ 26	1.00 ~ 1.05	8.2
	LM-25B	1.02 ~ 1.10	10.2 ~ 11.0	342 ~ 477	4.3 ~ 6.0	175 ~ 207	22 ~ 26	1.00 ~ 1.05	8.2
	LM-30B	1.10 ~ 1.17	11.0 ~ 11.7	477 ~ 636	6.0 ~ 8.0	215 ~ 247	27 ~ 31	1.00 ~ 1.05	8.2
	TS-18	0.83 ~ 0.88	8.3 ~ 8.8	480 ~ 640	6.0 ~ 8.0	136 ~ 151	17 ~ 19	1.01	8.3
	TS-20	0.88 ~ 0.94	8.8 ~ 9.4	480 ~ 640	6.0 ~ 8.0	151 ~ 167	19 ~ 21	1.01	8.3
	TS-22	0.90 ~ 0.96	9.0 ~ 9.6	440 ~ 640	5.5 ~ 8.0	167 ~ 183	21 ~ 23	1.01	8.3
	TS-24	0.94 ~ 1.00	9.4 ~ 10.0	400 ~ 600	5.0 ~ 7.5	183 ~ 199	23 ~ 25	1.01	8.3
TS-26	1.02 ~ 1.08	10.2 ~ 10.8	400 ~ 600	5.0 ~ 7.5	199 ~ 223	25 ~ 28	1.01	8.3	

Table 2.6

Varieties and magnetic characteristics of Nd-Fe magnets

Name of product ^a	Characteristics						Notes	
	Residual magnetic flux density, B_r		Coercive force, H_c		Maximum energy product, $(BH)_{max}$		Recoil permeability, μ_{rec}	Density, D
	(T)	(kG)	(kA/m)	(kOe)	(kJ/m ³)	(MG · Oe)	(G · Oe)	(g/cm ³)
NEOMAX-35	1.18 ~ 1.25	11.8 ~ 12.5	796 ~ 916	10.0 ~ 11.5	263 ~ 287	33 ~ 36	1.05	7.4
NEOMAX-30	1.12 ~ 1.19	11.2 ~ 11.9	677 ~ 836	8.5 ~ 10.5	223 ~ 247	28 ~ 31	1.05	7.4
NEOMAX-27	1.05 ~ 1.12	10.5 ~ 11.2	677 ~ 796	8.5 ~ 10.0	199 ~ 223	25 ~ 28	1.05	7.4
NEOMAX-30H	1.12 ~ 1.19	11.2 ~ 11.9	741 ~ 860	9.3 ~ 10.8	231 ~ 255	29 ~ 32	1.05	7.4
NEOMAX-27H	1.05 ~ 1.12	10.5 ~ 11.2	677 ~ 812	8.5 ~ 10.2	199 ~ 223	25 ~ 28	1.05	7.4

^a NECMAX: Sumitomo Special Metals Co., Ltd.

magnets are manufactured by a casting method, and partly processed by grinding when high accuracy is required. They have excellent mechanical strength, and can be manufactured up to a large size comparatively easily.

Table 2.3 lists the varieties and magnetic characteristics of Alnico magnets. MCA is a magnet [Ref. 11] whose magnetism is isotropic. MCB is an anisotropic magnet whose magnetism is greater in a particular direction. MCB has high residual magnetic flux density and low coercive force. It therefore needs to be magnetised after it is mounted on the motor. It is demagnetised when it is demounted from the motor. It is magnetically stable against temperature change, having a temperature coefficient of -0.002% per $^{\circ}\text{C}$.

Ceramic magnets

Ceramic magnets are properly defined as ferrite oxides of barium or strontium and exhibit the property known as ferromagnetism. Ferrite magnet has inferior residual magnetic flux density to that of Alnico magnet but it has very high coercive force. Some anisotropic ferrite magnets have coercive force of over 240 kA/m (3000 Oe). These features are understandable from the facts that in ferrite magnet the density of metallic atoms exhibiting magnetism is essentially low and that the theoretical value of saturated magnetism is 375 kA/m (4700 Oe ; $1 \text{ A/m} = 1.256 \times 10^{-2} \text{ Oersted}$)

Ferrite magnet does not contain noble or heavy metals. Its main component is iron oxide and therefore ferrite magnet is comparatively inexpensive. In addition, it can be made homogeneous by compression using ceramic techniques, which makes it most appropriate to mass production. Also, it has low density of $4.8\text{--}5.0 \text{ g cm}^{-3}$.

However, ferrite magnet is fragile with a low degree of impact tolerance. Moreover, it has a large temperature coefficient, $-0.8 \text{ to } -0.2\%$ per $^{\circ}\text{C}$, which is a hundred times larger than the temperature coefficient of Alnico magnet. The main varieties and magnetic characteristics of ferrite magnets are presented in Table 2.4, where MPA is an isotropic magnet, MPB is an anisotropic magnet.

Rare-earth cobalt magnets

Rare-earth cobalt magnet has nearly the same residual magnetic flux density as that of Alnico magnet and two to three times higher coercive force than that of ferrite magnet. Some rare-earth cobalt magnets have maximum energy product reaching 240 kJ/m^3 (30 MGOe ; $1 \text{ MGOe} = 7.958 \text{ kJ/m}^3$). These features are greatly improving the high performance of brushless motors and making them of lighter weight.

Two kinds of rare-earth cobalt magnets are produced:

- SmCo_5 series (1-5 series)
- SmCo_{17} series (2-17 series).

The latter series have more attractive features for higher performance. Rare-earth cobalt magnets have a small temperature coefficient of $-0.03 \text{ to } -0.05\%$ per $^{\circ}\text{C}$, which is close to that of Alnico magnet. However, it has high density of $8.0\text{--}8.5 \text{ g/cm}^3$, so that it is heavy. The main varieties and magnetic characteristics of rare-earth cobalt magnets are presented in Table 2.5. From a technical standpoint, SmCo magnets are ideal for rotating electric machine applications. However, there are major disadvantages for commercial use: very high material and manufacturing cost; and their strategic nature of cobalt.

Samarium is one of less plentiful rare-earth materials, and its processing costs are also high.

Neodymium-iron-boron magnets

NeFeB has the highest coercive force available in magnets [Ref. 6, 28, 30]. *NeFeB* magnets have a marvellous performance, with its maximum energy product close to 40 *MGOe* and consequently it has been applied to industrial use. Also, its residual flux density is relatively high, comparable to the best of the Alnicos. Moreover, *NeFeB* magnets are much cheaper than samarium cobalt. The main magnetic characteristics and varieties of neodymium-iron-boron magnets are presented in Table 2.6. The low operating temperature requires the use of a larger size for applications required to operate at elevated temperatures and, therefore, many of the reduced size and weight advantages of *NeFeB* are lost. The addition of cobalt or some other rare-earth materials to *NeFeB* is claimed to improve the thermal characteristics of this magnet [Ref. 28]. This material, which contains a large percentage of iron, is also subject to severe corrosion problems in many environments [Ref. 30], and may require additional weight and size in corrosion protection materials in some machine applications.

According to the proper electromagnetic design of electric machine, the permanent magnet material is seldom operated along the normal curve but, rather in regions of lesser energy products. In many motors, the most severe operating condition is that due to a blocked-rotor condition, which may occur during a motor start-up or a machine stall situation. Thus, the peak energy product of a PM machine, which is proportional to the product of the machine's airgap flux density and armature current, does indeed limit the power capability of the machine [Ref. 28]. Note that this limitation is different in many respects from the power limitation characteristics of machines with electrical field excitation. Such machines are generally limited by the steady-state thermal capacity of the electrical insulation and/or by related efficiency considerations. However, note that the energy product is actually an energy density. Therefore, power output of a PM machine can be increased the volume of the PMs. Also note that there are many geometrical and winding design factors such as: type of winding and winding layout, the airgap length, number of poles, etc. which variation provide a variety of power capabilities from a given volume or a given weight of the machine. Therefore, in conclusion, it can be said that, although there is a power limit imposed by the permanent magnets in a PM machine, this limit can be greatly varied by the quality of machine design.

Chapter 3

BRUSHLESS MOTOR CONTROL

Automatic control of brushless motors is of two kinds. The first one is sequential control (sequential starting and overload protection of motors). This utilises a sequential circuit that comprises a memory circuit and a logic circuit. The second one controls the dynamic system, including energy storage elements (inertia, inductor, capacitor, etc.). Let us deal with the second type of automatic control.

Control is classified into feedback control and feedforward control. Feedback control detects the controlled variables and then compares them with the control reference to determine the control variables. Feedback control is insensitive to disturbances (load torque fluctuations, source voltage oscillations, etc.) that disturb the behaviour of the system and to parameter variation (changes in inertia, resistance, and so on). Feedback control changes the structure of the control system.

Brushless motor control involves a regulator problem (e.g. constant angular velocity control), a servo problem (e.g. point-to-point control), and a tracking problem (e.g. continuous path control). The regulator problem is the stability of the system when the control instructions is zero. The servo problem is the control of the system when the control reference varies with passage of time. The tracking problem is the utilisation of future information for control when the control reference varies with passage of time and the future control reference (command) is known beforehand.

Control of a brushless motor requires the main frame of the motor, angle and angular velocity detectors, current, voltage, and magnetic flux detectors, a transistor PWM (pulse width modulation) inverter, and a semiconductor power converter including analogue and digital ICs for controlling those equipments. In addition, a brushless motor driver requires position, velocity, and force controllers (motion control) for controlling the whole system (see Fig.2.4, 2.5). The semiconductor power converter performs sinusoidal output current control, orthogonal control of magnetic flux and current, equivalent field-weakening control, and so on.

Performance of variable speed servo drives (brushless motors) is measured in terms of speed or position precision, speed range, and speed response to specific commands. The precision of speed or position response is directly related to torque position aspects mainly to torque ripples. The speed range is dependent on the machine's capability of flux weakening in the high speed area and this is related to rotor configuration (interior magnet, or pole-magnet). The availability of position, speed or torque control, speed and torque range, and dynamic performance of such drivers depends much on proper design. Therefore, in the following we will address in some detail the basic aspects of the permanent-magnet self-synchronous motor torque production.

3.1 Torque production

Investigations during the last decade have resulted in high performance brushless motor drivers. It is almost unanimously accepted that such drives should be current controlled (except in the high-speed portion of the speed range), through 120° or 180° voltage source transistor inverters [Ref. 23, 29, 39]. There are two fundamental current control waveforms envisaged: (a) rectangular current and (b) sinusoidal current. The first one requires only incremental position information every 60° (electrical). Sinusoidal current control requires more refined rotor position information, is more expensive but results in very small torque ripples, and is suitable for low speed operation.

3.1.1 Field and torque production with rectangular current

The ideal rectangular current consists of two 120° wide rectangular waveforms per period per phase. The torque is produced by the interaction between the airgap flux and stator currents. Notable insight into the phenomenon of torque production may be obtained via a linear model. A transverse view of the permanent magnet rotor is presented in Figure 2.6a. In a conventional cylindrical rotor synchronous motor, the torque is given by

$$T_{EM} = p \psi_F I_q \quad (3.1)$$

where

p is the pole pairs

ψ_F is a field flux linkage

I_q is a quadrature component of the armature current

Equation (3.1) suggests that only the stator magnetomotive force component which is 90° out of phase with respect to the magnet axis produces a torque. In other words, when the magnet induced voltages (E_a , E_b , and E_c in Figure 3.1) are in phase with the stator currents, maximum torque per ampere is obtained ($\alpha = 0$). In general, the rectangular current may be commanded in advance by an angle $\alpha > 0$. However, over a 60°-span of the rotor motion (stator windings with full-pitch coils arranged in 60°-span belts, number of slots/pole/phase -- $q = 1$), the stator currents remain ideally constant in the conducting phases (a and b). According to the model in Figure 3.2 the induced voltage in phase (a) at the moment is

$$E_a(t) = K_b W_b \omega_M \tau / \pi l p \int_{\theta_0 + \alpha}^{\theta_0 + \frac{\pi}{3} + \alpha} B(\theta) d(\theta) \quad (3.2)$$

where

$\theta_0 = \omega_M t$ varies from zero to $2\pi/3$

W_b is a number of turns per pole per phase

$K_b = 1$ is a winding factor (for full-pitch coil with $q = 1$)

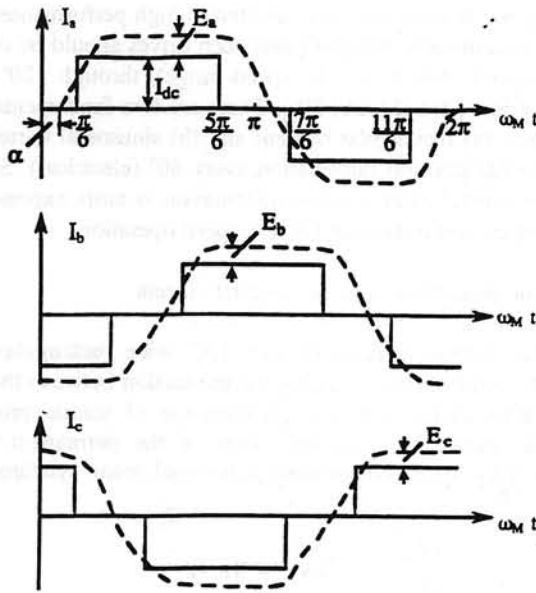


Figure 3.1 Ideal rectangular phase currents

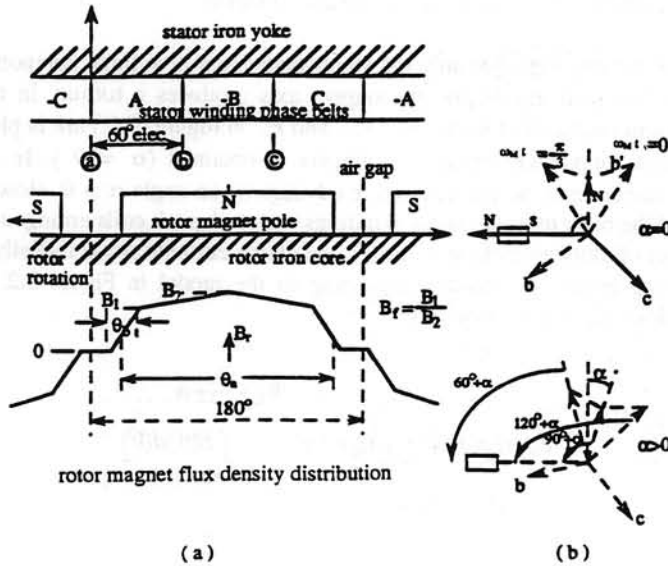


Figure 3.2 (a) Brushless motor model and radial flux-density distribution (b) Advanced angle, α

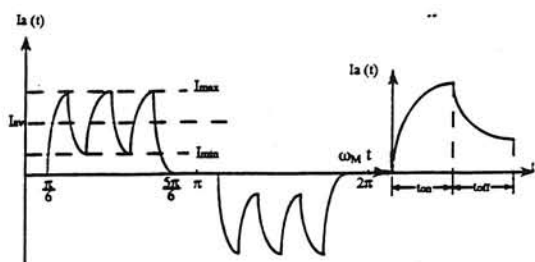


Figure 3.3 On-off rectangular current waveform

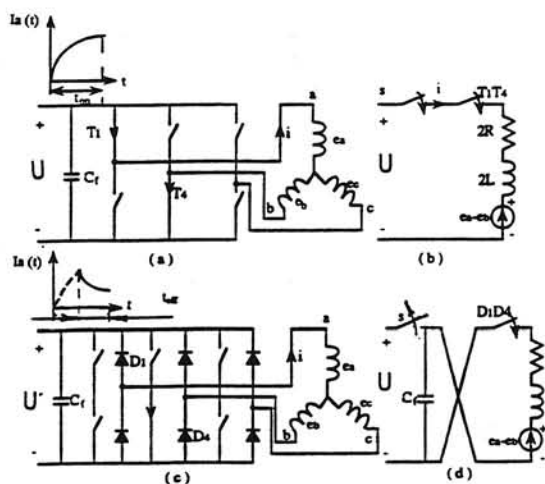


Figure 3.4 Inverter current flow in phase 'a'

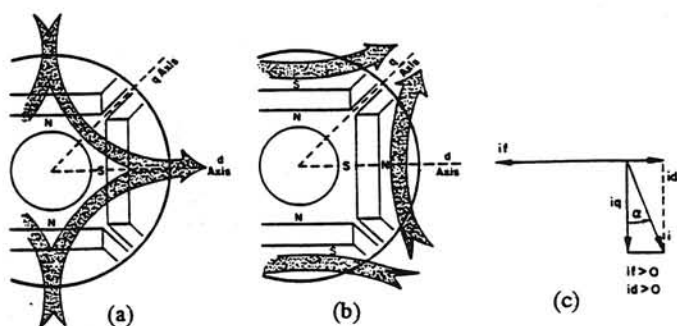


Figure 3.5 Flux path for (a) d-axis, (b) q-axis of an interior magnet rotor; (c) current phasors

- α is an advance angle for maximum torque per ampere position
 l is an axial length of the machine

The angle θ_0 accounts for the fact that during $\pi/3$ (or 60°) the stator conducting phases remain the same while the rotor is moving. The torque is given by

$$T_c(t) = 3 I_{dc} l p^2 W_b L \tau / \pi^2 \int_{\theta_0 + \alpha}^{\theta_0 + \frac{\pi}{3} + \alpha} B(\theta) d(\theta) \quad (3.3)$$

It may be expected that the torque pulsations can be reduced by modifying the span of the magnet [Ref. 9]. Unfortunately, the average torque modifies also. A compromise between the average torque and the torque pulsation values should be made since the average torque decreases in a monotone fashion when the permanent magnet space (θ_a) is reduced. To calculate the torque-speed characteristic for constant voltage running, the motor equations should be formulated.

3.1.2 Field and torque with sinusoidal current

Sinusoidal current control through advanced PWM techniques produces very low ripples, if the winding distribution and the permanent magnet airgap field distribution are adequately matched. Low torque ripple levels are required at very low speeds providing enough precision in speed. Sinusoidal current control is applicable to both surface-magnet and inset-magnet rotor motors. Inset permanent magnet rotors are characterised by higher flux leakage [Ref.28]. Consequently, more PM material is required for useful (airgap) flux. The inset PM rotor machine exhibits significant saliency on the rotor. The magnetic path along the d-axis contains the permanent magnets and thus exhibits a high magnetic reluctance. The path along the q-axis does not contain the PM and its magnetic reluctance is considerably smaller. It follows that the inductance along the d-axis, L_d , is smaller than that along the q-axis L_q . The expression for the torque resembles that of a nonsalient pole synchronous machine, and may be written as

$$T_e = 3/2 p [L_d I_f I_q + (L_d - L_q) I_d I_q] \quad (3.4)$$

This torque corresponds only to the fundamental components of the field mmf distribution. Because rare-earth permanent magnets have a recoil permeability $\mu_{rec} \approx (1.02 \text{ to } 1.05) \mu_0$, they may be considered as air zones for the armature reaction field. In general, a permanent magnet is modelled by an equivalent current fed (I_f) winding which is close to reality for linear demagnetisation curves such as those of SmCo_5 , strontium ferrite and NdFeB magnets with almost μ_0 recoil permeability. Equation (3.4) with $L_d < L_q$ suggests that the reluctance torque component is positive only if I_d is negative. With $I_d = 0$, no reluctance torque is developed. So the inset permanent magnet should in general be controlled with $I_d \neq 0$, and from zero speed -- unlike the surface-magnet rotor type -- in order to make full use of the reluctance torque component. The

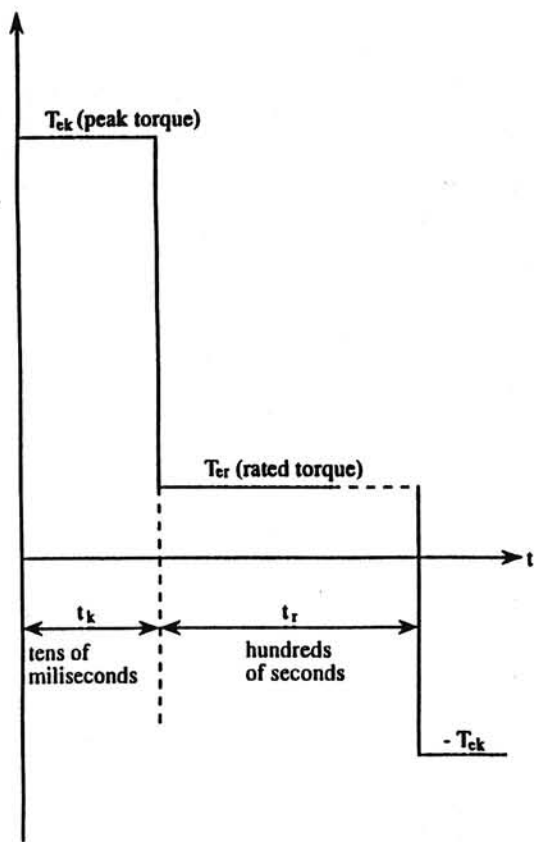


Fig. 3.6 Duty cycle of a brushless motor drive

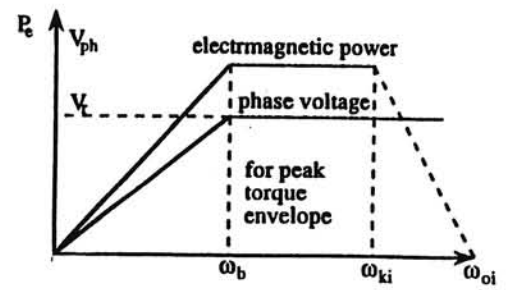
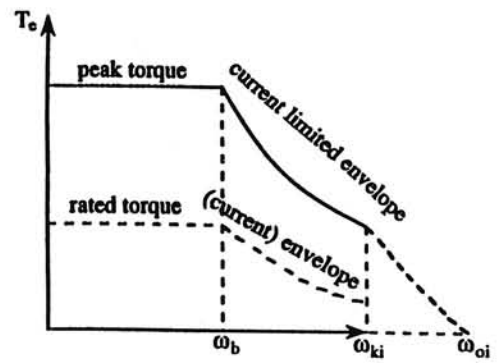


Fig. 3.7 Torque, power, and voltage design goals for a brushless motor drive

magnetic saturation along the q-axis (Figure 3.5)due to I_q uses more of the direct axis armature reaction field produced by it to return to the stator through the permanent magnets. The path along iron, though saturated, is more permeable with respect to the PM zone. Thus apparently the longitudinal inductance along the d-axis, L_d , increases with the reaction current I_d . But L_q decreases due to saturation. A cross coupling effect occurs [Ref. 28]. The reluctance torque component tends to decrease due to saturation since L_d increases and L_q decreases. The direct axis inductance voltage drop $\omega_M L_d I_d$ increases. An additional apparent field weakening effect occurs, which allows high speeds for given stator voltage. Thus in a wide-speed range application the interior PM rotor self-synchronous machines are superior to those having pole-magnet rotors. The presence of a notable reluctance torque may be exploited to reduce the PM weight and cost per unit torque, and extend the speed range through flux weakening with smaller currents than in the case of surface-magnet rotor.

3.1.3 Design of sinusoidal-fed PM motor

Variable speed drives are characterised by high dynamic performance. For example , acceleration times on no-load are typically included in catalogue descriptions of such drives. Other specifications include: dc link voltage, U_0 ; and maximum torque, T_{ek} , up to base speed. Duty cycle (Figure 3.6) is also important in designing the motor. These requirements, lead to torque, power and voltage requirements, such as those shown in Figure 3.7. Often a ratio of the three between the peak and rated torques has been found adequate to provide the desired acceleration on no-load for aircraft electromechanical applications.

The base speed, ω_b , is by definition the speed at which the maximum torque, T_{ek} is achievable at full voltage. The peak current is limited by the motor overheating, ratings of the inverter power transistors, and protection against demagnetisation of the permanent magnets [Ref. 23]. Given the specifications, the design may be initiated keeping in mind the airgap flux density, the stator mmf limitations, and taking into account the PM remnant flux density.

During the acceleration time, t_b , to the base speed, ω_b , the motor develops the peak torque, and the speed increases linearly as determined from

$$T_{ek} = \frac{J \Delta\omega}{p \Delta t} = \frac{J \omega_b}{p t_b} \quad (3.5)$$

And the ratio of the peak torque to the motor inertia is simply given

$$\frac{T_{ek}}{J} = \frac{1 \omega_b}{p t_b} \quad (3.6)$$

The approximate techniques for brushless motor design (permanent magnet geometry and stator dimensions, power considerations, heat losses, etc) are widely described in literature [Ref. 6, 16, 21, 43]. The basic simulation results for brushless motors are presented in Appendix 3. However, for a more refined design, for designed optimization, and for an exact comparison among several motor designs, more

sophisticated methods of electromagnetic field analysis will be required. Three-dimensional analysis (such as three-dimensional finite element analysis of electromagnetic field distribution) is required for brushless machines in which two-dimensional symmetry is inadequate to describe the complete machine configuration.

3.1.4 Square-wave current control system

Rectangular current control has emerged as a practical solution providing fast response and rapid speed reversal. A sample of the rectangular current control system is shown in Figure 3.8. A basic control scheme for the brushless motor consists of

- the PM synchronous motor
- control system
- the position transducer

The control system itself should include: a position controller, a speed controller, and a current (torque) controller. Providing an inphase voltage/current requires a position transducer (as mentioned earlier). A typical position transducer for square wave current control has six inductive (or optical) position sensors per double pole pitch of rotor periphery. They are shifted from each other by 60° (electrical). Each of the position sensors triggers on one power transistor in the inverter during 120° electrical per period. It follows from Figure 3.4 (a) that ideally only two transistors (phases) are conducting at a time. For example the position sensors $P-T_1$ and $P-T_6$ respectively provide positive and negative voltages (currents) in phase a; $P-T_3$, $P-T_4$ in phase b; and $P-T_5$, $P-T_2$ in phase c. Thus, the stator mmf vector ideally jumps after every 60° producing a "jumping" stator field. The mmfs of two phases in series are at standstill (over 60° rotor rotation) and 30° lagging the phase connected in the positive sense (Figure 3.8). If we now locate the position sensor that fires the transistor T_1 , 90° behind the phase a axis (with respect to the direction of motion) the power angle varies from 120° to 60° -- T_1T_2 conducting with an average power angle of 90° . Each phase conducts continuously for 120° . However, the voltage source inverter simply distributes the constant voltage between two phases at a time, in the sequence shown in Figure 3.4b. Square-wave current control may be achieved through a pulse-width modulation circuit (Figure 3.8) which turns on and off the transistor as needed to maintain the required current level, I_{dc} . Let us present the details of this on-off controller, since it gives a better insight into the motor behaviour.

3.1.5 On-off square-wave current controller

The initial current in stator phases is done by the position sensors as explained earlier, we let the current rise up to a maximum value I_{max} and then turn it off for a while until a minimum value I_{min} is reached. The duration of on and off intervals, t_{on} and t_{off} is given by the pulse-width modulation circuit where input is the error between the reference current (I_{dc}^*) and the measured input current of the inverter.

Negative reference current ($-I_{dc}$) implies torque reversal but regenerative braking is obtained only if all the position sensors are rotated through 180° ; that is, a^+ becomes a^- , b^+ becomes b^- , and c^+ becomes c^- . At the average power angle 90° , regenerative braking and speed reversal are easy to obtain and the machine behaves identically in both directions of motion. The on-off mode terminates after 120° when the position sensor of that phase goes off (Figure 3.4), that is, after 120° .

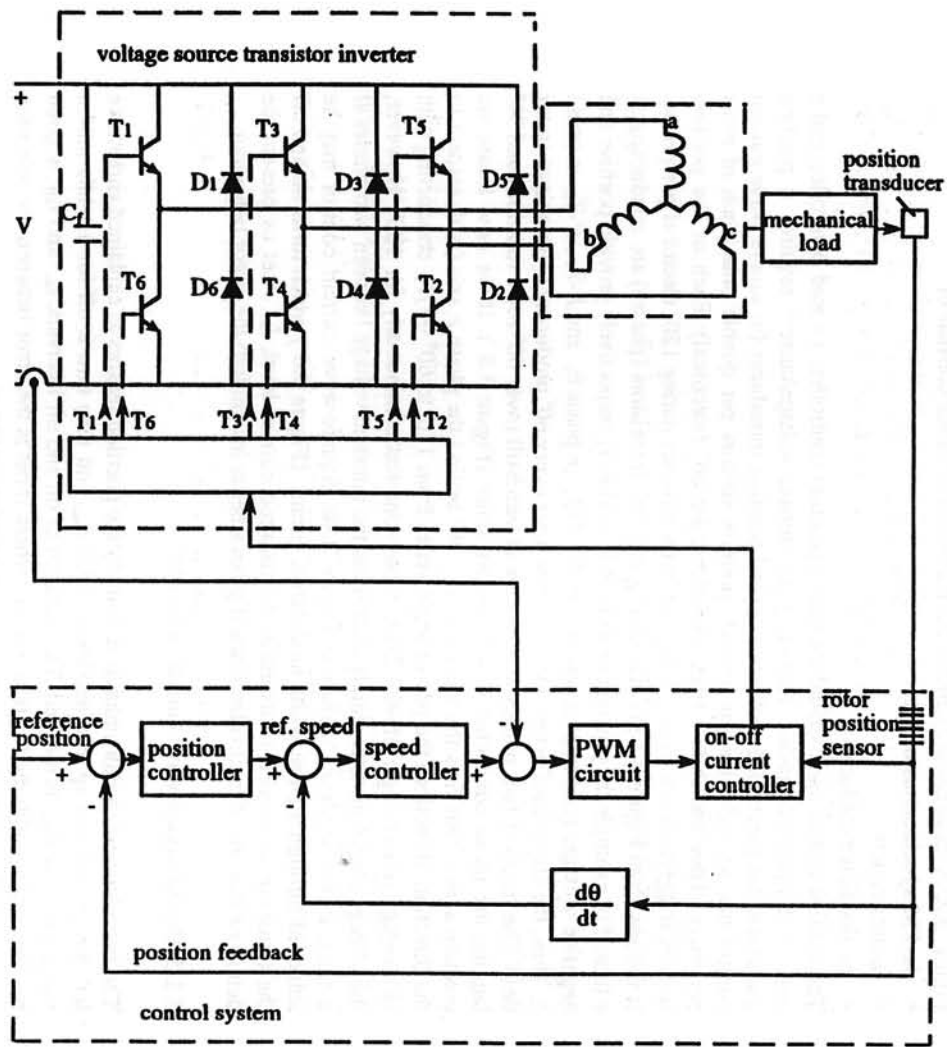


Fig. 3.8 Basic rectangular current control system for a brushless motor drive

Let us consider the inverter-motor equations during the on-off-time intervals. During on-time (Figure 3.4a), T_1 and T_4 are conducting. Thus, the current flows through phases a and b in series. The equivalent circuit is shown in Figure 3.4b which shows the phase induced voltage e_a, e_b , the phase resistors R , and the inductor L . The corresponding equation is

$$U = 2RI + 2L \frac{di}{dt} + (e_a - e_b) \quad (3.7)$$

$$e_a - e_b = 2E_a = E_0 = \text{a constant} \quad (3.8)$$

During the conducting period (120°) the line induced voltage varies only during 60° because $e_a - e_b$ is replaced by $e_a - e_c$ after the first 60° . As already demonstrated, E_0 is constant during the commutation interval, and I_a and I_b are ideally square waves. The solution of (3.7) can be written as

$$i(t) = \frac{\left(-\frac{1}{2} \int e^{\left(\frac{Rt}{L}\right)} U(t) + e^{\left(\frac{Rt}{L}\right)} E_0 dt + \frac{1}{L} \right) e^{\left(-\frac{Rt}{L}\right)}}{L} \quad (3.9)$$

in the interval $[0, t_{on}]$.

For current rise it is imperative to have $U > E_0$; it means that the motor (electrical machine) is under excited. For the off-time interval both T_1 and T_4 are turned off (Figure 3.4c) and the diodes D_1 and D_4 provide the path for the current which charges the filter capacitor C_f . The switch S (open this time) signifies the fact that the dc power source which supplies the inverter does not accept power retrieval. The circuit equation is now

$$U = 2RI + 2L \frac{di}{dt} - (e_a - e_b) + \frac{1}{C_f} \int Idt \quad (3.10)$$

Considering that the off-time process is initiated at $t_i = t_{on}$ or $t_i = t - t_{on}$, the solution to (3.10) is

$$i(t) = \frac{\left(\frac{1}{2} \int e^{\left(\frac{1}{2} \frac{t}{RC_f}\right)} \left(\frac{\partial}{\partial t} U(t) \right) dt + \frac{1}{R} \right) e^{\left(-\frac{1}{2} \frac{t}{RC_f}\right)}}{R} \quad (3.11)$$

in the interval $] t_{on}, t_{off}]$.

The PM circuit should adjust the t_{on} and t_{off} so as to meet the desired average current I_{dc}^* and torque. The expression for the torque $T_e(t)$ is

$$T_e(t) = \frac{(e_a - e_b)I(t)}{\omega / p} \quad (3.12)$$

with $I(t)$ obtained from (3.11) and (3.10).

The torque pulsates due to the on-off process. The frequency of pulsations is $6\omega_M$ whereas the on-off current pulsations have significantly higher frequency. The speed control (a proportional integral PI type) should eliminate their consequences through adequate design. A precisional position control should be used for both current wave forming and position feedback.

3.2 Mathematical models of brushless motor drive system

3.2.1 Mathematical model of brushless motor in d,q-axes presentation

The majority of research associated with the formulation of models for the simulation of synchronous machines is directed towards the synchronous generator. The aim of this chapter is to present single detailed machine formulations for synchronous motor (brushless) which, in addition to providing the basis for a more advanced study of the subject, may be used to advantage for a number of problems associated with practical EMA driving systems. Taking as a specific example the brushless machine shown schematically in Figure 2.6a, where motor is presented as 2p-poles 3-phase permanent magnet synchronous machine with the phase windings in a wye-connection. All mutuals between stator and rotor circuits are periodic functions of rotor angle position, and in addition, due to finite saliency, mutual inductances between stator phases are also periodic functions of rotor angle position. To simplify the mathematical description of the synchronous machine (brushless motor) and to facilitate a simulation a two-axes transformation of the stator and rotor quantities may be performed such that the basic equations possess constant coefficients. In accordance with Figure 3.9 the derived matrix equations can be presented in d, q -axes frame [Park R.H., 1929], and invariably stated in the per unit form

$$[U] = [R][I] + [L] \left[\frac{dI}{dt} \right] + [\psi] \omega \quad (3.13)$$

where

- $[U]$ voltage matrix
- $[I]$ current matrix
- $[\psi]$ flux linkage matrix is given by $[L][I]$
- $[R]$ resistance matrix
- $[L]$ inductance matrix

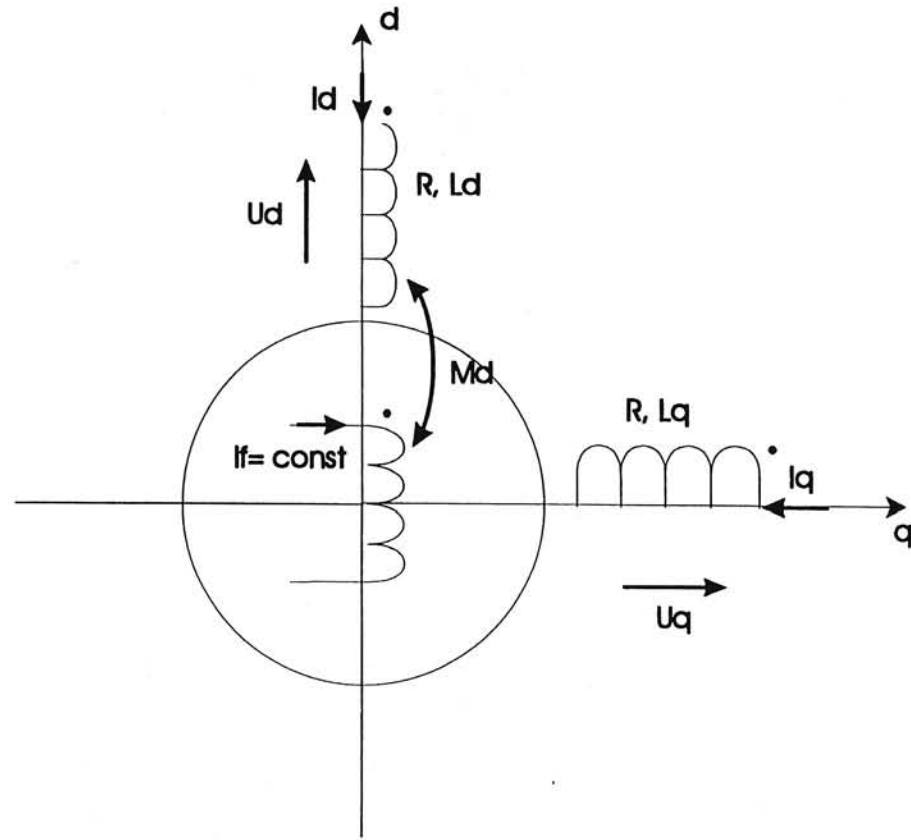


Fig. 3.9 Equivalent d,q - axes model of brushless motor

This is particularly advantageous in the study of machines because it provides a procedure of non-dimensionalising the variables and parameter values thereby introducing a simpler means of comparison of differing sizes of machines. Figure 2.6b depicts the electric circuit of this system which includes an inverter and a motor. The motor governing equations in the rotor reference frame (d, q -axes) variables can be represented as a set of differential equations as listed below.

$$\begin{aligned} U_d &= R I_d + d\psi_d / dt - \omega_M \psi_q p \\ U_q &= R I_q + d\psi_q / dt + \omega_M \psi_d p \end{aligned} \quad (3.14)$$

where

R is the motor resistance
 L_d, L_q are the motor d, q -axes inductances
 ψ_d, ψ_q are the d, q -axes flux linkages
 ω_M is the angular velocity of the brushless motor
 U_d, U_q are the d, q -axes voltages
 I_d, I_q are the d, q -axes currents
 p is the number of pole pairs

For further analysis, the permanent magnet should be changed by a single coil of an exciting winding along which a current I_f (is equal to the "fictitious" magnetomotive force F_{mf}) flows (Fig 3.9).

The flux linkages in d, q -axes presentation can be written as

$$\begin{aligned} \psi_d &= L_d I_d + M_d F_{mf} \\ \psi_q &= L_q I_q \end{aligned} \quad (3.15)$$

where

M_d is the mutual inductance in d, q -axes representation

In view of fact that

$$F_{mf} = I_f, \quad M_d I_f = \psi_m$$

where ψ_m is a flux linkage coefficient, the set of the differential equations can be rewritten as

$$\begin{aligned} U_d &= R I_d + L_d dI_d / dt - \omega_M p L_q I_q \\ U_q &= R I_q + L_q dI_q / dt + \omega_M p L_d I_d + \omega_M p \psi_m \end{aligned} \quad (3.16)$$

The electromechanical torque of the brushless motor is

$$T_{EM} = 3/2 p (\psi_d I_q - \psi_q I_d) = 3/2 p (L_d I_d I_q + M_d F_m I_q - L_q I_q I_d) = 3/2 p [(L_d - L_q) I_d I_q + \psi_m I_q] \quad (3.17)$$

and the equation of motion is

$$T_M = T_{EM} = J d\omega_M/dt + \xi\omega_M + T_{ML} \quad (3.18)$$

where

- J is the motor inertia
- ξ is the motor damping coefficient
- T_{ML} is the motor-load torque

3.2.2 Position control system of brushless motor using d,q-axes presentation

Figure 3.10 shows the basic diagram of the system (brushless motor) for further investigation. An input is setting by the user and is feeding to the controller. The controller can be configured either as a position or a velocity control system. In the case of the controller designing with generating a control law with state feedback, the sensing of the states and the control law will be discrete. The controller output changes the amplitude of the supply voltage to the motor phase windings via a PWM (pulse width modulation) scheme, which is achieved by means of the inverter. The inverter can be operated either in a 180° or 120° mode. Hence, 3-phase balanced voltages, determined by the motor angular position, are applied to the motor phase windings sequentially. A transformation from the phase voltages ($A B C$ - variables) to the rotor reference frame (d,q - axes variables) can be conducted in a fictitious transformation block. Since the rotor of a brushless motor rotates in continuous time, the transformation is also conducted in the continuous domain. The brushless motor "takes" the d,q - axes voltages and then generates the electromechanical torque with d,q - axes as the intermediate state variables. The d,q -axes currents are used as state feedback signals for the controller. Since the d,q -axes currents do not exist physically, the only available measurable variables are the ABC -axes currents. These will be converted to the d,q -axes currents in a virtual transformation. In the simulation, this can be done by lookup table and the real implementation time delay should be lumped into the computational delays. The load torque may be constant, step changing or as a random variable with normal or uniform distributions. The difference between the electromechanical and load torque is applied to the motor to produce the motor velocity via the equations of motion (3.15, 3.17, 3.18). The motor velocity is scaled down by a reduction gear of ratio $G_D : 1$ and then the system velocity and position are obtained. These final controlled variables are fed to the controller which acts as a feedback variable.

The dynamic system of a brushless motor is represented by a set of differential equations in d,q --axes coordinates

$$dI_d/dt = -R/L_d I_d + \omega_M p L_q /L_d I_q + U_d/L_d$$

$$dI_q/dt = -R/L_q I_q - \omega_M p L_d / L_q I_d - \omega_M p \psi_m / L_q + U_q / L_q \quad (3.19)$$

$$T_{EM} = 3/2 p [(L_d - L_q) I_d I_q + p \psi_m I_q]$$

The differential equations (3.19) for mathematical model are constructed in the d, q - axes frame (see Fig. 3.9). Therefore, the inverter block, after transforming, will produce the d, q -axes voltages from the modulated supply voltage (according to the actuation command) and the rotor position. For the simulation, a unity normalized actuation command can be taken as the input and the d, q -axes voltages be pre-computed and stored in a look-up table (MATLAB, SIMULINK) [Ref.32]. The resolution of position sensor will affect inverter performance and it should be selected in the simulation. It can be achieved by varying the angular interval in the pre-computation. The phase voltages, U_{Ap} , U_{Bp} , U_{Cp} , being physically measured parameters (variables), can be used for determination the d, q -axes voltages as

$$\begin{bmatrix} U_{As} \\ U_{Bs} \\ U_{Cs} \end{bmatrix} = 1/3 \begin{bmatrix} 2 & -1 & -1 \\ -1 & 2 & -1 \\ -1 & -1 & 2 \end{bmatrix} \begin{bmatrix} U_{Ap} \\ U_{Bp} \\ U_{Cp} \end{bmatrix} \quad (3.20)$$

and the d, q -axes voltages are given by

$$\begin{bmatrix} U_d \\ U_q \end{bmatrix} = \begin{bmatrix} \sin(\theta_M) & \sin(\theta_M - 2/3\pi) & \sin(\theta_M + 2/3\pi) \\ \cos(\theta_M) & \cos(\theta_M - 2/3\pi) & \cos(\theta_M + 2/3\pi) \end{bmatrix} \begin{bmatrix} U_{As} \\ U_{Bs} \\ U_{Cs} \end{bmatrix} \quad (3.21)$$

3.2.3 Mathematical model of brushless motor in phase coordinates

In brushless motor with concentrated full-pitch windings the stator-to-rotor mutual inductances do not vary sinusoidally, and instead of the dq -axes or space phasor presentation, the mathematical model in terms of phase coordinates is valid for modelling and simulation.

The stator phase main (L) and mutual (M) inductances are constant, and may be either calculated or measured. The voltages, e_a , e_b , and e_c , induced in the stator phases due to the field of the PM depend on the rotor (motor) speed, ω_M (ideally rectangular, actually trapezoidal). Thus, in terms of phase coordinates, the motor voltage equation may be written as

$$\begin{bmatrix} U_a \\ U_b \\ U_c \end{bmatrix} = \begin{bmatrix} R & 0 & 0 \\ 0 & R & 0 \\ 0 & 0 & R \end{bmatrix} \begin{bmatrix} I_a \\ I_b \\ I_c \end{bmatrix} + \begin{bmatrix} L & M & M \\ M & L & M \\ M & M & L \end{bmatrix} p \begin{bmatrix} I_a \\ I_b \\ I_c \end{bmatrix} + \begin{bmatrix} e_a(\theta_M) \\ e_b(\theta_M) \\ e_c(\theta_M) \end{bmatrix} \quad (3.22)$$

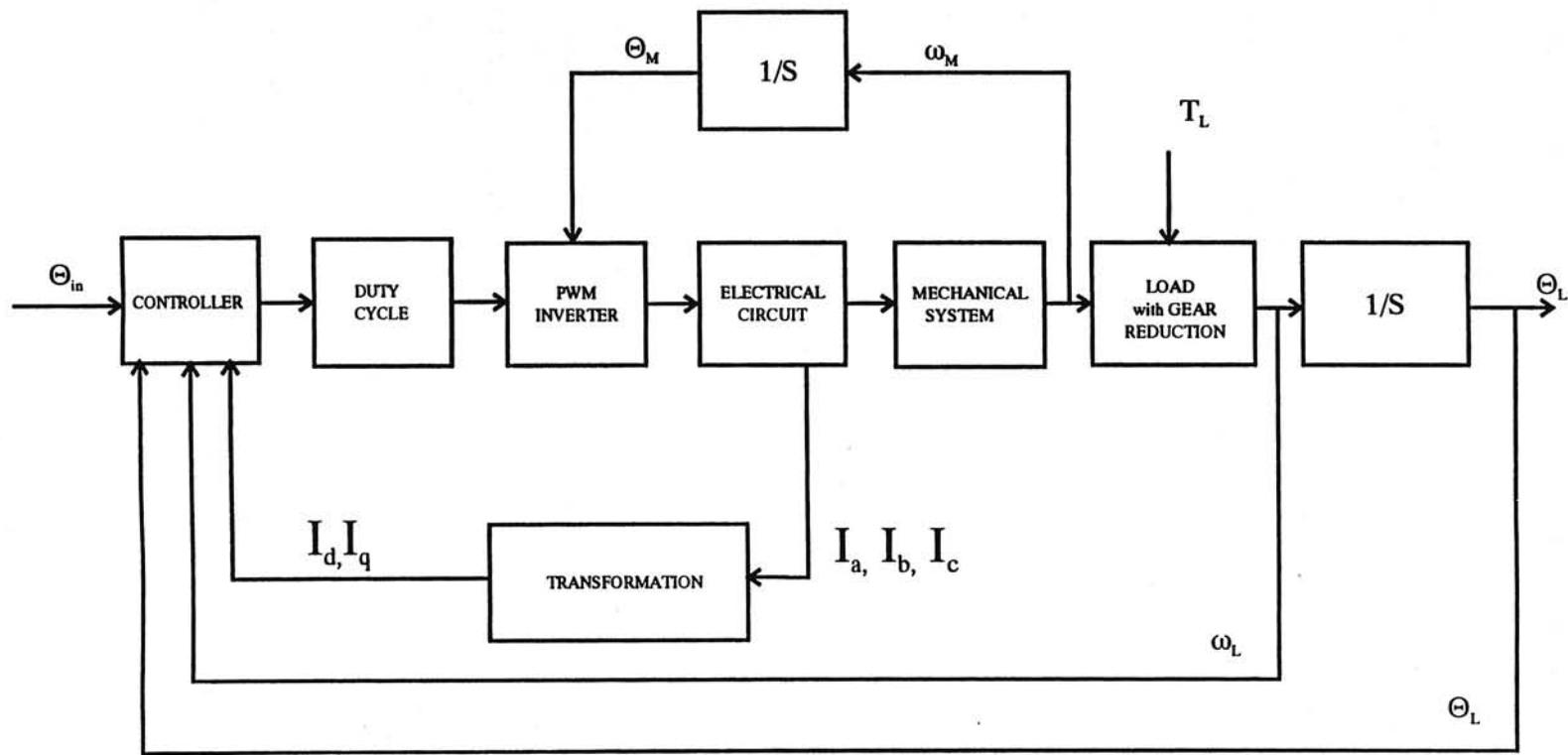


Fig. 3.10 Brushless motor control system block diagram

For wye-connected phases, we have

$$I_a + I_b + I_c = 0 \quad (3.23)$$

The inductance matrix in (3.22) may be diagonalized and (3.23) may be rewritten as

$$P \begin{bmatrix} I_a \\ I_b \\ I_c \end{bmatrix} = \begin{bmatrix} \frac{1}{L-M} & 0 & 0 \\ 0 & \frac{1}{L-M} & 0 \\ 0 & 0 & \frac{1}{L-M} \end{bmatrix} \left(\begin{bmatrix} U_a \\ U_b \\ U_c \end{bmatrix} - \begin{bmatrix} R & 0 & 0 \\ 0 & R & 0 \\ 0 & 0 & R \end{bmatrix} \begin{bmatrix} I_a \\ I_b \\ I_c \end{bmatrix} - \begin{bmatrix} \omega_M \psi_a(\theta_M) \\ \omega_M \psi_b(\theta_M) \\ \omega_M \psi_c(\theta_M) \end{bmatrix} \right) \quad (3.24)$$

where θ_M denotes the rotor (motor) position (in electrical degrees). The mechanical dynamics are given by

$$J_M d^2 \theta_M / dt^2 = T_M - T_{ML} - \xi_M d\theta_M / dt \quad (3.25)$$

where electromagnetic torque $T_M = T_e$ may be expressed as

$$T_e = p / \omega_M (e_a I_a + e_b I_b + e_c I_c) = \psi_a(\theta_M) I_a + \psi_b(\theta_M) I_b + \psi_c(\theta_M) I_c \quad (3.26)$$

Hysteresis (on-off), ramp comparison, or other current controllers may be used to control the 120° square waveforms of the stator currents. For a wye-connected stator, Table 3.1 shows the phase voltages for rectangular current control. Only

Table 3.1

Phase voltages for wye-connected stator				
DC link current		power transistor		voltage
I_a^*	I_a	T_1	T_4	U_a
≥ 0	$\leq (I_a - \Delta I)$	on	off	$+U_0 / 2$
≥ 0	$\geq (I_a - \Delta I)$	off	off	$-U_0 / 2, D_4$ on
0	$\geq (I_a - \Delta I)$	off	on	$-U_0 / 2$
0	$\leq (I_a - \Delta I)$	off	off	$+U_0 / 2, D_1$ on

the DC link current is measured and controlled, and then distributed to the other two phases. The switching frequency depends on the hysteresis window ($2\Delta I$), the machine parameters, and the voltage ceiling ($U_o - E_o$). In the ramp comparison controller the current error is measured and compared with a saw-tooth triangular waveform. The switching frequency, although constant, should be less than one-tenth the motor electrical time constant, in order to avoid delays affecting the control response. Proportional integral (PI) pseudo-derivative feedback (POF) or sliding mode speed controller may also be used to control a brushless motor.

3.3 Synthesis of controllers

An important direction of research for using brushless motors is the synthesis of controllers. The most usual strategy consists of selfcontrolling the motor, considering the currents as control variables [Ref.42, 47]. Some usual approximations are the following

- the speed dynamics are slow in comparison to those of the currents, so one traditionally controls separately these dynamics. Thus, the effects of the motor acceleration are not taken into account.
- in many applications, the effect of the induced electromotive forces created by the rotation of the motor is neglected in the control algorithms. Moreover, the coupling between the phases of the motor is also neglected.

The latter couplings are immediately observable in equations (3.16, 3.17). The presence of two non-linearities in the electrical and mechanical equations can be seen. For applying recent non linear control methods which bring a total linearization of the speed behaviour, with a current in a quadratic axis (an important torque component) for any speed variation [Ref. 17], the rapid DSP should be used. So, we present a decoupling controller which is based on a linear model using the general electrical equations. We obtain a total decoupling of the two phases d and q , and compensation of the magnetomotive forces in the aim to get asymptotic tracking of the torque reference, which can be implemented with a broadly diffused microprocessors.

Equations

Using as states

$$x = \begin{bmatrix} x_1 \\ x_2 \\ x_3 \end{bmatrix}, \quad x_1 = I_d, \quad x_2 = I_q, \quad x_3 = \omega_M \quad (3.27)$$

and as input variables

$$u = \begin{bmatrix} u_1 \\ u_2 \end{bmatrix}, \quad u_1 = U_d, \quad u_2 = U_q \quad (3.28)$$

We can rewrite the equations (3.16, 3.17) in the state form

$$\dot{x} = Ax + Bu \quad (3.29)$$

with

$$A = \begin{bmatrix} A_1 x \\ A_2 x \\ A_3 x \end{bmatrix}, \quad B = \begin{bmatrix} B_1 & 0 \\ 0 & B_2 \\ 0 & 0 \end{bmatrix} \quad (3.30)$$

where

$$A_1 x = -I_d / \tau_d + p I_q \frac{L_q}{L_d} \omega_M$$

$$A_2 x = -I_q / \tau_q - p I_d \frac{L_d}{L_q} \omega_M + p \frac{\psi_m}{L_q} \omega_M$$

$$A_3 x = p I_d I_q (L_d - L_q) / J + p \frac{\psi_m}{J} I_q - \omega_M / \tau_M - T_{ML} / J$$

$$\tau_M = J / \xi_M, \quad \tau_d = L_d / R, \quad \tau_q = L_q / R$$

3.3.1 Decoupling current control of a brushless motor

In this strategy we neglect the dynamic non-linear effects of the mechanical speed ω_M , considering that this is varying slowly. We can then rewrite the state equations, with only two state variables I_d and I_q , as follows

$$\dot{x} = Ax + Bu \quad (3.31)$$

with

$$A = \begin{bmatrix} -R/L_d & p\omega_M L_q/L_d \\ -p\omega_M L_d/L_q & R/L_q \end{bmatrix} \quad (3.32)$$

and

$$B = \begin{bmatrix} 1/L_d & 0 \\ 0 & 1/L_q \end{bmatrix} \quad (3.33)$$

with

$$x = \begin{bmatrix} I_d \\ I_q \end{bmatrix}, \quad u = \begin{bmatrix} U_d \\ U_q - p\psi_m \omega_M \end{bmatrix} \quad (3.34)$$

The aim of every classical machine control is to control at first the torque of the motor. As we can see from equation of the torque (3.17), if we can maintain I_d to zero we get

$$T_M = T_{em} = p\psi_m I_q \quad (3.35)$$

Thus, controlling the torque means controlling the current I_q . That is why we chose as output variables the currents I_d and I_q as follows

$$c = Dx \quad (3.36)$$

with

$$D = \begin{bmatrix} 1 & 0 \\ 0 & 1 \end{bmatrix} \quad (3.37)$$

We consider an input vector u , in order to obtain the following first order decoupled response for outputs

$$dI_d / dt = K_1 (I_{dref} - I_d) \quad (3.38)$$

$$dI_q / dt = K_2 (I_{qref} - I_q)$$

where I_{dref}, I_{qref} constant references.

The matrix B are being always non-singular, we get the necessary input vector

$$\begin{bmatrix} U_1 \\ U_2 \end{bmatrix} = B^{-1} \left\{ \begin{bmatrix} K_1(I_{dref} - I_d) \\ K_2(I_{qref} - I_q) \end{bmatrix} - Ax \right\} \quad (3.39)$$

and so

$$U_d = K_1 L_d (I_{dref} - I_d) + R I_q - pL_q \omega_M I_q \quad (3.40)$$

$$U_q = K_2 L_q (I_{qref} - I_q) + R I_d + pL_q \omega_M I_q + p\psi_m \omega_M$$

This strategy allows us to impose the steady states I_{dref}, I_{qref} , with the dynamics for the errors described by the equations

$$de_1 / dt = K_1 (I_{dref} - I_d) \quad (3.41)$$

$$de_2 / dt = K_2 (I_{qref} - I_q)$$

It is now very easy to place the poles of the system by adjusting the coefficients K_1 and K_2 . With stable poles, the errors converge to zero and the currents I_d and I_q converge to their references $I_{d\text{ref}}$ and $I_{q\text{ref}}$ respectively.

The Figure 3.11 gives the general structure of decoupling control of the currents I_d and I_q . The obtained resulting structure can be interpreted as an extension of the classical proportional regulations.

For implementation of this controller we should use a direct digital control strategy. This means that each variable which intervenes in the calculations, should be measured and immediately converted by an A/D converter linked to a microprocessor board [Ref. 2].

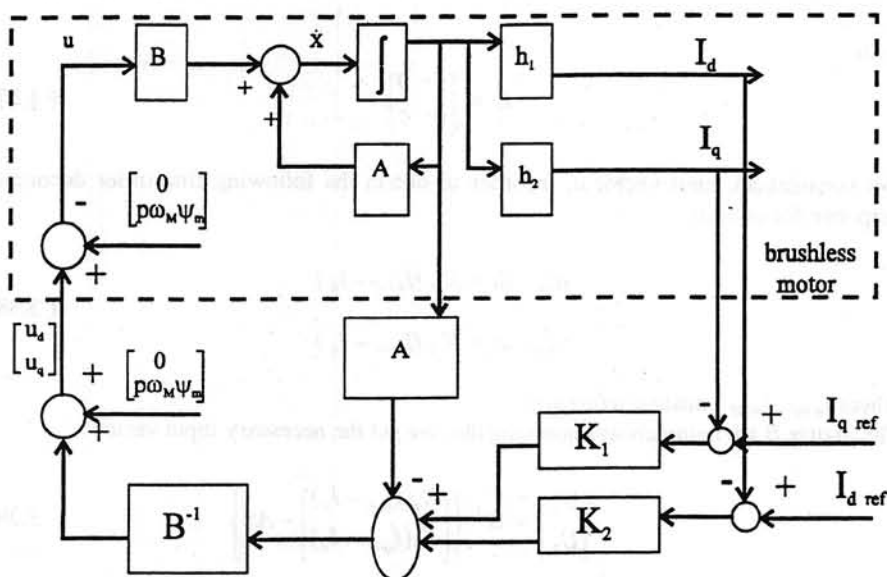


Fig.3.11 Decoupling controller for the brushless motor

The microprocessor provides successively

- the d,q -axes transformations I_d and I_q of the three phases currents of the motor
- the result of the control algorithm (required voltages U_d and U_q)
- the reference three phase voltages, calculated from U_d and U_q by reverse d,q -axes transformations.

The first remark is that such a control can only be implemented in d,q - frame (the referential linked with the rotor with direct and quadrature axes). Moreover, such a regulation asks much more calculations to the microprocessor than a simple proportional regulation. We can chose $K_1 = K_2 = K$ so that the reaction of the system will be as fast

in the direct axis than in the quadrature one. Moreover, in the purpose to accelerate the calculation time, we can chose for implementation this algorithm with $L_d = L_q$ in equations (3.32).

In order to impose to the motor the calculated voltages U_d and U_q , we should use a PWM inverter, linking the motor d,q -axes to the conduction rate CR_A, CR_B, CR_C by the following relation [Ref. 9]

$$\begin{bmatrix} U_d \\ U_q \end{bmatrix} = U_{DS} T_{32} \begin{bmatrix} CR_A \\ CR_B \\ CR_C \end{bmatrix} \quad (3.42)$$

where U_{DS} is the DC voltage of the inverter and T_{32} is transformation matrix from phase axes A,B,C to d,q - axes

$$T_{32} = \begin{bmatrix} \sin(\theta_M) & \sin(\theta_M - 2/3\pi) & \sin(\theta_M + 2/3\pi) \\ \cos(\theta_M) & \cos(\theta_M - 2/3\pi) & \cos(\theta_M + 2/3\pi) \end{bmatrix} \quad (3.43)$$

So the conduction rates $CR_{A,B,C}$ can be given as

$$\begin{bmatrix} CR_A \\ CR_B \\ CR_C \end{bmatrix} = \begin{bmatrix} 0.5 \\ 0.5 \\ 0.5 \end{bmatrix} + \frac{1}{U_{DS}} \begin{bmatrix} K_1 & K_2 & K_3 \\ K_3 & K_1 & K_2 \\ K_2 & K_3 & K_1 \end{bmatrix} \begin{bmatrix} I_A \\ I_B \\ I_C \end{bmatrix} + \frac{1}{U_{DS}} \sqrt{\frac{2}{3}} \begin{bmatrix} \cos(p\theta_M + \frac{\pi}{2}) \\ \cos(p\theta_M + \frac{\pi}{2} - \frac{2\pi}{3}) \\ \cos(p\theta_M + \frac{\pi}{2} + \frac{2\pi}{3}) \end{bmatrix} (KLI_{qref} + p\psi_m \omega_M) \quad (3.44)$$

with

$$\begin{aligned} K_1 &= R - KL \\ K_2 &= -1/2(R - KL) - \frac{\sqrt{3}}{2} pL\omega_M \\ K_3 &= -1/2(R - KL) + \frac{\sqrt{3}}{2} pL\omega_M \end{aligned} \quad (3.45)$$

The dynamics of the currents and the speed are different enough to consider that we should calculate with two scales of time. The slow scale should be used for calculations relative to the speed, and the fast one is for the currents and also for position control.

Chapter 4

PRELIMINARY SYSTEM APPROACH TO DESIGN OF ELECTROMECHANICAL ACTUATORS FOR AIRCRAFT CONTROL SURFACES

The system approach to design of electromechanical actuators for control surfaces is a complex engineering problem due to the numerous parameters, constraints, and performance requirements which must be satisfied. When this task is coupled with optimisation, the design becomes more difficult.

Generally, the solution of this scientific problem should include three interactive basic research levels:

- preliminary system analysis and evaluation design of the electromechanical actuators for aircraft flight control surfaces (ailerons, rudders, elevators, spoilers, etc.)
- the analysis, synthesis and design of the general electrical and secondary power systems for the aircraft according to the new abundant group of the electrical loads (electromechanical actuators)
- the integration of the electromechanical actuators into the power, control, digital avionics, and mechanical systems environment of the aircraft, in corresponding with the requirements for reliability, redundancy, electromagnetic compatibility, etc.

Let us consider the basic stages of the strategy for design of the electromechanical actuators for aircraft control surfaces. This first research level comprises the numerous essential design stages, and, particularly, includes

- the power considerations for electromechanical actuators
- the selection of the basic structure and hardware for electromechanical actuators (brushless motor, inverter, resolver, encoder, PWM, etc.)
- the creation of the software for the synthesis and analysis of the dynamic, steady-state behaviour and control operation (stability, observability) of the electromechanical actuators
- the design of the controllers for electromechanical actuators
- the estimation of the software and hardware compatibility

An important criteria in specifying an electromechanical actuation system (EMAs) is the duty cycle to which it should be designed and tested. Criteria used in the design of

controllers, inverters, and brushless motors will be power demand and efficiency. Power demand is determined by using actuator loads to find peak and average horsepower requirements during various phases of the flight. Efficiency is determined by measuring heat generated during each flight phase and expressing it as dissipated energy. As power requirements and heat generation values will be determined, weight, envelope, and system complexity can also be defined.

Surface loads The mission profile of an aircraft is separated into general flight phases (ground operation, take-off, climb, turbulence, descent, cruise, terrain following, approach, landing), and consequently each of them consists of the additional internal phases, and characterised by inherent elapsed time, velocity, altitude, etc. From the flight phases, loads are derived using altitude, dynamic pressure, amplitude of excursion from flight surface activity, and hinge moment coefficient considerations as shown below

$$H_M = 1/2 \rho V^2 C_{ha} S \bar{c} \quad (4.1)$$

where

- ρ is the air density (the function of temperature and altitude)
- V is the true air speed (TAS)
- C_{ha} is a hinge moment coefficient (a function of surface and tab position)
- S is the surface reference area
- \bar{c} is the mean aerodynamic chord

Hinge moment (4.1) is then transferred to the actuator to determine actuator load. Let us take into account the fact that the EMA system load demands are proportional to the torque demands of its actuators (hydraulic system load demands are proportional to the rate of its actuators) [Ref. 31]. The electric actuator requires peak power at stall and requires a continuous supply of power while holding against a constant load (conversely, a hydraulic actuator exhibits a peak demand at high surface rate, no-load conditions and no demand when required to hold against a constant load [Ref.19,31]).

Power The required power at the bus and system inefficiencies, expressed as a function of time should be the final result of the duty cycle calculations. The calculated values of the peak power for the rudder, elevators, ailerons, etc. should be used for the design of EMA flight control surfaces (FCS). Evaluating FCS peak power requirements during each flight phase requires a further power and heat analysis. The required power at the distribution bus should be expressed in Watts (kilowatts). The horsepower equation is

$$H_P = T_{ML} \omega_L 2\pi / 60 \quad (4.2)$$

where

- T_{ML} is the actuator (motor) load torque (flight control surface moment),
- ω_L is the load (surface) speed in revolutions per minute

From every flight phase a hinge moment should be used as the surface moment. An average surface rate can be obtained using number of cycles per second of surface activity. Rates in cycles/sec of surface activity can be derived from flight test traces of existing aircraft or from aerodynamic models based on the response of the aircraft given weight, inertia, and aerodynamic characteristics. Calculated horsepower is then changed to peak power in Watts at the surface and adjusted for motor, controller, actuator, and other inefficiencies. Efficiency values of the system components may range from 65% to 98% [Ref. 3]. An overall efficiency value of 85% can be used to determine the power required at the bus.

System inefficiencies or power dissipated as heat should be then calculated by subtracting the power required at the bus from the power required at the surface. All these calculations are required for the rudders, elevators and ailerons to complete the analysis of the system.

Using the aircraft's duty cycle to analyse components for power and heat dissipation is a valuable tool that helps to predict weight requirements and in some cases reduce them.

The further strategy of EMAs design is including:

- the estimation of variables that must be considered in the design phase of an electromechanical systems,
- the main constraints that must be addressed and analysed during preliminary design,
- the design methods and optimisation strategy for elements of electromechanical actuation system.

The principal issue of preliminary design in electromechanical actuation systems with rotary or linear outputs concerns brushless motor sizing and selection. The motor capabilities are determine the system performance, while motor design is dependent on external system parameters and internal design constraints. The problem is complex according to:

- Multidisciplinary design (electrical, mechanical, controls),
- Numerous design parameters (linear and non-linear),
- Numerous design constraints (imposed and inherent)
- Optimisation of numerous parameters in many cases.

The design problem for electromechanical actuation systems may be viewed as attempting to create a system which simultaneously satisfies requirements in the areas of performance, installation, and function.

Performance comprises the following specific requirements:

- Speed-Torque parameters --The required minimum speed attainable by electromechanical actuator at steady-state as a function of load torque.
- Frequency response --The effective bandwidth of the system. This is usually taken as the cross-over frequency of the open-loop system at a specified input amplitude; open-loop phase lag at the cross-over will typically be 120 deg or less for stability considerations.

- Trajectory Response -- System responses (usually position) as a function of time. These are specific response trajectories which must be capable of being reproduced for successful operation of the system.
- Duty Cycle -- Rate and torque as a function of time. The system must be capable of operating at the specified rates and torques without loss of performance in the preceding areas or failure.

Installation usually comprises of the following requirements:

- Envelope dimensions and weight for electromechanical actuator components (including invertors, brushless motors, gear boxes , etc.).
- Envelope dimensions and weight for the controllers.

Functional requirements are highly dependent on the application, but should address the following as a minimum:

- Electrical power source characteristics.
- Redundancy requirements.
- Operating requirements after failures
- Rotary or linear actuator configuration.
- System stiffness requirements (temperature, electromagnetic compatibility, etc.).

While the above is not by any means an exhaustive set of requirements, it is relatively complete for the purpose of sizing brushless motors, controllers, and actuators.

Models For analysing requirements and size system components, a previous model of an electromechanical actuation system is required. A simplified model is represented in Figure 4.1. The required parameters for further analysis are treated in the figure and summarised in Table 4.1. The model presented in Figure 4.1 includes mechanical dynamics, but not electrical dynamics; a detailed model of the brushless motor is required for this purpose (See Chapter 3). A simplified motor model is shown in Figure 4.2. The motor model includes both mechanical (rotor) and electrical (winding) dynamics.

Equations From the design models and references in the literature [Ref. 6, 11, 21, 38, 46], set of design governing equations can be developed for the motor and load (see Table 4.1,4.2 for equation nomenclature)

Motor equations can be written as

$$U_M = U_E + R_M I_M + L_M dI_M / dt \quad (4.3)$$

$$U_E = K_E d\theta_M / dt \quad (4.4)$$

The motor torque T_M is equal to the torque delivered to the load. Let the total moment of inertia (including rotor, motor shaft and gear 1) and damping coefficient on the motor shaft be J_M and ξ_M , respectively and those on the load shaft be J_L and ξ_L . Additionally, spring coefficient K_L , and viscous friction coefficient T_F are on the load

Electromechanical Actuation System Model Parameters

Table 4.1

Parameter	Description	Units
θ_A	Electromechanical actuator position reflected to the load	rad
θ_C	Commanded position	rad
θ_L	Load position	rad
θ_M	Brushless motor position	rad
$d\theta_M/dt$	Brushless motor speed	rad/sec
X_A	Actuator position	rad
η_A	Actuator efficiency	
$\dot{\xi}_L$	Load damping	N / sec
G_D	Drive ratio, motor-to-load	
I_M	Brushless motor current	A
I_S	Power source current	A
J_L	Load inertia	N m
J_M	Brushless motor inertia	N m
T_F	Load friction	N m
K_L	Load spring rate	N m / rad
T_L	Total load torque	N m
T_{LL}	Applied load torque	N m
T_M	Brushless motor torque	N m
U_E	Brushless motor back EMF	V
U_S	Power source voltage	V

Table 4.2

Motor Model Parameters

Parameter	Description	Units
θ_M	Motor position	rad
$d\theta_M/dt$	Motor speed	rad /sec
I_M	Motor current	A
ξ_M	Motor damping	N / sec
J_M	Motor inertia	kg m ²
K_E	Motor voltage constant	V / (rad/sec)
K_T	Motor torque constant	N m /A
L_M	Motor inductance	henry
R_M	Motor resistance	ohm
T_{ML}	Motor-load torque	N m
T_M	Motor torque	N m
U_M	Motor voltage	V

shaft. The torque T_M generated by the motor must drive J_M , overcome ξ_M and generate a torque T_{ML} at gear 1 to drive the second gear. Torque T_{ML} at gear 1 generates a torque T_L at gear 2, which in turn drives J_L , and overcomes ξ_L , K_L , T_F .

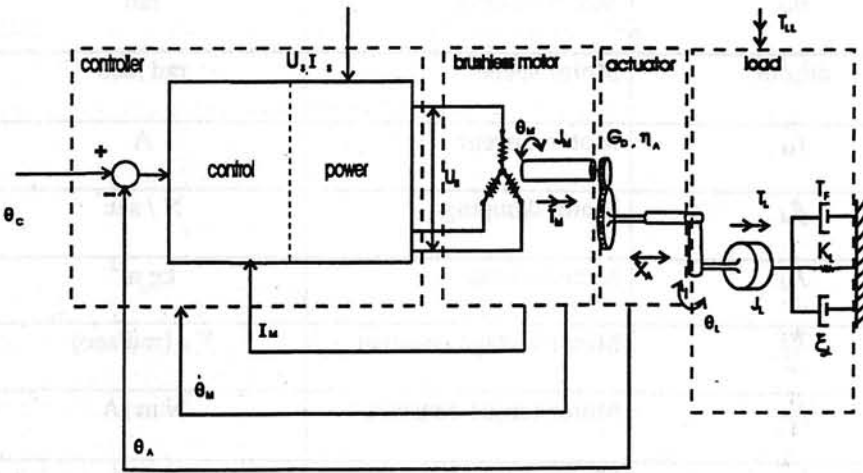


Fig. 4.1 Electromechanical actuation system Model

Thus we have

$$T_M = T_{ML} + \xi_M \frac{d\theta_M}{dt} + J_M \frac{d^2\theta_M}{dt^2} \quad (4.5)$$

$$T_M = K_T I_M \quad (4.6)$$

$$S_M = -R_M / (K_E K_T) \quad (4.7)$$

Load equations can be written

$$\theta_L = \theta_M / G_D \quad (4.8)$$

$$T_L = T_{LL} + T_F \text{sign}(d\theta_L/dt) + K_L \theta_L + \xi_L (d\theta_L/dt) + J_L (d^2\theta_L/dt^2) \quad (4.9)$$

$$T_L = \eta_A G_D T_M \quad (4.10)$$

$$S_L = S_M / (\eta_A G_D^2) \quad (4.11)$$

For a preliminary design let us assume

$$T_F \text{sign} (d\theta_L / dt) \approx T_F (d\theta_L / dt)$$

The substitution of the equations (4.8, 4.10) into (4.9) converts the load, friction, spring, and damping on the load shaft into the motor shaft. Transforming equations (4.3, 4.4, 4.5, 4.6, 4.9), we obtain governing equations

$$U_M = K_E d\theta_M / dt + R_M I_M + L_M dI_M / dt \quad (4.12)$$

$$K_T I_M = T_L / \eta_A G_D + \xi_M d\theta_M / dt + J_M d^2 \theta_M / dt^2 \quad (4.13)$$

$$T_L = T_{LL} + \frac{T_F}{G_D} d\theta_M / dt + \frac{K_L}{G_D} \theta_M + \frac{\xi_L}{G_D} d\theta_M / dt + \frac{J_L}{G_D} d^2 \theta_M / dt^2 \quad (4.14)$$

The equivalent model contains two input signals U_M and T_{LL} .

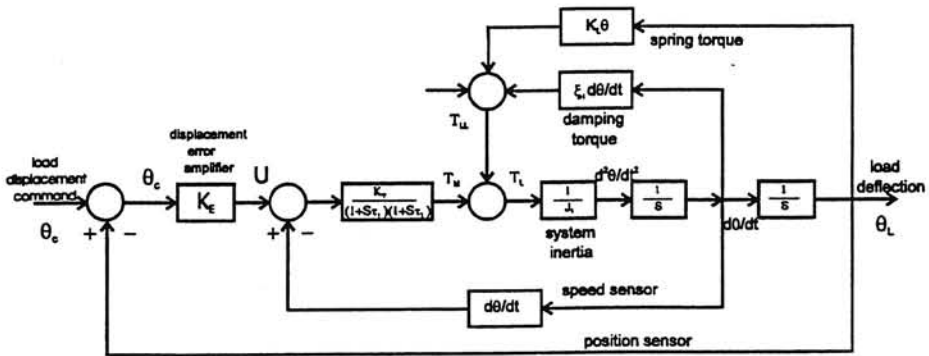


Fig. 4.2 Actuation closed-loop block diagram

Let us represent a transfer function of a such system (see Fig. 4.2). At first we consider the set of differential equations (4.12, 4.13, 4.14) on condition that $T_{LL} = 0$.

Using Laplace transformation, we obtain the set of governing equations

$$U_M (S) = K_E S \theta_M (S) + R_M I_M (S) + L_M S I_M (S)$$

$$K_T I_M (S) = T_L (S) / \eta_A G_D + \xi_M S \theta_M (S) + J_M S^2 \theta_M (S) \quad (4.15)$$

$$T_L (S) = T_F / G_D S \theta_M (S) + K_L / G_D \theta_M (S) + \xi_L / G_D S \theta_M (S) + J_L / G_D S^2 \theta_M (S)$$

Rearranging equations (4.15), we have

$$I_M (S)(R_M +L_M S) = U_M (S) - K_E S\theta_M (S)$$

$$I_M (S)= (U_M (S) - K_E S\theta_M (S))/ (R_M +L_M S) \quad (4.16)$$

$$\eta_A G^2_D K_T U_M (S)= [(T_F + \xi_L + \xi_M \eta_A G^2_D)S\theta_M (S)+$$

$$(J_L + J_M \eta_A G^2_D)S^2 \theta_M (S)](R_M +L_M S) + K_T K_E \eta_A G^2_D S\theta_M (S) \quad (4.17)$$

Representing J_1 and ξ_1 as follows

$$J_1 = J_L + J_M \eta_A G^2_D$$

$$\xi_1 = T_F + \xi_L + \xi_M \eta_A G^2_D$$

equation (4.17) becomes

$$\eta_A G^2_D K_T U_M (S)=S[(R_M +L_M S)(J_1 S + \xi_1) + K_T K_E \eta_A G^2_D] \theta_M (S) \quad (4.18)$$

Using equation (4.18), we obtain the transfer function $G_I (S)$ (with $T_{LL}(S) = 0$)

$$G_I (S)= \theta_M (S)/U_M (S) = \frac{K_T \eta_A G^2_D}{S[(R_M + L_M S)(J_1 S + \xi_1) + K_T K_E \eta_A G^2_D]} =$$

$$= \frac{K_T \eta_A G^2_D / L_M J_1}{S(S^2 + S(R_M J_1 + L_M \xi_1) / L_M J_1 + (K_T K_E \eta_A G^2_D + R_M \xi_1) / L_M J_1)} \quad (4.19)$$

For the next step we consider the set of differential equations (4.12, 4.13, 4.14) on condition that $U_M = 0$.

Using Laplace transformation, we obtain the set of governing equations

$$0 = K_E S\theta_M (S) + R_M I_M (S) + L_M S I_M (S)$$

$$K_T I_M (S)= T_L (S) / \eta_A G_D + \xi_M S\theta_M (S)+ J_M S^2 \theta_M (S) \quad (4.20)$$

$$T_L (S)=T_{LL}(S) + T_F / G_D S\theta_M (S) + K_L / G_D \theta_M (S)+$$

$$\xi_L / G_D S\theta_M (S) + J_L / G_D S^2 \theta_M (S)$$

Rearranging equations (4.20), we obtain

$$I_M(S)(R_M + L_M S) = -K_E S \theta_M(S)$$

$$I_M(S) = -K_E S \theta_M(S) / (R_M + L_M S) \quad (4.21)$$

$$T_{LL}(S)(R_M + L_M S) G_D = -\{[(T_F + \xi_L + \xi_M \eta_A G_D^2) S \theta_M(S) + (J_L + J_M \eta_A G_D^2) S^2 \theta_M(S)] / (R_M + L_M S) + K_T K_E \eta_A G_D^2 S \theta_M(S)\} \quad (4.22)$$

As before

$$J_1 = J_L + J_M \eta_A G_D^2$$

$$\xi_1 = T_F + \xi_L + \xi_M \eta_A G_D^2$$

equation (4.22) becomes

$$T_{LL}(S)(R_M + L_M S) G_D = -S\{[(R_M + L_M S)(J_1 S + \xi_1) + K_T K_E \eta_A G_D^2] \theta_M(S)\} \quad (4.23)$$

Using equation (4.23), we obtain the transfer function $G_2(S)$ (with $U_M(S) = 0$)

$$G_2(S) = \theta_M(S) / T_{LL}(S) = - \frac{(R_M + L_M S) G_D}{S[(R_M + L_M S)(J_1 S + \xi_1) + K_T K_E \eta_A G_D^2]} =$$

$$= - \frac{(R_M + L_M S) G_D / L_M J_1}{S(S^2 + S(R_M J_1 + L_M \xi_1) / L_M J_1 + (K_T K_E \eta_A G_D^2 + R_M \xi_1) / L_M J_1)} \quad (4.24)$$

Consequently, the transfer function $G_3(S)$ for no-load motor can be obtain from the equations (4.3, 4.4, 4.5)

$$G_3(S) = \theta_M(S) / U_M(S) = \frac{K_T}{S(L_M J_M S^2 + R_M J_M S + K_E K_T)} = \frac{K_T / L_M J_M}{S(\tau_1 S + 1)(\tau_2 S + 1)} \quad (4.25)$$

where

τ_1, τ_2 are the roots (poles) of the equation

$$S^2 + R_M / L_M + K_E K_T / L_M J_M \quad (4.26)$$

Table 4.3

Motor Design Constraints

Parameter	Description	Reasons for constraint	Units
j_c	Winding current density	Thermal	A/m ²
J_M	Rotor inertia	Acceleration	N m
L_M	Winding inductance	Commutation, current control, current response	henry
L_R / D_R	Rotor length/diameter	Manufacturing, installing magnets, maximum speed	
R_M	Winding resistance	Thermal, current response, stator dimensions	ohm
τ_E	Electrical time constant	Current control, current response	sec
τ_M	Mechanical time constant	Speed response	sec
dX_R / dt	Rotor surface velocity	Stress	m / sec

Constraints In addition to the design equations, there is a set of design constraints which must be applied to the general equations in order to ensure that the specified performance of an electromechanical actuator will be achieved. These constraints could be obtained from the performance requirements discussed above as speed-torque, frequency response, trajectory response, and duty cycle (Table 4.4, 4.5, 4.6)

Additionally we must include the constraints on brushless motor design geometry and electromagnetic characteristics observed so that the motor be practical to fabricate, and will accommodate the preceding requirements (Table 4.3).

Options Future size design and/or selecting a suitable brushless motor (servomotor) strategy must accommodate as many of the preceding design goals and constraints as possible. Two basic approaches are commonly used:

- select a motor design from the catalogues and evaluate it until a successful design is found
- design an optimal brushless motor for the application, compare with available designees and 1) use an existing design, or 2) build the new one.

Both approaches have advantages and are workable design strategies. However, the second strategy will determine an optimum design for an application. For these reasons, the latter strategy is pursued.

Approach Brushless motor acceleration is usually the critical dynamic performance constraint [Ref.14]. Knowing that acceleration is often critical, this information should be used for formulation a design algorithm for brushless motors. The basic principal steps can be presented in the following way

1. Selection of G_D and η_A by using a desired no-load $d\theta_M/dt$
2. Calculation of a maximum allowable J_M
3. Selection of a rotor length-to-diameter ratio (l_R/D_R)
4. Calculation of a D_R and l_R
5. Selecting of the permanent magnet rotor and stator winding configurations
6. Calculation of the stator's length l_S and diameter D_S
7. Check of design constraints (if design is feasible-- proceed; if design is infeasible--iteration of steps 3 or 5 above)

Table 4.4

Design Constraint Nomenclature

Parameter	Description	Units
$d\theta_{max}/dt$	Maximum actuator rate, loaded	rad /sec
$d^2\theta_{max}/dt^2$	Maximum actuator acceleration, loaded	rad / sec ²
$d\theta_{no-load} / dt$	Actuator required no-load rate	rad /sec
θ_{peak}	Maximum motor temperature (peak)	°C
θ_{cont}	Maximum motor temperature (continuous)	°C
ω_s	System bandwidth	rad / sec
A	Frequency response amplitude	rad
S_{min}	Minimum actuator speed-torque slope	(rad/sec) / N m
t	Time	sec
t_T	Trajectory duration	sec
T_{max}	Maximum actuator torque	N m
dT_{max} / dt	Maximum actuator torque-rate	N m / sec
T_{stall}	Actuator required stall torque	N m
W_{max}	Actuator output power	watt
dW / dt	Actuator output power rate	watt / sec

Table 4.5

DESIGN EQUATION NOMENCLATURE

Parameter	Description	Units
τ_1, τ_2	System time constants	sec
K_M	Transfer function gain	(rad/sec)/V
S	Laplace transform variable	sec ⁻¹
S_L	Actuator speed-torque slope	(rad/sec)/N m
S_M	Motor speed-torque slope	(rad/sec)/N m

GENERAL CONSTRAINTS FOR DESIGN OF AN ELECTROMECHANICAL ACTUATOR

Constraints	Description
Speed-torque	$d\theta_{max}/dt \geq d\theta_{no-load}/dt$
	$T_{max} \geq T_{stall}$
	$0 \geq S_{min} \geq S_L$
Frequency Response	$\omega_c \leq \min [\text{Mag} (1/\tau_1) , \text{Mag} (1/\tau_2)]$
	$d\theta_{max}/dt \geq A \omega_c$
	$d^2\theta_{max}/dt \geq A^2 \omega_c$
	$T_{max} \geq \max [T_L (t)]$
	$dT_{max}/dt \geq \max [dT_L / dt]$
	$dW_{max}/dt \geq \max [d\theta_L / dt T_L (t)]$
	$d^2 W_{max} / dt^2 \geq \max [d^2\theta_L / dt^2 T_L(t) + d\theta_L / dt dT_L / dt]$
Trajectory Response	$d\theta_{max}/dt \geq \max [d\theta_L / dt]$
	$d^2\theta_{max}/dt \geq \max [d^2\theta_L / dt^2]$
	$0 \leq t \leq t_T$
Duty Cycle	$\Theta_{peak} \geq \max [\Theta_M (d\theta_L / dt), T_L, t]_{peak}$
	$\Theta_{cont} \geq \max [\Theta_M (d\theta_L / dt), T_L, t]_{cont}$

These general steps should be used as a framework or startpoint for a larger, more detailed electromagnetic and electromechanical design algorithm for brushless motors.

REFERENCES

- [1] "ABB Semiconductor Catalogue" 1995/1996
- [2] Astrom K. J., Wittenmark B., 1990, "Computer controlled systems", Prentice-Hall Inc., N.J., USA
- [3] Bartley G., 1994, "Model 777 primary flight control system", Airliner, Oct-Dec
- [4] Bodson M., Chiasson J.N., Novotnak R.T., and Rekowski R.B., 1993, "High performance nonlinear feedback control of a permanent magnet stepper motor", IEEE Transactions on Control Systems Technology, 1, N1, 5-14
- [5] Bollinger J. G., Duffie N. A., 1993, "Computer control of machines and processes", Addison-Wesley Publishing Company, USA
- [6] Bout D.A., 1990, "Brushless electrical machines", Higher School, Moscow, Russia
- [7] Cronin M.J., 1990, "Advanced power generation systems for more electric aircraft", SAE Technical Paper Series, N 912186
- [8] Chi-Tsong Chen, 1991, "Analog and digital control system design: transfer-function, state-space, and algebraic methods", Saunders College Publishing
- [9] Doeuff R.L., Robert J. (eds), 1991, "Modelling and control of electrical machines: New trends", IMACS, Elsevier Science Publishers B.V., North-Holland
- [10] Dorf R.C., Bishop R. H., 1995, "Modern control systems", Seventh Edition, Addison-Wesley Publishing Company, USA
- [11] Dote Y., Kinoshita S., 1990, "Brushless servomotors: fundamentals and applications", Clarendon Press, Oxford, U.K.
- [12] Francis J. H., 1973, "Introduction to control system analysis and design", Prentice-Hall Inc., N.J., USA
- [13] Franklin G.F., Powell J.D., Workman M.L., 1990, "Digital control of dynamic systems", Second Edition, Addison-Wesley Publishing Company, USA
- [14] General Requirements of Synchronous Machines", ANSI Standard C50.10-1977, June, 1977
- [15] Isidory A., 1989, "Non linear control systems, an introduction", 2 edition, Springer-Verlag
- [16] Hanselman D.C., 1994, "Brushless permanent-magnet motor design", McGraw-Hill. Inc., USA
- [17] Hemati N., Thorp J.S., and Leu M.C., 1990, "Robust nonlinear control of brushless dc motors for direct-drive robotic applications", IEEE Transactions on Industrial Electronics, 37, N6, 460-468
- [18] Hoffman A.C., Hansen I.G., Beach R.F. et al, 1985, "Advanced secondary power system for transport Aircraft", NASA Technical Paper, 2463
- [19] Johnson T.W., 1977, "Primary flight control actuation with electric motors", NAECON, 1102-1107
- [20] Kassakian J.G., Schlecht M.F., Verghese G.C., 1991, "Principles of power electronics", Addison-Wesley Publishing Company
- [21] Kenjo T., Nagamori S., 1985 "Permanent-magnet and brushless DC motors", Clarendon Press, Oxford, U.K.
- [22] King R.J., 1983, Dissertation "Dynamic modeling of the series resonant DC-DC converter", The University of Toledo, USA
- [23] Kosow I.L., 1983, "Control of electric machines", Prentice-Hall Inc., N.J., USA

- [24] Kuo B.C., Hanselman D.C., 1994, "Matlab tools for control system analysis and design", Prentice Hall Englewood Cliffs, NJ, USA
- [25] Leonhard W., 1985, "Control of Electrical Drives", Springer-Verlag Berlin, Heidelberg, Germany
- [26] McMurray W., 1978, "Thyristor commutation in DC choppers -- a comparative study", IEEE Transactions on Industry and Applications, IA-14, N 6
- [27] Miller T.J.E., 1993, "Switched Reluctance Motors and their control", Magna Physics Publishing and Clarendon Press, Oxford, U.K.
- [28] Nasar S.A., Boldea I., Unnewehr L.E., 1993, "Permanent magnet, reluctance, and self synchronous motors", CRC Press, Inc., Florida, USA
- [29] Nasar S.A., Unnewehr L.E., 1983, "Electromechanics and Electric machines", Second edition, John Wiley & Sons, Canada
- [30] Neomax - a super energy rare earth magnet", Sumitomo Technical Brochure, No 580602, Sumitomo Special Metals Co. Ltd., Osaka, Japan
- [31] Niggemann R. E., Peecher S., Rozman G.I., 1993, "270-Vdc/hybrid 115 Vac electric power generating system technology demonstrator evolution to a dual -- channel, more electric aircraft technology development testbed", SAE Technical Paper Series, N 912183
- [32] Ogata K., 1994, "Solving control engineering problems with MATLAB", Prentice-Hall, Inc, NJ, USA
- [33] Radun A., Richter E., 1993, "A detailed power inverter design for a 250 kW switched reluctance aircraft engine starter/generator", SAE Technical Paper Series, N 931388
- [34] Roffel B., Vermeer P.J., Chin P.A., 1989, "Simulation and implementation of self-tuning controllers", Prentice Hall, Englewood Cliffs, NJ 07632
- [35] Rosswurm M.A., 1981, "Design considerations of DC-Link Aircraft Generation Systems", SAE Technical Paper Series, N811081
- [36] Rowe S.A., 1985, "Preliminary Design of Electromechanical servosystems", SAE Technical Paper Series, N 851759
- [37] Segrest J.D., Cloud W.W., 1981, "Evolution and development of high voltage (270 volt) DC aircraft electric systems in the United States", SAE Technical Paper Series, N 811087
- [38] Silvester P.P., 1990, "Advances in Electrical Engineering Software", Computational Mechanics Publications, Southampton Boston, USA
- [39] Silvester P.P., 1993, "Software applications in Electrical Engineering", Computational Mechanics Publications, Southampton Boston, USA
- [40] Silvester P.P., Ferrari R.L., 1990, "Finite Elements for Electrical Engineers", Second edition, Cambridge Univ. Press, U.K.
- [41] Simsic C.J., 1991, "Electric actuation system duty cycles", IEEE, N2, 540-545
- [42] Smith J.R., 1990, "Response analysis of AC electrical machines: computer models and simulation", Wiley, New York, USA
- [43] Sokira J., Wolfgang J., 1990, "Brushless DC motors: electronic commutation and controls", Tab Books Inc., USA
- [44] Tailor E., Croke D., Speck E., 1993, "The use of high voltage direct current in aircraft electrical systems -- a navy perspective", SAE Technical Paper Series, N 912173

- [45] Veltman A., 1994, "The Fish method - Interaction between AC-machines and switching power converters", Ph.D. thesis, TUDelft, The Netherlands
- [46] Williams B.W., 1992, "Power electronics - devices, drivers, applications and passive components", Second edition, McGraw-Hill, Inc., USA
- [47] Yasuhiko D., 1990, "Servo motor and motion control using digital signal processors", Prentice-Hall Inc., N.J., USA
- [48] Zribi M., Chiasson J.N., 1991, "Position control of a PWM stepper motor by exact linearization", IEEE Transactions on Automatic Control, **36**, N5, 620-625

Appendix 1

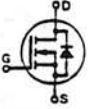
Brushless motor specifications

Due the great diversity in size, shape, and applications of brushless motors, there is still no single standard nor group of standards that covers this class of machine. General requirements for all types of synchronous machines above fractional horsepower ratings are given in ANSI C50. 10-1977 [Ref. 14].

However, when purchasing a new machine or requesting the development of a machine, the principal items must be specified:

- terminal voltage rating of the machine, V
- frequency of the terminal voltage, f, Hz
- approximate waveform of the terminal voltage-sinusoidal, square, etc.
- synchronous speed, related to frequency by $RPM (synch) = 120 f/p$ (where p = number of poles, f = frequency in Hz)
- continuous power rating (shaft power - W or horse power)
- duty cycle of load
- short time peak power of load
- terminal voltage variations
- power factor of motor
- permissible temperature rise and ambient temperature
- type of housing - drip-proof, hermetic, etc.
- other potentially adverse environmental factors
- stability considerations, paralleling, etc.
- motor response time and other dynamic considerations
- mass, size or shape limitations

Standard Power MOSFETs and MegaMOS™ FETs

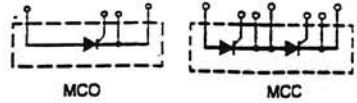


N-Channel Enhancement-Mode


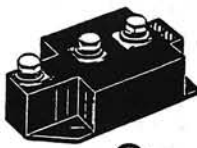
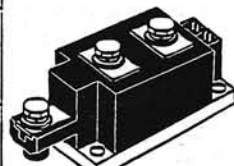
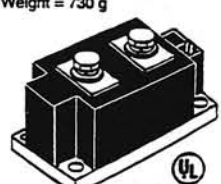
Type	V _{DS} max.	I _{DS}	R _{DS(on)}	C _{iss}	C _{oss}	t _{rr}	Q _g	R _{th(jc)}	P _D	Fig. No.	Package style
T _{amb} = 150°C		T _c = 25°C	T _c = 25°C	typ.	typ.	typ.	max.	max.	max.		
► New	V	A	Ω	pF	pF	ns	nC	K/W	W		Outlines on pages 33/34 S = Source, D = Drain, G = Gate, KS = Kelvin Source
IXTH 67N10	100	67	0.025	4500	550	300	260	0.42	300	4	Fig. 4 TO-247 AD Weight = 6 g
IXTH 75N10		75	0.02								
IRFP 250	200	30	0.085	2600	180	360	140	0.65	190		
IXTH 42N20		42	0.06	4600	285	400	220	0.42	300		
IXTH 50N20		50	0.045								
IRFP 254	250	23	0.14	2990	150	370	140	0.65	190		
IXTH 35N30	300	35	0.1	4600	240	400	220	0.42	300		
IXTH 40N30		40	0.085								
IXTH 12N50A	500	12	0.4	2800	70	600	120	0.7	180		
IRFP 450		14	0.4	2800	150	500	150	0.65	190		
IXTH 21N50		21	0.25	4200	135	600	190	0.42	300		
IRFP 470		24	0.23								
IXTH 24N50		24	0.23								
IXTH 30N50		30	0.17	4900	300	850	250*	0.35	360		
IXTH 15N60	600	15	0.5	4500	140	600	170	0.42	300		
IXTH 20N60		20	0.35								
IXTH 15N70	700	15	0.45	4500	140	600	170	0.42	300		
IXTU 01N80	800	0.1	80	80	1.8	280	10	3	42	8	Fig. 5a TO-204 AE Fig. 5b TO-204 AA Weight = 12 g
IXTU 01N100	1000										
IXTH 6N80	800	6	1.8	2800	100	900	130	0.7	180	4	Fig. 6 TO-264 AA Weight = 10 g
IXTH 6N80A		6	1.4								
IXTH 11N80		11	0.95	4500	65	800	170	0.42	300		
IXTH 13N80		13	0.8								
IXTH 6N90	900	6	1.8	2600	45	900	130	0.7	180		
IXTH 6N90A		6	1.4								
IXTH 10N90		10	1.1	4500	65	900	170	0.42	300		
IXTH 12N90		12	0.9								
IXTH 5N100	1000	5	2.4	2600	45	900	130	0.7	180		
IXTH 5N100A		5	2.0								
IXTH 10N100		10	1.2	4000	70	1000	170	0.42	300		
IXTH 12N100		12	1.05								
IXTH 14N100		14	0.82	5650	150	850	195*	0.35	360		
IXTK 21N100		21	0.55	8400	110	1000	250	0.25	500	6	
IXTH 13N110	1100	13	0.92	5650	150	850	195*	0.35	360	4	
IXTN 79N20	200	85	0.025	9000	600	400	450	0.31	400	7	Fig. 7 SOT-227B miniBLOC Weight = 30 g
IXTN 36N50	500	36	0.12	8500	300	600	350	0.31	400		
IXTN 15N100	1000	15	0.6	8000	150	1000	350	0.31	400		
IXTN 21N100		21	0.55	8400	110	1000	250	0.24	520		
IXTM 67N10	100	67	0.025	4500	550	300	260	0.42	300	5a	Fig. 8 TO-251AA Weight = 1 g
IXTM 75N10		75	0.02								
IXTM 42N20	200	42	0.06	4600	285	400	220	0.42	300		
IXTM 50N20		50	0.045								
IXTM 35N30	300	35	0.1	4600	240	400	220	0.42	300		
IXTM 40N30		40	0.088								
IXTM 12N50A	500	12	0.4	2800	70	600	120	0.7	180	5b	
IXTM 21N50		21	0.25	4200	135	600	190	0.42	300	5a	
IXTM 24N50		24	0.23								
IXTM 15N60	600	15	0.5	4500	140	600	170	0.42	300		
IXTM 20N60		20	0.35								
IXTM 6N80	800	6	1.8	2800	100	900	130	0.7	180	5b	Fig. 8 TO-251AA Weight = 1 g
IXTM 6N80A		6	1.4								
IXTM 11N80		11	0.95	4500	65	800	170	0.42	300		
IXTM 13N80		13	0.8								
IXTM 6N90	900	6	1.8	2600	45	900	130	0.7	180		
IXTM 6N90A		6	1.4								
IXTM 10N90		10	1.1	4500	65	900	170	0.42	300		
IXTM 12N90		12	0.9								
IXTM 5N100	1000	5	2.4	2600	45	900	130	0.7	180		
IXTM 5N100A		5	2.0								
IXTM 10N100		10	1.2	4000	70	1000	170	0.42	300		
IXTM 12N100		12	1.05								

⊠ Not for new design. ⊡ Either terminal can be used as Kelvin or Main. Data at 25°C unless otherwise specified * Typical value

Thyristor Modules, Single and Double

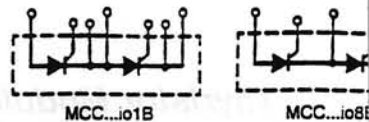


$I_{TAV} = 130-500 \text{ A}$

Type	V_{RSM} V_{DRM} V	I_{TAV} A	T_C °C	I_{TSM} A	I_{TSM} 45°C 10 ms A	V_{T0} V	r_T mΩ	T_{VM} °C	$R_{th(jc)}$ per chip K/W	$R_{th(jc)}$ per chip K/W	Fig. No.	Package style See outlines on page 34
► New MCC132-081o1 MCC132-121o1 MCC132-141o1 MCC132-161o1 MCC132-181o1	800 1200 1400 1600 1800	130	85	300	5500	0.8	1.5	125	0.23	0.1	28	Fig. 28 Weight = 125 g 
► MCC161-201o1 ► MCC161-221o1	2000 2200	175	85	300	6000	0.8	1.3	125	0.155	0.07		
► MCC162-081o1 ► MCC162-121o1 ► MCC162-141o1 ► MCC162-161o1 ► MCC162-181o1	800 1200 1400 1600 1800	181	85	300	6000	0.8	1.15	125	0.155	0.1		
► MCC170-121o1 ► MCC170-141o1 ► MCC170-161o1 ► MCC170-181o1	1200 1400 1600 1800	203	85	350	5400	0.8	1.0	130	0.164	0.04	31	
► MCC220-081o1 ► MCC220-121o1 ► MCC220-141o1 ► MCC220-161o1	800 1200 1400 1600	250	85	400	8500	0.9	1.0	140	0.139	0.04	29	Fig. 29 Weight = 320 g 
► MCC224-201o1 ► MCC224-221o1	2000 2200	240	85	400	8000	0.8	0.76	130	0.139	0.04	31	
► MCC225-121o1 ► MCC225-141o1 ► MCC225-161o1 ► MCC225-181o1	1200 1400 1600 1800	221	85	400	8000	0.8	0.76	130	0.16	0.04		
► MCC250-081o1 ► MCC250-121o1 ► MCC250-141o1 ► MCC250-161o1 ► MCC250-181o1	800 1200 1400 1600 1800	287	85	450	9000	0.85	0.82	140	0.129	0.04	29	
► MCC255-121o1 ► MCC255-141o1 ► MCC255-161o1 ► MCC255-181o1	1200 1400 1600 1800	250	85	450	9000	0.8	0.68	130	0.14	0.04	31	Fig. 31 Weight = 750 g 
► MCC310-081o1 ► MCC310-121o1 ► MCC310-141o1 ► MCC310-161o1 ► MCC310-181o1	800 1200 1400 1600 1800	320	85	500	9200	0.8	0.82	140	0.112	0.04	29	
► MCC312-121o1 ► MCC312-141o1 ► MCC312-161o1 ► MCC312-181o1	1200 1400 1600 1800	320	85	520	9200	0.8	0.68	140	0.12	0.04	31	Fig. 32 Weight = 730 g 
► MCO500-121o1 ► MCO500-141o1 ► MCO500-161o1	1200 1400 1600	500	85	785	15000	0.8	0.6	140	0.06	0.02	32	

Data according to DIN / IEC 747 and refer to a single thyristor unless otherwise stated.

Thyristor Modules



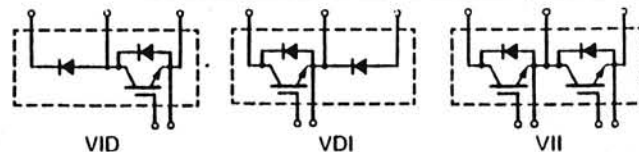
$I_{TAV} = 18-116 A$

Type	V_{RRM} V_{DRM}	I_{TAV}	T_C	I_{TRMS}	I_{TSM} 45°C 10 ms	V_{TO}	r_T	T_{VM}	R_{thJC} per chip	R_{thCK} per chip	Fig. No.	Package style
▶ New	V	A	°C	A	A	V	mΩ	°C	K/W	K/W		See outlines on page 35
MCC19-08lo1B	800	18	85	40	400	0.85	18	125	1.3	0.2	24	
MCC19-12lo1B	1200											
MCC19-14lo1B	1400											
MCC19-16lo1B	1600											
MCC19-08lo8B	800	18	85	40	400	0.85	18	125	1.3	0.2	27	
MCC19-12lo8B	1200											
MCC19-14lo8B	1400											
MCC19-16lo8B	1600											
MCC26-08lo1B	800	27	85	50	520	0.85	11	125	0.88	0.2	24	
MCC26-12lo1B	1200											
MCC26-14lo1B	1400											
MCC26-16lo1B	1600											
MCC26-08lo8B	800	27	85	50	520	0.85	11	125	0.88	0.2	27	
MCC26-12lo8B	1200											
MCC26-14lo8B	1400											
MCC26-16lo8B	1600											
MCC44-08lo1B	800	49	85	80	1150	0.85	5.3	125	0.53	0.2	24	
MCC44-12lo1B	1200											
MCC44-14lo1B	1400											
MCC44-16lo1B	1600											
MCC44-18lo1B	1800											
MCC44-08lo8B	800	49	85	80	1150	0.85	5.3	125	0.53	0.2	27	
MCC44-12lo8B	1200											
MCC44-14lo8B	1400											
MCC44-16lo8B	1600											
MCC44-18lo8B	1800											
MCC56-08lo1B	800	60	85	100	1500	0.85	3.7	125	0.45	0.2	24	
MCC56-12lo1B	1200											
MCC56-14lo1B	1400											
MCC56-16lo1B	1600											
MCC56-18lo1B	1800											
MCC56-08lo8B	800	60	85	100	1500	0.85	3.7	125	0.45	0.2	27	
MCC56-12lo8B	1200											
MCC56-14lo8B	1400											
MCC56-16lo8B	1600											
MCC56-18lo8B	1800											
MCC72-08lo1B	800	85	85	180	1700	0.85	3.2	125	0.3	0.2	24	
MCC72-12lo1B	1200											
MCC72-14lo1B	1400											
MCC72-16lo1B	1600											
MCC72-18lo1B	1800											
MCC72-08lo8B	800	85	85	180	1700	0.85	3.2	125	0.3	0.2	27	
MCC72-12lo8B	1200											
MCC72-14lo8B	1400											
MCC72-16lo8B	1600											
MCC72-18lo8B	1800											
▶ MCC94-20lo1B	2000	104	85	180	1700	0.85	3.2	125	0.22	0.2	24	
▶ MCC94-22lo1B	2200											
MCC95-08lo1B	800	116	85	180	2250	0.8	2.4	125	0.22	0.2		
MCC95-12lo1B	1200											
MCC95-14lo1B	1400											
MCC95-16lo1B	1600											
MCC95-18lo1B	1800											
MCC95-08lo8B	800	116	85	180	2250	0.8	2.4	125	0.22	0.2	27	
MCC95-12lo8B	1200											
MCC95-14lo8B	1400											
MCC95-16lo8B	1600											
MCC95-18lo8B	1800											


Fig. 24/27
TO-240 AA
Weight = 90 g



IGBT Modules



High Short Circuit SOA Capability

Type \ominus	V_{CES}	I_c	I_c		$V_{CE(sat)}$	$E_{on} \ominus$	E_{off}	R_{thJC}	P_c	Package style
$T_{JM} = 150^\circ C$		$T_c = 25^\circ C$	$80^\circ C$	$100^\circ C$	typ.	typ.	typ.	max.	max.	See outlines on page 35
► New	V	A	A	A	V	125°C mJ	125°C mJ	K/W	W	
low $V_{CE(sat)}$	► VII 50-12G3	1200	50	49	2.6	10	18	0.35	360	Fig. 33 Weight = 130 g 
	► VII 75-12G3		75	56	2.9	12	22	0.31	400	
	► VII 100-12G3		100	75	2.9	20	29	0.23	540	
High speed	► VII 50-12S3	1200	50	45	3.4	8	8	0.31	400	
	► VII 75-12S3		75	64	3.4	12	12	0.22	570	
	► VII 100-12S3		100	68	3.7	20	14	0.21	600	
	► VID 50-12S3	1200	50	45	3.4	8	8	0.31	400	
	► VID 75-12S3		75	64	3.4	12	12	0.22	570	
	► VID 100-12S3		100	68	3.7	20	14	0.21	600	
low $V_{CE(sat)}$	► VII 100-12G4	1200	100	84	2.6	16	29	0.20	625	
	► VII 125-12G4		125	110	2.9	16	37	0.15	830	
	► VII 150-12G4		150	129	2.8	20	46	0.13	960	
► VII 200-12G4	200		153	2.9	29	58	0.11	1130		
High speed	► VII 100-12S4	1200	100	90	3.4	14	14	0.20	625	
	► VII 125-12S4		125	119	3.7	16	18	0.15	850	
	► VII 150-12S4		150	138	3.7	20	23	0.13	950	
	► VII 200-12S4		200	168	3.7	29	29	0.11	1130	
	► VID 125-12S4	1200	125	119	3.7	16	18	0.15	850	
	► VID 150-12S4		150	138	3.7	20	23	0.13	950	
	► VID 200-12S4		200	168	3.7	29	29	0.11	1130	
	► VDI 125-12S4		1200	125	119	3.7	16	18	0.15	850
► VDI 150-12S4	150	138		3.7	20	23	0.13	950		
► VDI 200-12S4	200	168		3.7	29	29	0.11	1130		

i E_{on} including turn-on energy caused by commutation of free-wheeling diode

Appendix 3

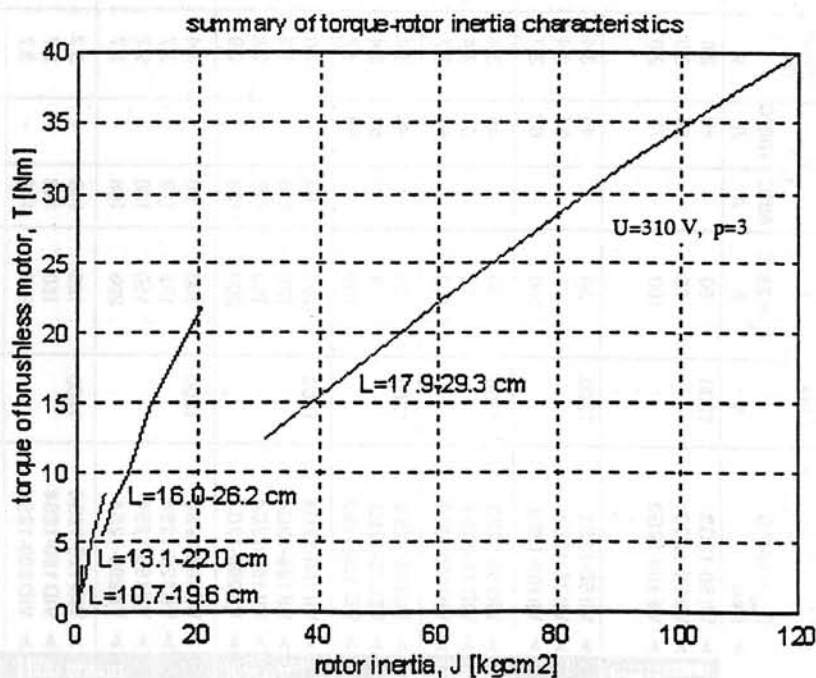
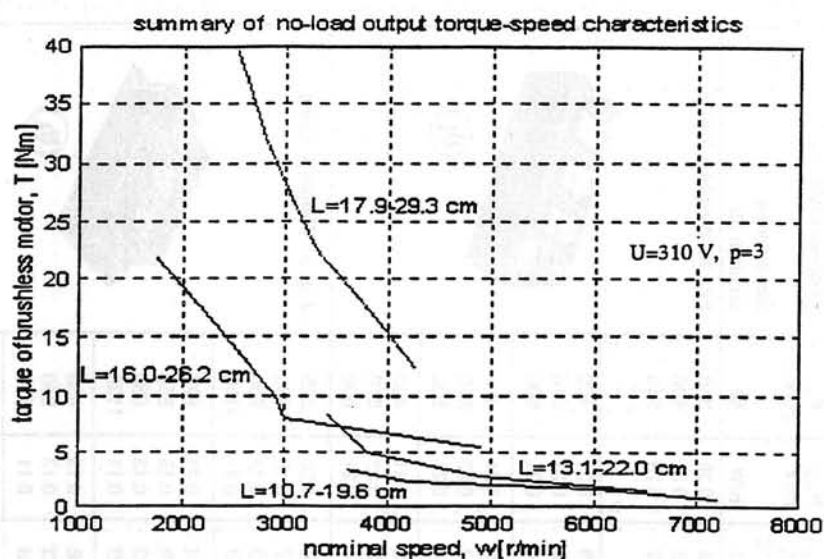
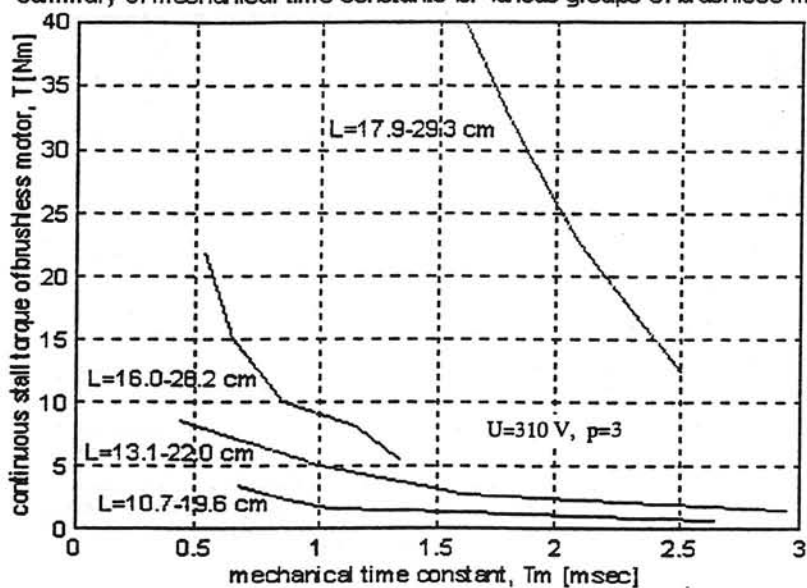


Figure A3-1 Brushless motor characteristics (power inverter with IGBT, $m=3$)

summary of mechanical time constants for various groups of brushless motors



summary of the electrical time constants for various groups of brushless motors

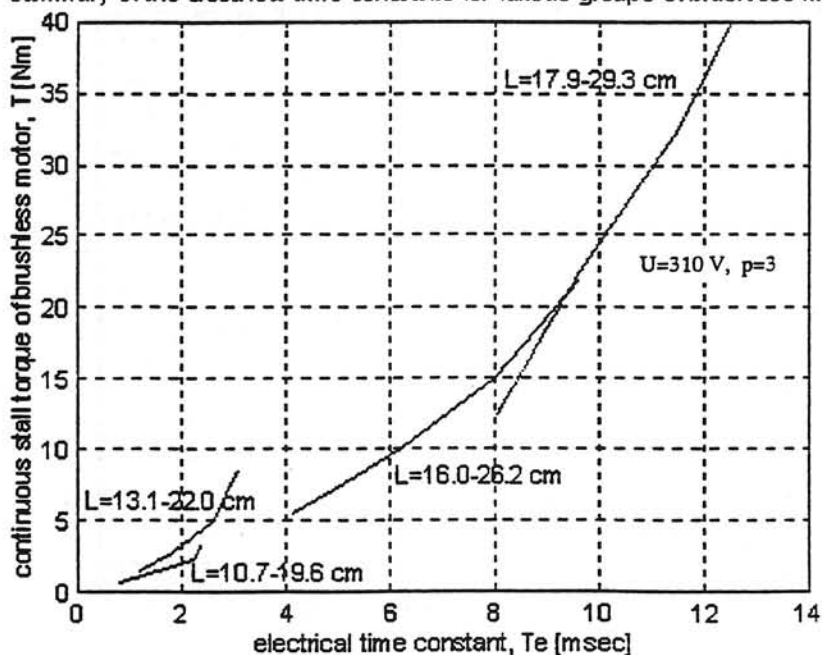


Figure A3-2 Brushless motor characteristics (power inverter with IGBT, $m=3$)

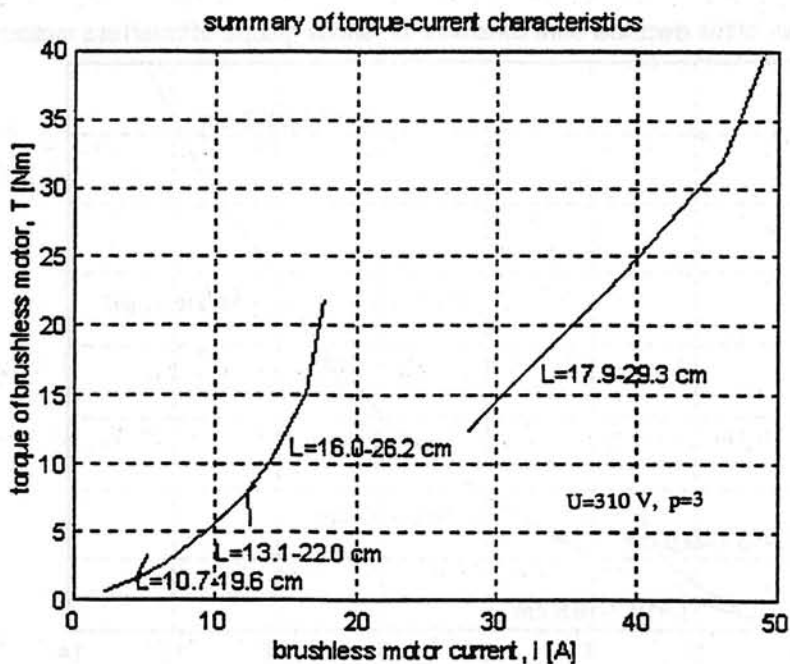
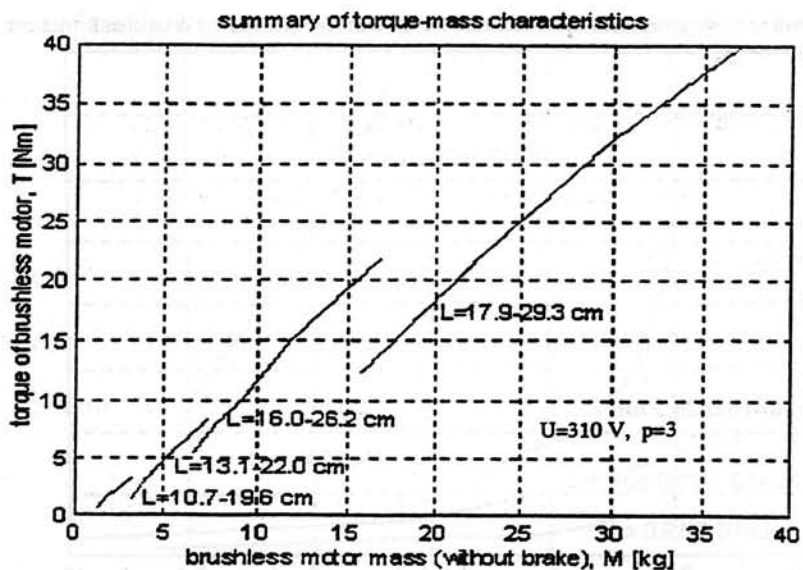


Figure A3-3 Brushless motor characteristics (power inverter with IGBT, $m=3$)

Appendix 4 Frequency Transfer Function of Electromechanical Servosystem

The equivalent model (see Fig. 4.2) contains two input signals

$$U_M \sim U_{OM} \sin \omega t \text{ and } T_{LL} \sim T_{OLL} \sin (\omega t + \varphi_0),$$

and one output signal

$$d\theta_M / dt = \dot{\theta}_M = A \sin (\omega t + \varphi) = A_M \sin (\omega t + \varphi_M) + A_{LL} \sin (\omega t + \varphi_{LL}),$$

conformed to the sine wave of frequency functions with different amplitudes, and phases, where

$$A_M = U_{OM} |K_M|, A_{LL} = T_{OLL} |K_{LL}|, \varphi_M = \arg(K_M),$$

$$\varphi_{LL} = \arg(K_{LL}) + \varphi_0, K_U = I_{mag} \{ \dot{\theta}_M / U_M \} = j\omega\theta_{OM} U_{OM}$$

Let us represent a frequency transfer function of a such system (see Fig. 4.2). At first we consider the set of differential equations (4 .10, 4 .11, 4.12) on condition that $T_{LL} = 0$.

In view of the fact that

$$U_M = U_{OM} e^{j\omega t}; I_M = I_{OM} e^{j\omega t}; T_L = T_{OL} e^{j\omega t}; \theta_M = \theta_{OM} e^{j\omega t}; K_U = \frac{j\omega\theta_{OM}}{U_{OM}},$$

we obtain

$$U_{OM} = K_E j\omega\theta_{OM} + R_M I_{OM} + L_M j\omega I_{OM}$$

$$K_T I_{OM} = T_{OL} / \eta_A G_D + \xi_M j\omega\theta_{OM} + J_M (-\omega^2)\theta_{OM} \quad (\text{A4.1})$$

$$T_{OL} = j\omega\theta_{OM} T_F / G_D + \theta_{OM} K_L / G_D + j\omega\theta_{OM} \xi_L / G_D - \omega^2 \theta_{OM} J_L / G_D$$

$$U_{OM} = K_E j\omega\theta_{OM} + I_{OM} (R_M + j\omega L_M)$$

$$I_{OM} = T_{OL} / K_T \eta_A G_D + \theta_{OM} (\xi_M j\omega + J_M (-\omega^2)) / K_T \quad (\text{A4.2})$$

$$T_{OL} = \theta_{OM} (j\omega T_F + K_L + j\omega \xi_L - \omega^2 J_L) / G_D$$

Allow the symbols

$$\alpha = j\omega K_E, \quad \beta = R_M + L_M,$$

$$\gamma = 1 / (K_T \eta_A G_D), \quad \delta = (j\omega \xi_M - \omega^2 J_L) / K_T,$$

$$\varepsilon = (j\omega T_F + K_L + j\omega \xi_L - \omega^2 J_L) / G_D$$

the set of equations (A4.2) become

$$U_{OM} = \alpha \theta_{OM} + \beta I_{OM}$$

$$I_{OM} = \gamma T_{OL} + \delta \theta_{OM} \quad (A4.3)$$

$$T_{OL} = \varepsilon \theta_{OM}$$

$$U_{OM} = \alpha \theta_{OM} + \beta I_{OM}$$

$$I_{OM} = \theta_{OM} (\gamma \varepsilon + \delta)$$

$$U_{OM} = \theta_{OM} (\alpha + \beta(\gamma \varepsilon + \delta))$$

$$K_U = \frac{j\omega}{\alpha + \beta(\gamma \varepsilon + \delta)} \quad (A4.4)$$

Reasoning by the same way for the condition $U_M = 0$, we obtain the frequency transfer function (A4.5)

$$K_{LL} = - \frac{j\omega \beta \gamma}{\alpha + \beta(\gamma \varepsilon + \delta)} \quad (A4.5)$$

Series 01: Aerodynamics

01. F. Motallebi, 'Prediction of Mean Flow Data for Adiabatic 2-D Compressible Turbulent Boundary Layers'
1997 / VI + 90 pages / ISBN 90-407-1564-5
02. P.E. Skåre, 'Flow Measurements for an Afterbody in a Vertical Wind Tunnel'
1997 / XIV + 98 pages / ISBN 90-407-1565-3
03. B.W. van Oudheusden, 'Investigation of Large-Amplitude 1-DOF Rotational Galloping'
1998 / IV + 100 pages / ISBN 90-407-1566-1
04. E.M. Houtman / W.J. Bannink / B.H. Timmerman, 'Experimental and Computational Study of a Blunt Cylinder-Flare Model in High Supersonic Flow'
1998 / VIII + 40 pages / ISBN 90-407-1567-X
05. G.J.D. Zondervan, 'A Review of Propeller Modelling Techniques Based on Euler Methods'
1998 / IV + 84 pages / ISBN 90-407-1568-8
06. M.J. Tummers / D.M. Passchier, 'Spectral Analysis of Individual Realization LDA Data'
1998 / VIII + 36 pages / ISBN 90-407-1569-6
07. P.J.J. Moeleker, 'Linear Temporal Stability Analysis'
1998 / VI + 74 pages / ISBN 90-407-1570-X
08. B.W. van Oudheusden, 'Galloping Behaviour of an Aeroelastic Oscillator with Two Degrees of Freedom'
1998 / IV + 128 pages / ISBN 90-407-1571-8
09. R. Mayer, 'Orientation on Quantitative IR-thermography in Wall-shear Stress Measurements'
1998 / XII + 108 pages / ISBN 90-407-1572-6
10. K.J.A. Westin / R.A.W.M. Henkes, 'Prediction of Bypass Transition with Differential Reynolds Stress Models'
1998 / VI + 78 pages / ISBN 90-407-1573-4
11. J.L.M. Nijholt, 'Design of a Michelson Interferometer for Quantitative Refraction Index Profile Measurements'
1998 / 60 pages / ISBN 90-407-1574-2
12. R.A.W.M. Henkes / J.L. van Ingen, 'Overview of Stability and Transition in External Aerodynamics'
1998 / IV + 48 pages / ISBN 90-407-1575-0
13. R.A.W.M. Henkes, 'Overview of Turbulence Models for External Aerodynamics'
1998 / IV + 40 pages / ISBN 90-407-1576-9

Series 02: Flight Mechanics

01. E. Obert, 'A Method for the Determination of the Effect of Propeller Slipstream on a Static Longitudinal Stability and Control of Multi-engined Aircraft'
1997 / IV + 276 pages / ISBN 90-407-1577-7
02. C. Bill / F. van Dalen / A. Rothwell, 'Aircraft Design and Analysis System (ADAS)'
1997 / X + 222 pages / ISBN 90-407-1578-5
03. E. Torenbeek, 'Optimum Cruise Performance of Subsonic Transport Aircraft'
1998 / X + 66 pages / ISBN 90-407-1579-3

Series 03: Control and Simulation

01. J.C. Gibson, 'The Definition, Understanding and Design of Aircraft Handling Qualities'
1997 / X + 162 pages / ISBN 90-407-1580-7
02. E.A. Lomonova, 'A System Look at Electromechanical Actuation for Primary Flight Control'
1997 / XIV + 110 pages / ISBN 90-407-1581-5
03. C.A.A.M. van der Linden, 'DASMAT-Delft University Aircraft Simulation Model and Analysis Tool. A Matlab/Simulink Environment for Flight Dynamics and Control Analysis'
1998 / XII + 220 pages / ISBN 90-407-1582-3

Series 05: Aerospace Structures and Computational Mechanics

01. A.J. van Eekelen, 'Review and Selection of Methods for Structural Reliability Analysis'
1997 / XIV + 50 pages / ISBN 90-407-1583-1
02. M.E. Heerschap, 'User's Manual for the Computer Program Cufus. Quick Design Procedure for a CUt-out in a FUSelage version 1.0'
1997 / VIII + 144 pages / ISBN 90-407-1584-X
03. C. Wohlever, 'A Preliminary Evaluation of the B2000 Nonlinear Shell Element Q8N.SM'
1998 / IV + 44 pages / ISBN 90-407-1585-8
04. L. Gunawan, 'Imperfections Measurements of a Perfect Shell with Specially Designed Equipment (UNIVIMP)'
1998 / VIII + 52 pages / ISBN 90-407-1586-6

Series 07: Aerospace Materials

01. A. Vašek / J. Schijve, 'Residual Strength of Cracked 7075 T6 Al-alloy Sheets under High Loading Rates'
1997 / VI + 70 pages / ISBN 90-407-1587-4
02. I. Kunes, 'FEM Modelling of Elastoplastic Stress and Strain Field in Centre-cracked Plate'
1997 / IV + 32 pages / ISBN 90-407-1588-2
03. K. Verolme, 'The Initial Buckling Behavior of Flat and Curved Fiber Metal Laminate Panels'
1998 / VIII + 60 pages / ISBN 90-407-1589-0
04. P.W.C. Provó Kluit, 'A New Method of Impregnating PEI Sheets for the *In-Situ* Foaming of Sandwiches'
1998 / IV + 28 pages / ISBN 90-407-1590-4
05. A. Vlot / T. Soerjanto / I. Yeri / J.A. Schelling, 'Residual Thermal Stresses around Bonded Fibre Metal Laminate Repair Patches on an Aircraft Fuselage'
1998 / IV + 24 pages / ISBN 90-407-1591-2
06. A. Vlot, 'High Strain Rate Tests on Fibre Metal Laminates'
1998 / IV + 44 pages / ISBN 90-407-1592-0
07. S. Fawaz, 'Application of the Virtual Crack Closure Technique to Calculate Stress Intensity Factors for Through Cracks with an Oblique Elliptical Crack Front'
1998 / VIII + 56 pages / ISBN 90-407-1593-9
08. J. Schijve, 'Fatigue Specimens for Sheet and Plate Material'
1998 / VI + 18 pages / ISBN 90-407-1594-7

Series 08: Astrodynamics and Satellite Systems

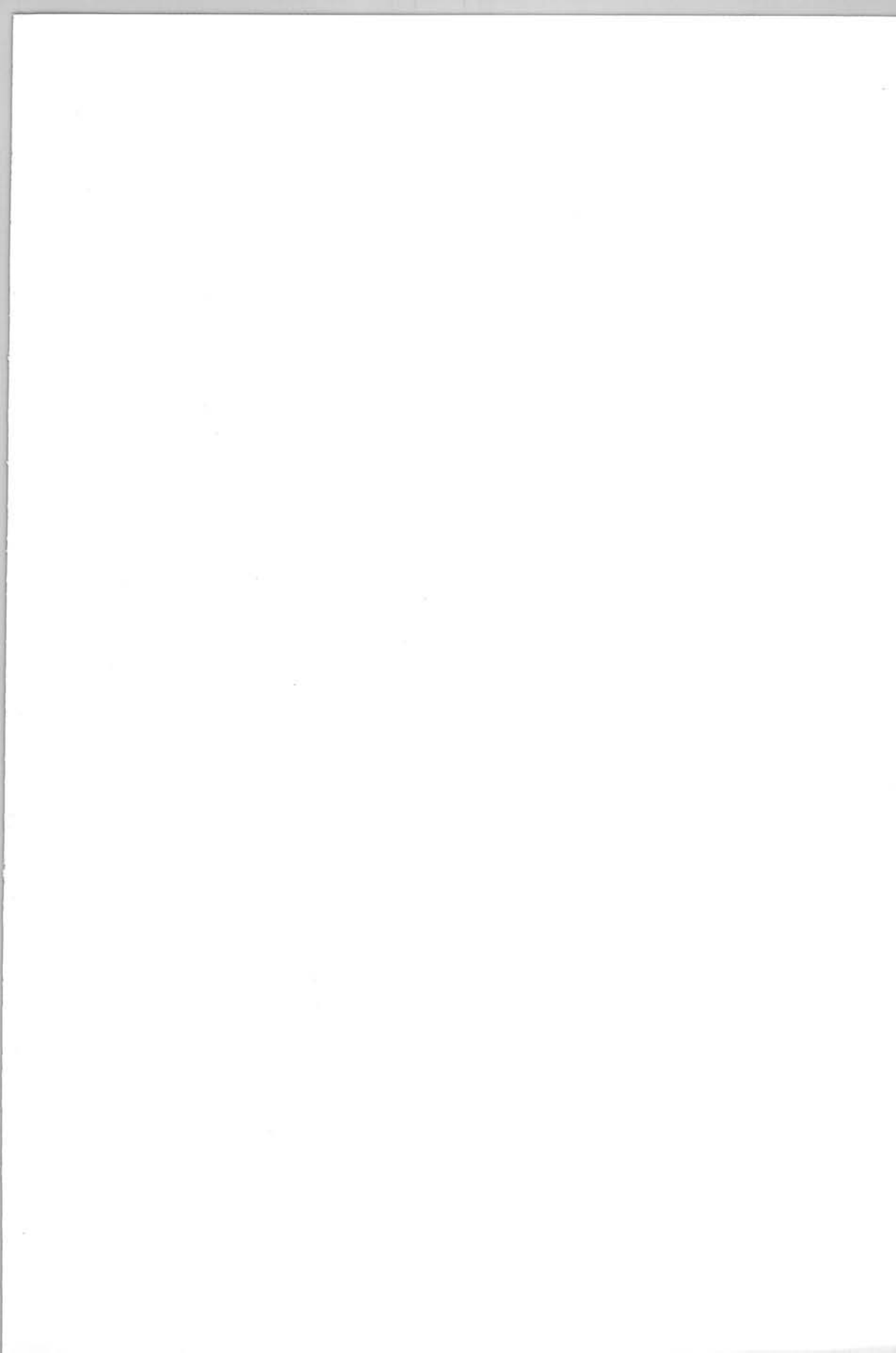
01. E. Mooij, 'The Motion of a Vehicle in a Planetary Atmosphere'
1997 / XVI + 156 pages / ISBN 90-407-1595-5
02. G.A. Bartels, 'GPS-Antenna Phase Center Measurements Performed in an Anechoic Chamber'
1997 / X + 70 pages / ISBN 90-407-1596-3
03. E. Mooij, 'Linear Quadratic Regulator Design for an Unpowered, Winged Re-entry Vehicle'
1998 / X + 154 pages / ISBN 90-407-1597-1

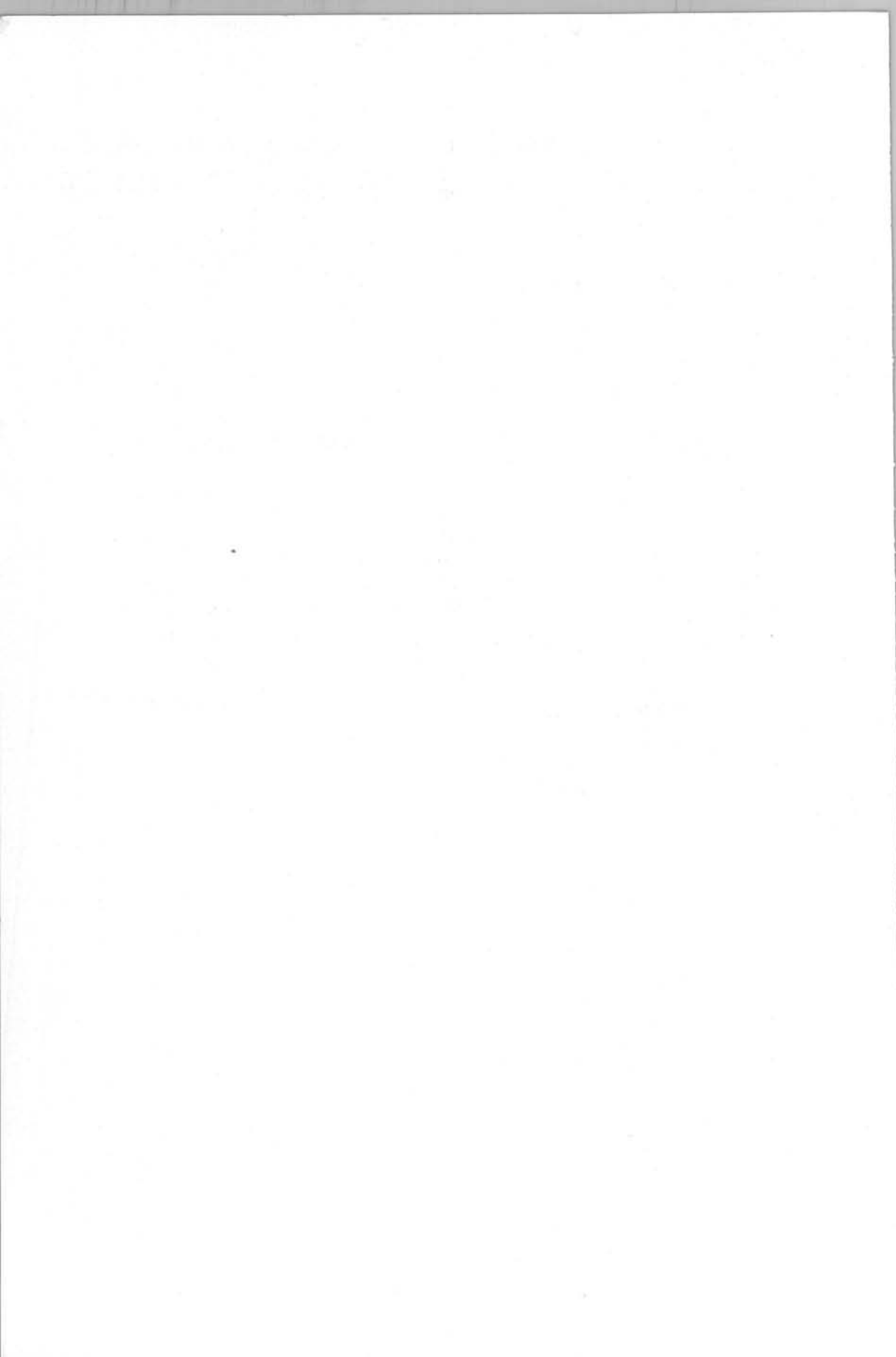
Section 10: Miscellaneous

- 10.1. The following items are to be included in the 1978 TO Budget:
 - 10.1.1. The cost of the 1978 TO Budget.
 - 10.1.2. The cost of the 1978 TO Budget.
 - 10.1.3. The cost of the 1978 TO Budget.
 - 10.1.4. The cost of the 1978 TO Budget.
 - 10.1.5. The cost of the 1978 TO Budget.
 - 10.1.6. The cost of the 1978 TO Budget.
 - 10.1.7. The cost of the 1978 TO Budget.
 - 10.1.8. The cost of the 1978 TO Budget.
 - 10.1.9. The cost of the 1978 TO Budget.
 - 10.1.10. The cost of the 1978 TO Budget.

Section 11: Administration and Finance

- 11.1. The following items are to be included in the 1978 TO Budget:
 - 11.1.1. The cost of the 1978 TO Budget.
 - 11.1.2. The cost of the 1978 TO Budget.
 - 11.1.3. The cost of the 1978 TO Budget.
 - 11.1.4. The cost of the 1978 TO Budget.
 - 11.1.5. The cost of the 1978 TO Budget.
 - 11.1.6. The cost of the 1978 TO Budget.
 - 11.1.7. The cost of the 1978 TO Budget.
 - 11.1.8. The cost of the 1978 TO Budget.
 - 11.1.9. The cost of the 1978 TO Budget.
 - 11.1.10. The cost of the 1978 TO Budget.





3021886

An overview is presented of the emergence of the ALL Electric flight control system (FCS) or power-by-wire (PBW) concept. The concept of fly-by-power refers to the actuator using electrical rather than hydraulic power. The development of the primary flight control Electromechanical Actuators (EMAs) is one of the essential steps in the implementation of the ALL Electric Aircraft. There is a great deal of interest in the application of brushless motors (BM) with rare-earth magnet rotors using external commutation as EMAs flight control systems. The increased complexity of the converter is caused by the fact that thyristor inverters with forced commutation involve additional components and a more complicated mechanical design but a simple control structure, the BM machine must be fed with alternating currents of variable amplitude, frequency and phase. It is for these reasons that no standard solution for the control of brushless motors has emerged as in the case of the DC motor. The purpose of this book is to present a theoretical investigation of EMAs based on the BM description: electromechanical architecture, magnet materials, operating principles, electromagnetic processes, etc. In order to design current, position, torque, and speed controllers for BM, the general theory of electromechanical and electromagnetic processes in electrical machines in electrical and power converters is used. This book describes a basic approach to the creation of mathematical models for BM with rectangular and sinusoidal current waves. It presents the hardware for position, torque, and current control systems for EMAs. This work also treats the analysis and synthesis of different aircraft power systems with EMAs. Finally, the basic approach for the preliminary design of EMAs is presented.

ISBN 90-407-1581-5



9 799040 715814

